Chem Soc Rev

Negative thermal expansion in functional materials: Controllable thermal expansion by chemical modifications

Journal:	*Chemical Society Reviews*
Manuscript ID:	CS-REV-12-2014-000461.R1
Article Type:	Review Article
Date Submitted by the Author:	17-Mar-2015
Complete List of Authors:	Chen, Jun; University of Science and Technology Beijing, Department of Physical Chemistry Hu, Lei; University of Science and Technology Beijing, Department of Physical Chemistry Deng, Jinxia; University of Science and Technology Beijing, Department of Chemsitry Xing, Xianran; University of Science and Technology Beijing, School of Metallurgical and Ecological Engineering

Chem Soc Rev

RSCPublishing

REVIEW ARTICLE

Negative thermal expansion in functional materials: Controllable thermal expansion by chemical modifications

Cite this: DOI: 10.1039/x0xx00000x

Received ooth January 2012,
Accepted ooth January 2012

DOI: 10.1039/x0xx00000x

www.rsc.org/

Jun Chen, Lei Hu, Jinxia Deng and Xianran Xing*

Negative thermal expansion (NTE) is an intriguing physical property of solids, and exhibits a complex interplay among lattice, phonon, and electron. Interestingly, a large number of NTE materials have been found in various types of functional materials. In the last two decades good progress has been achieved to discover new phenomena and mechanisms of NTE. In the present review article, NTE is reviewed in functional materials of ferroelectrics, magnetics, multiferroics, superconductors, temperature-induced electron configuration change and so on. Zero thermal expansion (ZTE) of functional materials is emphasized due to the importance for practical applications. The NTE functional materials present a general physical picture to reveal a strong coupling role between physical properties and NTE. There is a general nature of NTE for both ferroelectrics and magnetics, in which NTE is determined by either ferroelectric order or magnetic one. In NTE functional materials, a multi-way to control thermal expansion can be established through the coupling roles of ferroelectricity-NTE, magnetism-NTE, change of electron configuration-NTE, open-framework-NTE, and so on. Chemical modification has been proved to be an effective method to control thermal expansion. Finally, challenges and questions are discussed for the development of NTE materials. There remains a challenge to discover a "perfect" NTE material for each specific application for chemists. The future studies on NTE functional materials will definitely promote the development of NTE materials.

1. Background

1.1 Basic knowledge of thermal expansion in solids

Thermal expansion is an important issue for solid state chemistry. It generally correlates with crystal structure, electronic structure, microstructure, defects and so on. The thermal expansion of solid materials shows a strong dependence on chemical composition. The problem caused from thermal expansion exists in many fields varying from large structural components such as road, railroad tracks, container of liquefied natural gas and bridges, to precision instruments and electronic devices such as telescopes, standard rulers, solid-oxide fuel cells (SOFCs), actuators, core wires of long-distance power cables, catalyst support and thin films.[1-10] The modern applications require functional materials to display not only good physical properties, but also controllable thermal expansion. Controllable thermal expansion undoubtedly enhances the reliability of devices and prolongs lifetime.

Before we review progress in NTE of functional materials, some basic knowledge of thermal expansion should be introduced in order. It is well known that most materials expand upon heating, such as α-Al_2O_3 (α_V = 2.6×10^{-5} K^{-1}, 293-1773 K),[11] TiO_2 (anatase, α_V = 2.2×10^{-5} K^{-1}, 300-575 K),[12] and $SrTiO_3$ (α_V = 3.4×10^{-5} K^{-1}, 300-1173 K).[13] Thermal expansion can be explained by the simplest model of the asymmetric shape of the potential energy well of a simple diatomic molecule. As molecules are warmed, higher vibrational levels are excited, e.g., from r_0 at T_0 to r_6 at T_6, resulting in the thermal expansion in distance of molecules (Fig. 1). Thermal expansion of solids is formally explained by the Grüneisen relationship between phonon and thermal expansion.[14]

$$\alpha_V = \frac{\gamma C_v K}{V} \quad (1)$$

where α_V is the coefficient of thermal expansion (CTE), C_V specific heat at constant volume, K isothermal compressibility ($K = -(1/V)(\partial V/\partial P)_T$), V volume, γ the Grüneisen parameter ($\gamma = -\mathrm{d}(\ln v)/\mathrm{d}(\ln V)$). Normal solids have a nearly temperature-independent K, and γ which is in range of 1 to 3. Therefore, α_V is normally correlated to C_V which can be basically estimated by C_{Debye}:

$$C_{\text{Debye}} = 9\text{N}k_B(\frac{T}{\theta})^3 \int_0^{\theta/T} dx \frac{x^4 e^x}{(e^x-1)^2} \quad (2)$$

Therefore volume V depends on temperature T as:

$$V(T) = V_0 + \frac{9\text{N}k_B\gamma}{K} T(\frac{T}{\theta})^3 \int_0^{\theta/T} \text{d}x \frac{x^3}{e^x-1} \quad (3)$$

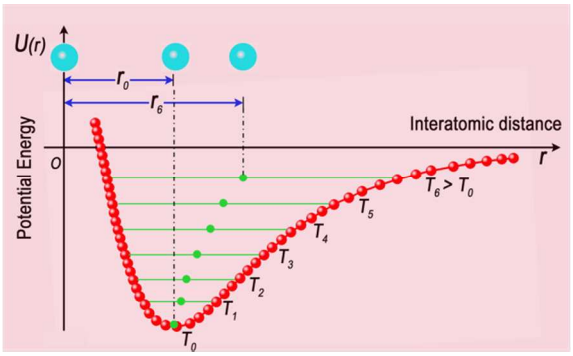

Fig. 1 Schematic diagram of potential energy well of pair atoms.

We can adopt the Debye-Grüneisen equation 3 to theoretically estimate thermal expansion of solids from phononic contribution. With given K and γ, unit cell volume can be fitted from experimental data with a refinement of parameter θ. The details of equation 3 can be referred to the literature.[15] The Debye-Grüneisen equation 3 is quoted here in order for the understanding the NTE mechanism in functional solids. After deduction of component contributed from anharmonic phonon vibration, the contribution to NTE or anomalous thermal expansion can be directly and quantitatively estimated from physical properties such as ferroelectric or magnetic order. According to equations 1 and 3, it is well known that thermal expansion is expected to be low in low temperature, and reaches zero at absolute zero Kelvin. And it approaches to a constant value above the Debye temperature. In a real structure of material, different vibrational modes have different energy and depend on temperature. The actual population of modes should be considered. The average Grüneisen parameter is estimated by $\gamma_{av} = \sum c_i\gamma_i/c_i$, where c_i weights the contribution of a mode to the overall C_V. In the present review, if thermal expansion of one material deviates from the theoretical thermal expansion estimated from the Debye-Grüneisen equation 3, we generally state this material displays anomalous thermal expansion. In such case, thermal expansion could be more positive, lower, or negative.

The CTE can be defined by either of the following equations:

$$\alpha_l = \frac{(l-l_0)}{l_0\times(T-T_0)} \text{ or } \alpha_l = \frac{\text{d}l}{l_0\times\text{d}T} \quad (4)$$

$$\alpha_V = \frac{(V-V_0)}{V_0\times(T-T_0)} \text{ or } \alpha_V = \frac{\text{d}V}{V_0\times\text{d}T} \quad (5)$$

where α_l and α_V are linear and volume CTE, respectively. NTE material means it exhibits negative α_V in a certain temperature range. Positive thermal expansion (PTE) means the value of α_V is positive. For a cubic material, there is an equation of $\alpha_l = 1/3\cdot\alpha_V$. However, for materials with anisotropic crystal structure thermal expansion is different along different axis. The relationship between α_l and α_V is complex. Simply, we could also use the equation of $\alpha_l = 1/3\cdot\alpha_V$ to basically estimate the relationship between average α_l and α_V. It needs to note that because CTE is sometimes dependent to temperature range, especially for those materials with nonlinear thermal expansion, the temperature range should be quoted for any value CTE. In the present review, the CTE value is default to be volume one which is derived from unit cell volume, unless there are specific notes for CTE data.

The data of CTE are generally determined by two methods. One is diffraction techniques, such as x-ray and neutron diffraction, to determine lattice parameters as function of temperature. The correspondingly calculated CTE presents the intrinsic thermal expansion property. The other is apparent measurement of length of bulk samples as a function of temperature by means of dilatometry. The calculated result represents the apparent linear CTE. It is important to note that there is normally a difference between intrinsic and apparent values of CTE, especially for those materials with high anisotropy. For the apparent measurement, the result of thermal expansion is unavoidably affected by extrinsic factors of microcracks, pores, and grain boundaries. In anisotropic materials, microcracks can be produced by the local stress of neighbouring grains in bulk ceramics due to anisotropic thermal expansion. The occurrence and healing of microcracks can introduce an additional contribution to lower thermal expansion.[4] The study of thermal expansion by apparent measurement should be paid much attention on the quality of sintered ceramics and drawing a conclusion. For example, $NaZr_2(PO_4)_3$ (NZP) was reported to have an apparent thermal expansion as negative as α_l = -4.0×10^{-7} K^{-1} (298~1273 K),[16] however, its intrinsic one is positive (α_l = 4.5×10^{-6} K^{-1}, 298~1273 K).[17] The other examples could be observed in anisotropic materials of $Sc_2(WO_4)_3$.[2,18]

1.2 NTE materials

The studies on NTE became one of the hot topics in solid state chemistry after the discovery of isotropic NTE in ZrW_2O_8 (α_V = -2.73×10^{-5} K^{-1}, 0~300 K) in 1996 by Sleight *et al.*[1] The first observation concerning the phenomenon of NTE can be traced back several hundred years ago to the discovery of the "density anomaly of water". Water has the highest density at 277 K. The nature of Invar effect in $Fe_{0.65}Ni_{0.35}$ alloys discovered by Guillaume in 1897 was actually related to NTE.[8,19] Thermal shrinkage of a solid was first documented by Scheel in 1907 for quartz and vitreous silica at low temperatures.[20,21] The low thermal expansion was found in lithium aluminium silicates in 1948,[22,23] and the NZP family in 1979.[16] During this period, these compounds were usually referred to "low thermal expansion" or "anomalous thermal expansion" instead of "negative thermal expansion" material. The term of "negative thermal expansion" was used only sporadically before the 1990s. After the discovery of isotropic NTE in ZrW_2O_8 in

1996, the studies on NTE have been paid much attention, and are growing rapidly.[1]

The majority of crystal structures of NTE materials have a common feature of two-coordinate M_1-O-M_2 linkage for cation polyhedra which build 3D lattice. These linkages are typical for those NTE materials with open-framework structure feature. The transverse vibration about M_1-O-M_2 linkage is the key factor for the occurrence of NTE with open-framework structure, sine the transverse vibrations are much energy favourable than longitudinal ones. For a strong bond of M_1-O-M_2 linkage, the length of M_1-M_2 contracts by the transverse vibrations of oxygens, while expands by longitudinal one. It was first pointed out in the 1950's that low energy transverse modes may have negative Grüneisen parameter and contribute to NTE.[24] It is also true for the coupled rotation of polyhedra in those open-framework NTE materials. The rocking of these two-coordinated linked polyhedra results from the transverse vibration mode of M_1-O-M_2 linkages. A concept of rigid unit modes (RUMs) is generally adopted to describe the NTE phenomenon in flexible framework materials.[25,26] There are a number of classes of materials with open-framework structure, such as NZP family,[16] ZrW_2O_8,[1] AM_2O_7 (A = Ti, Zr, Hf, M = P, V),[2,3] $Sc_2(WO_4)_3$,[18] zeolites,[27] $Fe[Co(CN)_6]$,[28] metal-organic frameworks,[29 - 31] $Zr_{0.4}Sn_{0.6}Mo_2O_8$,[32] and ScF_3.[33 - 39] The best example of NTE is that of liquid water and ice. Liquid water exhibits an increased density between 273 to 277 K, and solid ice itself exhibits NTE below 75 K, which is correlated to the low energy transverse vibrational modes (<50 cm^{-1}).[40,41] The NTE materials with open-framework structure are only briefly introduced in the present review, since the main task of the present topic focuses on the NTE in functional materials. Readers who interest in those NTE materials with open-framework structure can be referred to the excellent reviews.[2,3,5-7]

The discovery of NTE provides a good opportunity to simultaneously control both physical properties and thermal expansion of functional materials. Actually, NTE distributes in various type of materials such as metals, alloys, oxides, nitrides, sulfides, and fluorides. NTE has been found in various functional materials such as magnetics, ferroelectrics, semiconductors, Mott-insulators, and superconductors. One method is to form composite by adding NTE materials. Many effective studies have been carried out in various composites such as metals or oxides with ZrW_2O_8.[42-44] The other method is to control thermal expansion in single-phase compounds. The progress on the NTE functional materials has shown a general physical picture that NTE can be correlated with physical properties, such as ferroelectricity, magnetism, charge-transfer, and superconductivity. Thermal expansion of functional materials could be tailored through modulating their NTE-related physical properties.

1.3 Applications for controllable thermal expansion

For applications of those functional materials which undergo large temperature fluctuation, thermal expansion should be as low as possible. In such case, ZTE is desirable. For example, high performance of catalyst carrier needs to be refractory to survive hot corrosive exhaust and good thermal shock resistance in order for the requirements of greener vehicles with lower emission. A principal advantage of ceramic catalyst supports has to be low thermal expansion with a linear CTE located between $\alpha_l = \pm 2.0\times10^{-6}$ K^{-1}, because thermal stress σ of a material is dominated by CTE according to the equation: $\sigma = E\alpha_l\Delta T/(1-\nu)$, where E is Young's modulus, ν is Poisson's ratio, and ΔT is temperature difference.[4] Low or zero thermal expansion is critical for the application of precise instruments. For the application of electrostrictive materials, relaxor ferroelectrics like $Pb(Mg_{1/3}Nb_{2/3})O_3$-based ceramics exhibit large electrostrictive effect, which is benefited from the advantage of ZTE. Due to the feature of ZTE ($\alpha_l = 1\times10^{-6}$ K^{-1}, -173~373 K), the strain induced by thermal fluctuation is far smaller than the electrostrictive strain, which is an advantage for the micropositioner applications.[45]

The applications of functional devices generally need good matched CTE between different components. For example, the design for all-ceramic device of SOFC should pay much attention on the maintenance of structural integrity and compatibility during high temperature fabrication and repeatedly operating procedures in the range 673~1273 K, which is highly correlated to the difference in the CTE of different components. In addition to good electrochemical performance, the finding of new candidates of fuel electrode should take care of compatible thermal expansion with the electrolyte.[9,46] High temperature piezoelectric materials, which are desired for applications of structural health monitoring, non-destructive evaluation of the next generation turbines, more efficient jet engines and so on, can function at high temperatures without failure. High temperature operation condition requires controlled thermal expansion property in different component during the package of piezoelectric sensors in order to ensure mechanical reliability during thermal cycling.[47] In electronic packaging systems, the match of CTE among various materials is a key issue for the development of the next generation of electronic packaging with high system reliability. The undesirable mismatched CTE leads to thermal-stress accumulation at interfaces which deteriorates performance.[9] The applications of many thin structural components such as beams, plates and shells require stable shape against temperature fluctuation. The thermal expansion of different components should be well controlled. Otherwise, thermal deformation occurs, such as in-plane expansion or out-of-plane bending.[48] In the electronic industry, multilayer ceramic capacitors (MLCCs) are widely applied and an inseparable part of integrated circuits such as automotive industry, instrumentation, medical, laptops, and telecom. Because MLCCs consist of interleaved layers of ceramic dielectric and metal electrodes, MLCCs are sensitive to thermal shock during device construction. The mismatched CTE in MLCCs and the surrounding material is one of major problems for cracking and deterioration of devices, when the heat generated by the silicon chip will heat up surrounding components and thermal cycling. The thermal shock as the

cause of cracks is responsible for about 20 to 25% of MLCCs failure.[49]

For thin film devices, the control of biaxial elastic strain in epitaxial film, which is induced by mismatched lattice parameter or CTE between thin film and substrate is an important approach in order to enhance physical properties such as mobility of transistors, catalytic activity, superconducting, ferromagnetic, and ferroelectric,[50 - 52] or to produce new phenomena.[53 - 55] Strain engineering in film is a very useful method and commonly used to improve physical properties and get new phenomena by means of control of CTE mismatch between film and substrate. For example, $BiFeO_3$ is one of a small number of materials, which show simultaneously ferroelectric and magnetic order above room temperature. In its unstrained state, $BiFeO_3$ has rhombohedral symmetry (*R*3*c*). However, after the introduction of an in-plane biaxial compressive strain, $BiFeO_3$ is transformed to monoclinic or tetragonal state, resulting in much improved multiferroic property.[56] The engineering of control of CTE has succeeded in enhancement of superconducting transition temperature T_C. The biaxial tensile strain MgB_2 films show enhanced T_C (41.8 K) with 2 K higher than the bulk value (39.8 K), based on the well control of CTE between MgB_2 film and substrates.[51] T_C of $La_{1.9}Sr_{0.1}CuO_4$ superconductor was doubled to 49.1 K using epitaxial strain by controlling lattice mismatch and CTE between substrate and thin film. As a comparison, the bulk state of $La_{1.9}Sr_{0.1}CuO_4$ superconductor has a T_C = 25 K.[52]

In this review, we will focus on the topic of NTE in functional materials. NTE has been found in many functional materials with various types of physical properties. The main four types of NTE functional materials will be reviewed: NTE functional materials with ferroelectricity, magnetism, multiferroicity, and change of electron configuration. In the section for each NTE functional material, the contents including NTE phenomena, control of thermal expansion, and mechanism will be reviewed and discussed. After the review of these four types of NTE functional materials, one section is emphasized for the progresses of ZTE functional materials, since ZTE is an important topic for both fundamental study and practical applications. Finally, a summary and outlook will be given. The general mechanism and questions for NTE in functional materials will be discussed. The development of NTE functional materials will be suggested, such as discovery of new materials and mechanism.

2. NTE in ferroelectrics

2.1 NTE phenomena in ferroelectric solids

Ferroelectricity is one of important properties of functional materials. Ferroelectricity is defined as the existence of spontaneous polarization (P_S) which is electrically switchable. Ferroelectricity was first discovered in single-crystal Rochelle salt in 1921.[57] The story of the discovery of ferroelectric materials became fascinating in the early 1940s. Since that time, some important types of ferroelectrics were found, such as the perovskite (ABO_3) group, the tungsten-bronze group, the bismuth layer-structure group, and the pyrochlore group. Ferroelectric functional materials are widely applied in the fields of high electric constant capacitors, piezoelectric transducers, positive temperature coefficient devices, ferroelectric thin-film memories and so on. Among these ferroelectrics, the perovskite-based ferroelectricity is particular important one, such as $PbTiO_3$ (PT), $BaTiO_3$, $BiFeO_3$, $(K,Na)NbO_3$, $Pb(Mg_{1/3}Nb_{2/3})O_3$, and $(Bi_{1/2}Na_{1/2})TiO_3$.[57]

It is interesting to observe that many ferroelectrics have been found to exhibit NTE or anomalous thermal expansion below T_C, such as PT,[58] PT-based ferroelectrics,[13, 59 - 73] $Pb(Mg_{1/3}Nb_{2/3})O_3$ ferroelectric relaxors,[74,75] tungsten bronze,[76-80] and other ferroelectrics.[81,82] The NTE data are tabulated in Table 1. Among all these ferroelectrics, PT-based ferroelectrics exhibit an interestingly controllable NTE, which have been extensively studied in the past decade by the Xing group. The studies on crystal structure and phase transition of PT can be traced back to early 1950s. The temperature dependence of lattice parameters was measured in the temperature range of room temperature (RT) to 808 K by x-ray diffractometer in 1951.[83] Several other groups determined the crystal structure of PT as function of temperature in the following half century.[84] Even though the phenomenon of unit cell volume contraction with increasing temperature could be observed, NTE of PT was not paid attention.

In 2003, Xing *et al*. studied the thermal expansion property of PT in the temperature range of 123~1223 K. The temperature dependence of unit cell volume of PT is shown in Fig. 2. PT exhibits an interesting thermal expansion property from low-temperature ferroelectric phase to high-temperature paraelectric one (Fig. 3), in which slightly PTE is observed from 123 to 298 K, NTE from 298 K to T_C (763 K), and then again PTE above T_C.[58] The CTE of PT in the paraelectric phase is similar to most perovskites of $A^{1+}B^{5+}O_3$, $A^{2+}B^{4+}O_3$, or $A^{3+}B^{3+}O_3$ which have a CTE order of ~3.0×10^{-5} K^{-1}.[85] However, the thermal expansion in the ferroelectric phase below its T_C is unusual. In the temperature range of 298~763 K, the *c* axis continually decreases while *a*(*b*) axes slightly increase with increasing temperature. Unit cell volume contracts and reaches a minimum at T_C (Fig. 2). The average volume CTE is negative (α_V = -1.99×10^{-5} K^{-1}, 298~763 K).[59] Such strong NTE in PT is unusual when compared with most oxides behaving PTE, such as α-Al_2O_3,[11] TiO_2 (anatase),[12] and $SrTiO_3$.[13] It also needs to be mentioned that even though thermal expansion of PT is positive below 298 K, the CTE is very small and close to zero. For example, the CTE is 7.1×10^{-6} K^{-1} at 123 K.[58] The crossover from positive to negative thermal expansion at room temperature is unconventional, since there is no phase transition. Such crossover results from the balance between two competitive factors of anharmonic phonon vibration and ferroelectric order which contribute to positive and negative thermal expansion, respectively. The mechanism of NTE will be reviewed in the section 2.4 in detail.

Table 1 Negative thermal expansion properties in ferroelectrics

Materials	Composition	α_V (10^{-5} K^{-1})[a]	Temp. range (K)	Method[b]	Ref.
$PbTiO_3$		-1.99	298~763	XRD	58,59
		3.72	763~1173		
$(Pb_{1-x}Cd_x)TiO_3$	$x = 0.03$	-2.16	298~743	XRD	60
	$x = 0.06$	-2.40	298~743		
$(Pb_{1-x}La_x)TiO_3$	$x = 0.05$	-1.02	298~653	XRD	59
	$x = 0.1$	-0.77	298~563		
	$x = 0.15$	-0.50	298~493		
	$x = 0.2$	-0.11	298~403		
$(Pb_{1-x}Sr_x)TiO_3$	$x = 0.15$	-1.11	298~673	XRD	13
	$x = 0.2$	-0.52	298~623		
$(Pb_{0.5}Ba_{0.5})TiO_3$		1.15	298~603	XRD	61
$(Pb_{1-x}Bi_x)TiO_3$	$x = 0.05$	-1.25	298~773	XRD	62
	$x = 0.1$	-0.56	298~823		
$(1-x)PT-x(La_{1/2}K_{1/2})TiO_3$	$x = 0.1$	-1.0	298~683	XRD	63
	$x = 0.2$	-0.71	298~573		
$(Pb_{0.7}Ca_{0.3})TiO_3$		-1.11	343~570	XRD	63
$Pb(Ti_{1-x}Fe_x)O_3$	$x = 0.05$	-1.49	298~548	XRD	65
	$x = 0.10$	-1.13	298~738		
$Pb(Ti_{1-x}Zr_x)O_3$	$x = 0.25$	-0.11 (α_l)	RT~728	Dilto.	86
	$x = 0.5$	0.23 (α_l)	RT~651		
$Pb(Ti_{1-x}Hf_x)O_3$	$x = 0.2$	-0.51	300~705	NPD	87,88
	$x = 0.8$	-1.0	410~515		
$0.8PT-0.2Pb(Fe_{1/2}Nb_{1/2})O_3$		-0.29 (α_l)	300~453	XRD	89
$0.1PT-0.9Pb(Mg_{1/3}Nb_{2/3})O_3$		0.1 (α_l)	173~373	Dilto.	45,90
$(1-x)PT-xBiFeO_3$	$x = 0.3$	-2.38	298~823	XRD	66
	$x = 0.6$	-3.92	298~948		
$0.7PT-0.3BiFeO_3$		-0.92 (160 nm)	303~813	SPD	66
		-0.46 (140 nm)	303~793		
		0.96 (110 nm)	303~773		
$(1-x)PT-xBiScO_3$	$x = 0.1$	-1.23	298~798	XRD	68
	$x = 0.2$	-0.624	298~773		
$0.5PT-0.5(Bi_{1-x}La_x)FeO_3$	$x = 0.0$	-4.06	300~873	XRD	73
	$x = 0.1$	-3.55	300~773		
	$x = 0.2$	-0.71	300~673		
$0.7PT-0.3Bi(Zn_{1/2}Ti_{1/2})O_3$		-0.6	298~773	XRD	69
$0.6PT-0.3\ Bi(Zn_{1/2}Ti_{1/2})O_3-0.1\ BiFeO_3$		-0.31	298~773	XRD	69
$(1-x)PT-xBi(Ni_{1/2}Ti_{1/2})O_3$	$x = 0.1$	-0.881	298~798	XRD	70
	$x = 0.2$	0.121	298~798		
	$x = 0.3$	0.846	298~723		
$(1-x)PT-xBi(Mg_{1/2}Ti_{1/2})O_3$	$x = 0.2$	-0.494	298~823	XRD	70
	$x = 0.4$	0.083	298~798		
	$x = 0.6$	1.2	298~773		
$(1-x-y)PT-xBi(Ni_{1/2}Ti_{1/2})O_3-yBiFeO_3$	$x = 0.20, y = 0.10$	0.029 (α_l)	298~773	Dilto.	72
	$x = 0.25, y = 0.15$	0.27 (α_l)	298~763		
	$x = 0.25, y = 0.20$	0.308 (α_l)	298~753		
	$x = 0.30, y = 0.25$	0.641 (α_l)	298~723		
$Pb(Mg_{1/3}Ta_{2/3})O_3$		0.088 (α_l)	<180	NPD	91
$Pb(Zn_{2/3}Nb_{1/3})O_3$		-0.3	340~384	NPD	74
		0.54	4.2~340		
$Pb(Mg_{1/3}Nb_{2/3})O_3$		0.036	70~240	NPD	75
$Pb(Fe_{1/2}Nb_{1/2})O_3$		0.6	300~393	XRD	89
$Pb(Fe_{2/3}W_{1/3})O_3$		0.45	<300	NPD	92
$(NH_4)_2SO_4$		-15	170~223	XRD	81
$Sn_2P_2S_6$		-18.8	306~332	Dilto.	82

[a] The default value of CTE is α_V, and the linear CTE is noted with α_l.

[b] XRD: x-ray diffraction; SPD: synchrotron powder diffraction; NPD: neutron powder diffraction; and Dilto.: dilatometry.

By taking advantage of the NTE of PT, we are able to explore many ferroelectrics to obtain controllable NTE, *i.e.*, adjustable CTE and NTE temperature range, by means of chemical modifications to form solid solutions with the end member of PT. For example, the NTE can be tailored in the *A*-site chemically substituted systems like $(Pb_{1-x}La_x)TiO_3$,[59] $(Pb_{1-x}Sr_x)TiO_3$,[13] $(Pb_{1-x}Bi_x)TiO_3$,[62] $(Pb_{1-x}Cd_x)TiO_3$,[60] and $(Pb_{1-x}(La_{1/2}K_{1/2})_x)TiO_3$,[63] the *B*-site chemically substituted systems like $Pb(Ti_{1-x}Fe_x)O_3$,[65] $Pb(Ti_{1-x}Zr_x)O_3$,[86] and $Pb(Ti_{1-x}(Fe_{0.5}Nb_{0.5})_x)O_3$,[89] and the *A*/*B* sites co-substituted systems like $(1-x)PT-xBiFeO_3$,[66, 93, 94] $(1-x)PT-xBiScO_3$,[68] $(1-x)PT-xBi(Zn_{1/2}Ti_{1/2})O_3$,[69] $(1-x)PT-xBi(Ni_{1/2}Ti_{1/2})O_3$,[70] and $(1-x)PT-$

xBi($Mg_{1/2}Ti_{1/2}$)O_3.[71] The control of NTE for PT-based compounds will be discussed in the section 2.3 in detail.

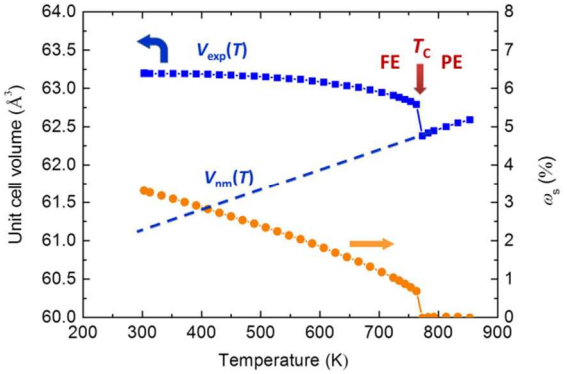

Fig. 2 Temperature dependence of unit cell volume ($V_{exp}(T)$) and nominal volume ($V_{nm}(T)$), and spontaneous volume ferroelectrostriction (SVFS, ω_s) for $PbTiO_3$. The data were determined from high-energy synchrotron x-ray diffraction. FE and PE mean ferroelectric and paraelectric, respectively.

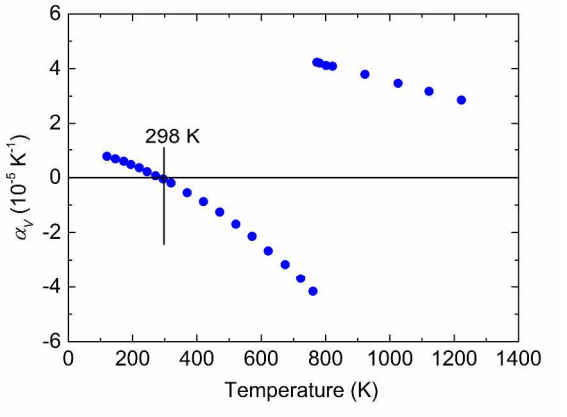

Fig. 3 Volume coefficient of thermal expansion, α_V, of $PbTiO_3$. (Reprinted with permission from ref. 58. Copyright 2003, The Nonferrous Metals Society of China.)

Apart from the NTE in PT-based ferroelectrics, NTE or anomalous thermal expansion has been observed in other ferroelectrics, antiferroelectrics, and relaxor ferroelectrics. For example, $Sn_2P_2S_6$ shows NTE below its T_C along three directions of crystal axes (α_V = -1.88×10^{-4} K^{-1}, 306~332 K).[82] In $BaTiO_3$ ferroelectric a slight contraction occurs at the transition temperatures of orthorhombic-to-tetragonal (289 K), and tetragonal-to-cubic (T_C, 393 K).[95,96] In Pb($Zn_{2/3}Nb_{1/3}$)O_3 a NTE occurs in a small temperature range (α_V = -3.0×10^{-6} K^{-1}, 340~384 K) just below the phase transition of rhombohedral ($R3m$) to cubic ($Pm\bar{3}m$).[74] NTE was observed in ferroelectric ammonium sulfate, $(NH_4)_2SO_4$, which undergoes a first-order ferroelectric phase transition from $Pnma$ to $Pna2_1$ at ~223 K.[81] With increasing temperature the a axis of $(NH_4)_2SO_4$ contracts, while the other two axes expand normally. In the ferroelectric phase, with increasing temperature unit cell volume first gradually expands, to the maximum value, and then begins to contract until reaching its T_C (223 K). Above T_C it is normally PTE. Note that NTE of $(NH_4)_2SO_4$ does not occur in the whole ferroelectric phase but only in a narrow temperature range near T_C. There is a crossover of PTE-to-NTE at ~160 K. The CTE of $(NH_4)_2SO_4$ is α_V = 2.7×10^{-5} K^{-1}, -1.5×10^{-4} K^{-1}, and 1.08×10^{-4} K^{-1}, for the temperature ranges of 4.2-160 K, 170~223 K, and above 223 K, respectively.[81] $(NH_4)_2SO_4$ ferroelectric shows a similar thermal expansion trend to PT. The progress in the nature of NTE for PT could be helpful for the understanding that of $(NH_4)_2SO_4$. The NTE of $(NH_4)_2SO_4$ should be correlated to its ferroelectricity, which can be supported by the experimental fact that the NTE disappears by substituting non-ferroelectric activity alkali ion of Rb.[97] In the family of tungsten bronzes, NTE occurs along the polar direction, such as $(Ba_{1-x}Sr_x)Nb_2O_6$:$(Na_{1-y}K_y)NbO_3$ solid solutions (c axis),[76] $Rb_5Nb_3OF_{18}$ (c axis),[77] (Ba,Sr)Nb_2O_6 (c axis),[78,79] and $Pb_2KNb_5O_{15}$ (b axis).[80]

NTE has been observed in phase transitions between antiferroelectric (AFE), ferroelectric (FE), and paraelectric (PE) in antiferroelectrics. For example, Pb(Zr,Sn,Ti)O_3 antiferroelectrics have various distorted perovskite-type structures including antiferroelectric orthorhombic AFE_O, antiferroelectric tetragonal AFE_T, low-temperature ferroelectric rhombohedral FE_L, high-temperature rhombohedral FE_H, and paraelectric phase PE. The thermal expansion is complex during phase transitions between these structures. Strong PTE for the phase transitions of $AFE_O \rightarrow AFE_T$, $FE_L \rightarrow FE_H$, AFE→FE, and AFE→PE, while NTE for phase transitions of FE→AFE, and FE→PE (Fig. 4).[98,99] For example, a strong linear contraction appears at the phase transition of $FE_L \rightarrow AFE_T$ (Fig. 4b).[100] In (Pb,Ba)ZrO_3 and Pb($Ti_{1-x}Zr_x$)O_3, PTE and NTE were also observed at phase transitions of AFE-to-FE and FE-to-PE, respectively.[86,100,101]

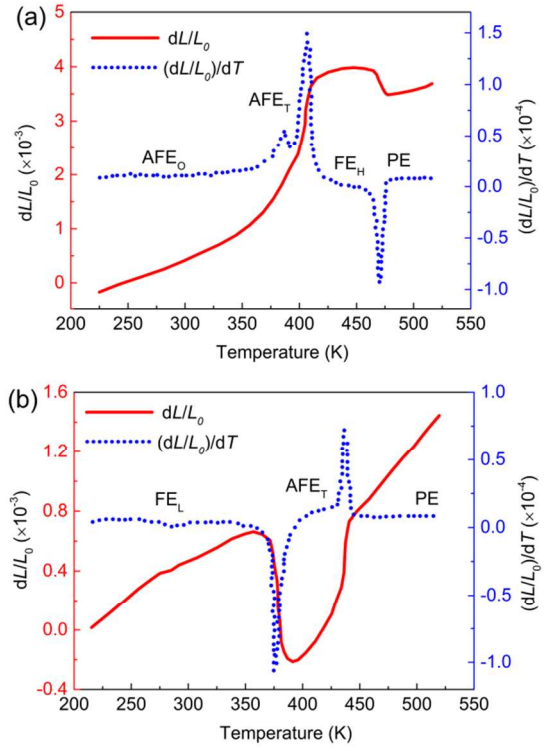

Fig. 4 (a) Thermal expansion of $Pb_{1-x/2}Nb_z[(Zr_{1-x}Sn_x)_{1-y}Ti_y]_{1-z}O_3$ (100*x*/100*y*/100*z*:10/3/2) with the sequence of phase transition $AFE_O \rightarrow AFE_T \rightarrow FE_H \rightarrow PE$. (b) Thermal expansion of $Pb_{1-x/2}Nb_z[(Zr_{1-x}Sn_x)_{1-y}Ti_y]_{1-z}O_3$ (100*x*/100*y*/100*z*:30/7/2) with the sequence of phase transition $FE_L \rightarrow AFE_T \rightarrow PE$. Data were collected by dilatometry. (Reprinted with permission from ref. 98. Copyright 2002, Science China Press.)

For Pb-based perovskite-type relaxors of $Pb(B'_{1-x}B''_x)O_3$, ZTE is often observed and is thought to a common thermal property for lead-based relaxor ferroelectrics. Below the so-called Burns temperature (T_B), the temperature at which polar nano-regions (PNRs) appear, its thermal expansion begins to deviate from the linear thermal expansion of high temperatures, such as $Pb(Mg_{1/3}Nb_{2/3})O_3$ (Fig. 5). Above the T_B, the relaxor ferroelectrics exhibit normal PTE similar to most perovskites. ZTE occurs normally below T_m which is the temperature at which dielectric constant reaches the maximum. [102 - 104] For example, the CTE of $Pb(Mg_{1/3}Nb_{2/3})O_3$ is as low as α_V = 3.6×10^{-7} K^{-1} (70~240 K), and 3.5×10^{-5} K^{-1} above T_B (~620 K).[75] A similar ZTE is in $Pb(Zn_{2/3}Nb_{1/3})O_3$ (α_V = 5.4×10^{-6} K^{-1}, 4.2~340 K),[74] and $Pb(Fe_{1/2}Nb_{1/2})O_3$ (α_V = 6.0×10^{-6} K^{-1}, 300~393 K).[89] Furthermore, low or zero thermal expansion can be also achieved in the ferroelectric relaxors based solid solutions, such as (1-*x*)$Pb(Mg_{1/3}Nb_{2/3})O_3$-*x*PT ceramics (α_l is 1.6, 2.0, 2.4, 3.2 $\times10^{-6}$ K^{-1} (263~373 K) for *x* = 0, 0.2, 0.3, and 0.35, respectively),[105] and $0.8Pb(Fe_{1/2}Nb_{1/2})O_3$-0.2PT ($\alpha_l$ = -2.9×10^{-6} K^{-1}, 300~453 K).[89] In lead-free relaxor ferroelectrics,[103,106,107] thermal expansion deviates from linear behaviour in $Ba(Zr,Ti)O_3$ as temperature decreasing below T_B~440 K.[103,106]

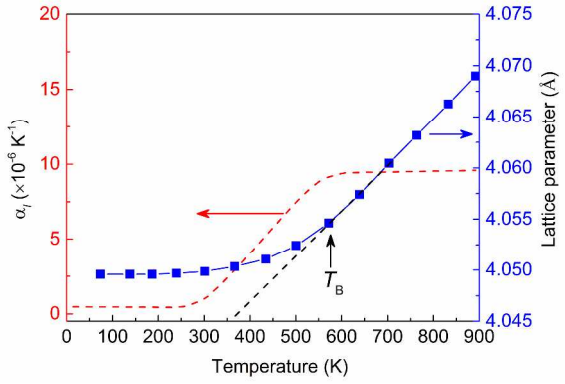

Fig. 5 Temperature dependence of lattice parameter and linear CTE α_l of $Pb(Mg_{1/3}Nb_{2/3})O_3$. (Reprinted with permission from ref. 75. Copyright 1991, Elsevier.)

In ferroelectric materials, domain motion can introduce NTE phenomena in poled ferroelectrics, which is ascribed to the process of thermal depoling. Especially for those compositions near morphotropic phase boundaries (MPB) having large piezoelectric property, poled ceramics can produce a large NTE along electric poling direction. For example, for the unpoled state piezoelectric ceramics of $Pb(Ti_{0.45}Zr_{0.55})O_3$ exhibits near ZTE (α_l = 1.4×10^{-6} K^{-1}, RT~650 K), while after electric poling strong NTE occurs (α_l = -1.1×10^{-5} K^{-1}, RT~650 K). The NTE phenomenon is a result of polar axis shrinkage and thermal depoling induced domain switching.[108] Note that this NTE phenomenon is irreversible after thermal depoling, and can only be recovered by electric re-poling. The NTE property of poled ferroelectric materials can be utilized to study the thermal depoling property for piezoelectric materials.

2.2 Crystal structure of $PbTiO_3$-based NTE ferroelectrics

As shown in Fig. 6, PT has a typical tetragonal perovskite structure in the ferroelectric phase (space group *P*4*mm*), which consists of corner-linked TiO_6 octahedra and Pb atoms fill the PbO_{12} polyhedra. The RT tetragonality (*c*/*a*), and T_C are 1.064 and 763 K, respectively. Its ferroelectricity and piezoelectricity originate from P_S, which consists of *c*-axis aligned dipoles at both *A*-site of PbO_{12} and *B*-site of TiO_6 polyhedra. At RT the P_S displacements of δz_{Ti} and δz_{Pb} are 0.299 Å and 0.468 Å, respectively.[109] PT transforms from tetragonal ferroelectric phase to cubic paraelectric one at T_C.

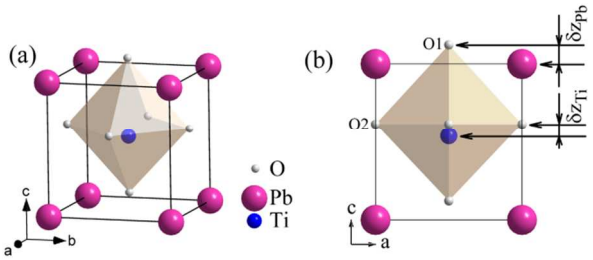

Fig. 6 (a) Perovskite structure of $PbTiO_3$, and (b) P_S displacements of δz_{Ti} in TiO_6 octahedron and δz_{Pb} in PbO_{12} polyhedron which are aligned the *c* axis.

The hybridization between the Ti 3*d* and O 2*p* states is important for the origin of ferroelectricity in perovskite-based titanates such as PT or $BaTiO_3$ by first-principles calculation and Rietveld/maximum entropy method (MEM).[110, 111] Furthermore, the hybridization between Pb 6*s* with O 2*p* plays a critical role for the strong ferroelectricity to maintain large *c*/*a* and high T_C for PT.[110] Most chemical substitutions in PT reduce both *c*/*a* and T_C, such as $Pb(Ti_{1-x}Zr_x)O_3$, and $(Pb_{1-x}La_x)TiO_{3+\delta}$. They normally distribute in the region of III as shown in Fig. **7**. However, a recently found new type of Pb/Bi based binary system, PT-Bi*Me*O_3 where *Me* consists of cations with an average valence of 3+, exhibits unusual crystal structure, NTE, ferroelectric and piezoelectric properties. For example, (1-*x*)PT-*x*$BiScO_3$ exhibits an excellent high temperature piezoelectric performance with large d_{33} (460 μC/N) and high T_C (723 K) at the MPB composition (*x* = 0.36), which is superior to the conventional piezoelectric of $Pb(Ti_{1-x}Zr_x)O_3$.[112] Interestingly, there are several PT-Bi*Me*O_3 (*Me* = Fe, $Zn_{1/2}Ti_{1/2}$, and $Zn_{3/4}W_{1/4}$) systems showing much enhanced T_C and *c*/*a*.[113-116] They lie in the region I of Fig. 7. These systems with high T_C provide potential candidates for high temperature applications of ferroelectric and piezoelectric materials.[112,117,118] There are also several compositions lying in the region II, showing a normally reduced *c*/*a* but an unusually non-monotonic trend of T_C, such as (1-*x*)PT-*x*$BiScO_3$, (1-*x*)PT-*x*$Bi(Mg_{1/2}Ti_{1/2})O_3$, and (1-*x*)PT-*x*$Bi(Zn_{1/2}Zr_{1/2})O_3$.[119,120] In these systems, T_C shows a parabolic-like curve as function of Bi*Me*O_3 content, where T_C firstly increases, reaches the maximum value, and then declines

as function of Bi*Me*O_3 content. It should be mentioned that such non-monotonic trend of T_C does not arise from a phase transition, since all these compositions stay in the tetragonal phase.

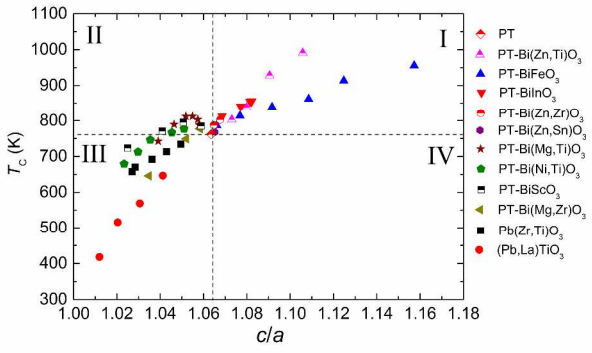

Fig. 7 The relationship between T_C and c/a in $PbTiO_3$-based tetragonal compounds.

The unusual crystal structure and ferroelectricity in PT-Bi*Me*O_3 have been studied by first-principles calculations and crystal structure investigations.[66,119-126] The unusual structural properties, such as enhanced c/a and T_C, and non-monotonic trend of T_C originate from the critical behaviour of P_S, which is stemmed from different hybridization ability. In tetragonal PT-based perovskites, Ti-O2 bonds along $a(b)$ axes are rather strong than Ti-O1 bonds along the polar c axis, and there is a significant energy cost for compressing Ti-O2 bonds.[127] Generally, c axis can be more easily elongated or shortened than $a(b)$ axes by chemical substitution. The strongly enhanced c/a in PT-Bi*Me*O_3 originates from the strong hybridization between cations with oxygens, which allows the formation of short and covalent chemical bonding, and enables favourable coupling between A-site and B-site displacements of P_S.[122] For example, in (1-x)PT-xBi($Zn_{1/2}Ti_{1/2}$)O_3 the increase in the c axis is driven by the large P_S displacements of A-site Bi and B-site Zn and their coupling. The P_S displacements of ions are very large in the composition of 0.75PT-0.25Bi($Zn_{1/2}Ti_{1/2}$)O_3 obtained by density functional theory calculations (δz_{Pb} = 0.49 Å, δz_{Bi} = 0.82 Å, δz_{Zn} = 0.38 Å, and δz_{Ti} = 0.32 Å). The unusual large P_S displacement of Zn is due to the strong hybridization of Zn (4s,4p) and O 2p orbitals.[122] The investigations of first-principles calculations on the dependence of c/a on local structure in a variety of ferroelectric perovskites demonstrate that c/a is strongly coupled to the P_S displacement of B-site cations and weakly to the A-site ones.[123] It can be understood that the P_S displacement at B-site cations strongly affect the B-O bond orders, while the P_S displacement at A-site cations leads to a small changes in the A-O bond length and its bond order.

The abnormal crystal structures of enhanced c/a in Pb/Bi based perovskites have been studied by structural refinements. Enhanced P_S and interesting chemical bonding were found in those systems such as (1-x)PT-xBi($Zn_{1/2}Ti_{1/2}$)O_3,[122,125] (1-x)PT-xBiFeO_3,[66,126] (1-x)PT-xBi($Zn_{3/4}W_{1/4}$)O_3,[128] (1-x)PT-xBiInO_3,[129] $PbVO_3$,[130] and pure Bi-based perovskites of Bi*Me*O_3 (*Me* = Co and $Zn_{1/2}Ti_{1/2}$).[131,132] In principle, there are many possible Pb/Bi based perovskites. Here we only focus on the structure information for those tetragonal phases showing usually enhanced c/a. Furthermore, those compositions of PT-Bi*Me*O_3 reviewed here show interesting NTE properties, which will be reviewed in the following paragraphs. As for those PT-Bi*Me*O_3 (*Me* = Fe,[113] In,[114] $Zn_{1/2}Ti_{1/2}$,[115] and $Zn_{3/4}W_{1/4}$[116]), there is a common feature that T_C and c/a are both enhanced by the Bi*Me*O_3 chemical substitution. For example, compared with PT (c/a = 1.064 and T_C = 763 K), 0.4PT-0.6BiFeO_3 has a large c/a = 1.165 and T_C = 865 K,[66,113] and 0.7PT-0.3Bi($Zn_{1/2}Ti_{1/2}$)O_3 has a similar larger c/a = 1.077 and T_C = 973 K.[115,125] All the four compositions were found to have enhanced P_S displacements at both A-site and B-site. For example, δz_A and δz_B are, respectively, 0.726, and 0.538 Å, in 0.4PT-0.6BiFeO_3,[66] 0.498 and 0.384 Å in 0.7PT-0.3Bi($Zn_{1/2}Ti_{1/2}$)O_3,[125] and 0.566 and 0.362 Å in 0.8PT-0.2BiInO_3,[129] 0.492 and 0.325 Å in 0.0PT-0.1Bi($Zn_{3/4}W_{1/4}$)O_3.[128] The enhancement in the P_S displacements is coupled in A-site and B-site ions. Furthermore, due to the difference in ion size and ferroelectric activity, the B-site cation splitting was observed by neutron powder diffraction refinements. For example, Fe has a larger P_S displacement than that of Ti in 0.7PT-0.3BiFeO_3,[66] and Zn has a larger P_S displacement than that of Ti in 0.7PT-0.3Bi($Zn_{1/2}Ti_{1/2}$)O_3.[125]

The abnormally enhanced c/a and T_C can be well understood from the studies of electron density distribution on detailed chemical bonding by Rietveld/MEM technique for a typical example of 0.4PT-0.6BiFeO_3.[126] As shown in Fig. 8, in cubic phase (1000 K), no charge density is distributed between Pb/Bi-O bonds, suggesting an ionic bond nature. Ti/Fe-O bonds are isotropic and weak covalency (minimum electron density, MED = 0.85 $Å^{-3}$). However, in ferroelectric phase (303.4 K) interesting covalent bonds of Pb/Bi-O2 and Ti/Fe-O take place. Pb/Bi-O2 bond becomes covalent, while Ti/Fe-O covalent bonds become extremely anisotropic. The MED of Pb/Bi-O2 (0.61 $Å^{-3}$) and Ti/Fe-O1 (2.3 $Å^{-3}$) is much larger than that of PT

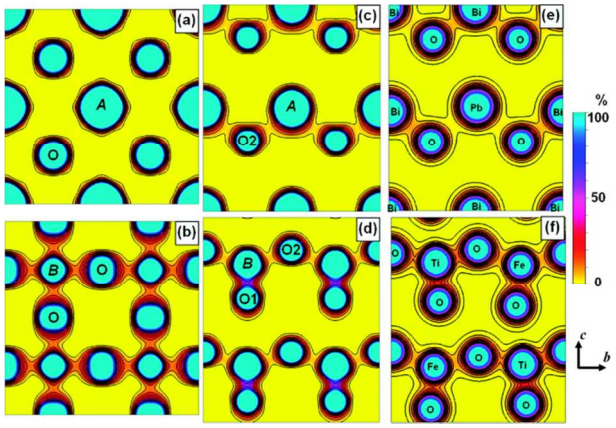

Fig. 8 Electron density distributions on the bc planes of 0.4PT-0.6BiFeO_3 with large c/a determined by Rietveld/MEM analysis from synchrotron powder diffraction (a-d), and by first-principles calculations (e-f). Electron density distributions on (a) Pb/Bi-O plane and (b) Ti/Fe-O plane of cubic phase at 1000 K, (c) Pb/Bi-O2 plane and (d) Ti/Fe-O plane at 303.4 K. Electron density distributions in (e) Pb/Bi-O plane and (f) Ti/Fe-O plane of $Pb_4Bi_8Ti_4Fe_8O_{36}$ through first-

principles calculations. (Reprinted with permission from ref. 126. Copyright 2011, American Chemical Society.)

(Pb-O2: 0.45 Å^{-3} and Ti-O1: 1.25 Å^{-3}),[111] showing experimental evidence that 0.4PT-0.6$BiFeO_3$ has a nature of even stronger covalent bonding. Further first-principles calculations indicate that the hybridization between Bi(6*s*,6*p*) and O(2*p*) orbitals is stronger than that between Pb(6*s*,6*p*) and O(2*p*), which is responsible for the enhanced ferroelectricity, *c*/*a*, and the increased in T_C in PT-$BiFeO_3$.[126]Apart from the structural refinement investigations to determine the P_S in those compositions of PT-Bi*Me*O_3, such large P_S can be successfully measured in high quality thin films of PT-$BiFeO_3$ (P_r = 50 μC·cm^{-2}),[133] and PT-Bi($Zn_{1/2}Zr_{1/2}$)O_3 (P_r = 55 μC·cm^{-2}).[134] However, it is well known that the direct measurement of polarization is very difficult in ceramics by hysteresis loop due to extremely large *c*/*a*. Alternatively, the P_S property can be easily and rapidly estimated according to the A_1(1TO) soft mode by measurement of Raman lattice dynamics,[128] since the A_1(1TO) soft mode represents the opposing vibration between *A*-site atoms with BO_6 octahedra along the P_S direction. As shown in Fig. 9, it is interesting to find that the A_1(1TO) soft mode increases linearly with the P_S displacement for those compounds of PT-Bi*Me*O_3 (*Me* = Fe, $Zn_{1/2}Ti_{1/2}$, and $Zn_{3/4}W_{1/4}$). The P_S could be basically judged from the variation of A_1(1TO) in the PT-based compounds not only with normally reduced *c*/*a* but also with unusually enhanced *c*/*a*.[128]

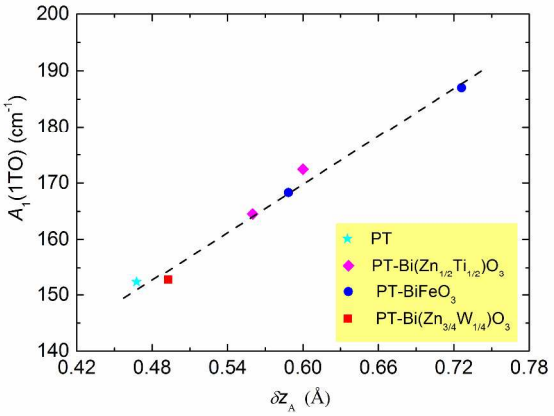

Fig. 9 Soft mode A_1(1TO) vs. P_S displacement of δz_A in tetragonal PT-Bi*Me*O_3 compounds with enhanced *c*/*a*. (Reprinted with permission from ref. 128. Copyright 2007, American Institute of Physics.)

With assistance of solid state reaction under high pressure and high temperature conditions, several tetragonal polar Pb or Bi based metastable perovskites with extremely large *c*/*a* have been achieved such as $PbVO_3$ (*c*/*a* = 1.23),[130] $BiCoO_3$ (*c*/*a* = 1.27),[131] and Bi($Zn_{1/2}Ti_{1/2}$)O_3 (*c*/*a* = 1.21).[132] All these tetragonal compounds exhibit extremely large P_S (100 μC·cm^{-2} for $PbVO_3$,[130] 130 μC·cm^{-2} for $BiCoO_3$,[131] and 158 μC·cm^{-2} for Bi($Zn_{1/2}Ti_{1/2}$)O_3).[132] Due to their metastable nature, the compounds decompose at temperatures far below T_C. More information of structural and physical properties of Bi*Me*O_3 can be found in a review literature and references therein.[135]

In ferroelectric perovskite, there is an important concept of ferroelectric activity to describe the ability to form displacement of P_S for ions (Table 2). The ferroelectric activity can help understand properties in crystal structure, NTE, and ferroelectric by chemical substitutions. The ferroelectric activity of ions can be quantitatively described by the magnitude of P_S displacement. Higher value means a stronger ferroelectric activity, smaller one means weaker ferroelectric activity. For example, *B*-site ions of Zn (0.25 Å) and Ti (0.25 Å), and *A*-site ions of Pb (0.45 Å) and Bi (0.80 Å) are strongly ferroelectrically active, while *B*-site ions of Mg (0.08 Å) and Sc (0.11 Å), and *A*-site ions of Ba (0.05 Å), K (0.05 Å) and La (0.05 Å) are weakly ferroelectrically active.[120,124] It means that ferroelectrics consisting of strongly ferroelectrically active ions generally have large P_S, high T_C, and large *c*/*a*, such as PT and 0.7PT-0.3Bi($Zn_{1/2}Ti_{1/2}$)O_3, while those consisting of weakly ferroelectrically active ions generally have relatively small P_S, low T_C, and small *c*/*a*, such as $BaTiO_3$ and PT-Bi($Mg_{1/2}Zr_{1/2}$)O_3.[120] Despite similar ionic size (0.72 Å for Mg and 0.74 Å for Zn) and the same valence, Zn-containing perovskites such as PT-Bi($Zn_{1/2}Ti_{1/2}$)O_3 and Pb($Zn_{1/3}Nb_{2/3}$)O_3 exhibits higher T_m than Mg-containing counterparts such as PT-Bi($Mg_{1/2}Ti_{1/2}$)O_3 and Pb($Mg_{1/3}Nb_{2/3}$)O_3. Table 2 lists ferroelectric activity of ions at *A*-site and *B*-site in ferroelectric perovskites.[120,124]

Table 2 The P_S displacements (Å) for *A*-site and *B*-site ions in perovskite ferroelectrics[120,124]

A-site ions									
K	Na	Ag	Ba	Pb	Sr	Ca	Cd	Bi	La
0.05	0.05	0.35	0.05	0.45	0.05	0.05	0.35	0.80	0.05
B-site ions									
Cd	Mn[a]	Zn	Mg	Ni	Yb	In	Sc	Fe	Mn[b]
0.11	0.08	0.25	0.08	0.08	0.08	0.08	0.11	0.17	0.13
Zr	Hf	Ti	Nb	Ta	W				
0.13	0.13	0.25	0.17	0.17	0.10				

[a] Mn has a larger radius of 0.83 Å.

[b] Mn has a smaller radius of 0.645 Å.

The unusually enhanced and nonmonotonic T_C trends in PT-Bi*Me*O_3 perovskites has been studied by first-principles density functional theory calculations and experimentally structural investigations.[119,120] The relationships between atomic properties and overall structure were studied in four compositions of PT-Bi($B^{2+}_{1/2}$,$B^{4+}_{1/2}$)O_3 (B^{2+} = Mg, Zn; B^{4+} = Zr, Ti) solid solutions in which B^{2+} and B^{4+} consist of strongly or weakly ferroelectrically active ions. PT-Bi($Zn_{1/2}Ti_{1/2}$)O_3 and PT-Bi($Mg_{1/2}Ti_{1/2}$)O_3 show enhanced and reduced T_C, respectively, and PT-Bi($Mg_{1/2}Ti_{1/2}$)O_3 and PT-Bi($Zn_{1/2}Zr_{1/2}$)O_3 show non-monotonic T_C trend. There is a good correlation

between calculated P_S and T_C.[120] T_C is well quantitatively correlated to P_S^2 following the Laudau theory relationship:[136]

$$T_C = \alpha P_S^2 \quad (6)$$

The nonmonotonic T_C trend in (1-x)PT-xBiScO$_3$ has also been experimentally studied based on Rietveld refinement by means of neutron powder diffraction.[119] The same nonmonotonic trend was observed in the P_S displacements of A-site Pb/Bi and B-site Ti/Sc. The nature of high T_C for the composition near the MPB of (1-x)PT-xBiScO$_3$ is mainly contributed from A-site Pb/Bi polarization, *e.g.*, 76 % for 0.65PT-0.35BS. Here, we summarize the data of T_C and δz_A^2 for some tetragonal PT-based compositions (Fig. 10). There is a strong correlation between T_C and P_S, which is an experiment evidence for the fact that T_C is determined by P_S. Such correlation offers us useful information to design the temperature range for the control of NTE of PT-based compounds, since NTE only occurs in the ferroelectric phase below T_C. The control of NTE, *i.e.*, magnitude of CTE and temperature range, will be discussed in the next section 2.3 in detail.

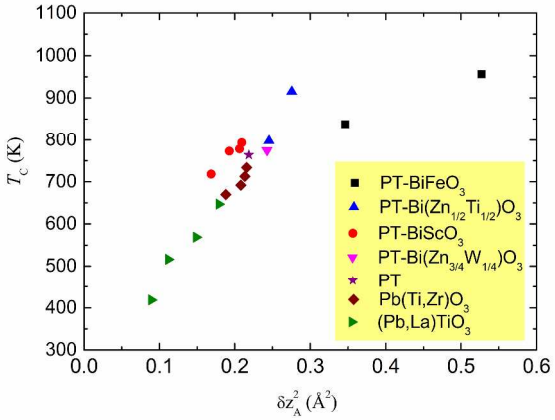

Fig. 10 The relationship between T_C and δz_A^2 in tetragonal PT-based compounds.

2.3 Controllable NTE

Controllable thermal expansion is one of key issues for NTE materials. Controllable thermal expansion means not only CTE but also temperature range can be tailored. The NTE of PT-based ferroelectrics can be well controlled by various methods, such as chemical modification, size effect, and physical route of applying pressure. Among these methods, chemical modification is the generally used method. It needs to be noted that a precondition to achieve controllable thermal expansion is that a NTE compound should have a good ability to accommodate hetero-atoms to form solid solution, which allows us to possibly adjust structure and thermal expansion by various chemical substitutions. For examples, for the prototype NTE compound of cubic ZrW_2O_8, it is unacceptable that the control of NTE is in a small CTE range (α_l = -7.3~-8.7×10^{-6} K^{-1}) due to the fact of low solubility limit for chemical substitution.[137] However, CTE can be well controlled over the range α_l = -5.9~+7.9×10^{-6} K^{-1} (12-500 K) in the (Zr$_{1-x}$Sn$_x$)Mo$_2$O$_8$ solid solutions, which is benefited to the higher A-site solubility range than that in other AM_2O_8 systems.[32] A single-phase ceramic material of $Al_{2x}(Hf,Mg)_{1-x}(WO_4)_3$ was found to have a CTE range of α_V = -2.3~4.5×10^{-6} K^{-1}.[138] The orthophosphate group of NZP has been widely studied with various substitutions at different sites to exhibit a CTE range of -1.7~1.9×10^{-6} K^{-1}.[16] Perovskites allow many kinds of atoms to substitute at A-site and B-site, due to the advantage of flexible structure. The NTE property of PT can theoretically be effectively controlled. The NTE of PT has been comprehensively studied by the A-site, B-site, or A/B combined chemical substitutions. The NTE properties of those PT-based compounds are listed in Table 1.

According to the thermal expansion properties, those PT-based compounds can be classified into four categories: Enhanced NTE, weakened NTE, ZTE, and PTE. Among these four categories, it is interesting but rare to observe enhanced NTE and ZTE. So far there are only two compounds which have been found to exhibit the enhanced NTE, compared with PT (α_V = -1.99×10^{-5} K^{-1}, 298~763 K). They are (Pb$_{1-x}$Cd$_x$)TiO$_3$ (*e.g.*, x = 0.06, α_V = -2.4×10^{-5} K^{-1}, 298~743 K, Fig. 11),[60] and (1-x)PT-xBiFeO$_3$ (*e.g.*, x = 0.6, α_V = -3.92×10^{-5} K^{-1}, 298~923 K, Fig. 12).[66] A linear strong NTE was observed in the 0.7PT-0.3BiFeO$_3$ (α_V = -2.38×10^{-5} K^{-1}, 298~823 K).[66]

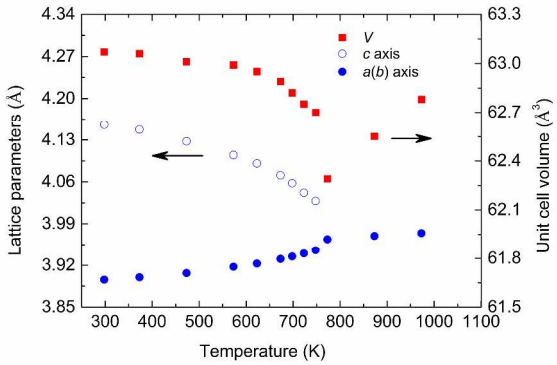

Fig. 11 Temperature dependence of lattice parameters and unit cell volume of (Pb$_{0.94}$Cd$_{0.06}$)TiO$_3$. (Reprinted with permission from ref. 60. Copyright 2005, American Institute of Physics.)

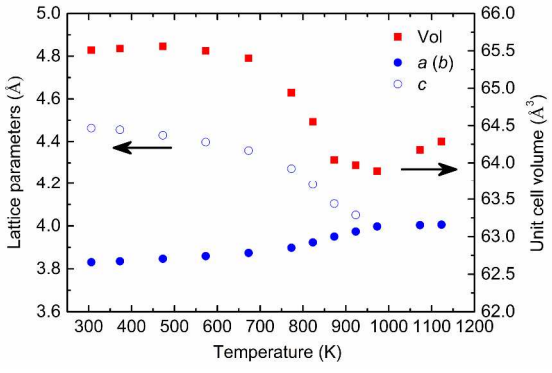

Fig. 12 Temperature dependence of lattice parameters and unit cell volume of 0.4PT-0.6BiFeO$_3$. (Reprinted with permission from ref. 66. Copyright 2006, American Institute of Physics.)

Most chemical substitutions for the *A*-site Pb or the *B*-site Ti reduce the NTE property in PT-based compounds. T_C is reduced, which means that the temperature range of NTE is simultaneously reduced. *A*-site substitutions have been investigated in $(Pb_{1-x}Ba_x)TiO_3$,[61] $(Pb_{1-x}Sr_x)TiO_3$,[13] $(Pb_{1-x}Ca_x)TiO_3$,[64] $(Pb_{1-x}La_x)TiO_3$,[59] $(Pb_{1-x}Bi_x)TiO_3$,[62] and (1-*x*)PT-*x*$(La_{1/2}K_{1/2})TiO_3$.[63] $(Pb_{0.95}La_{0.05})TiO_3$ exhibits weakened NTE (α_V = -1.02×10^{-5} K^{-1}, 298~653 K).[59] Similar weakened NTE is in $(Pb_{0.85}Sr_{0.15})TiO_3$ (-1.11×10^{-5} K^{-1}, 298~673 K)[13] and $(Pb_{0.9}(La_{1/2}K_{1/2})_{0.1})TiO_3$ (-1.0×10^{-5} K^{-1}, RT~683 K).[63] As for the *B*-site substitutions, $Pb(Ti_{0.9}Fe_{0.1})O_3$ shows weakened NTE (-1.13×10^{-5} K^{-1}, 298~738 K).[65] In the tetragonal $Pb(Ti_{1-x}Zr_x)O_3$ solid solutions, thermal expansion is weakened by the substitution of Zr. The composition of $Pb(Ti_{0.75}Zr_{0.25})O_3$ shows a reduced NTE (α_l = -1.1×10^{-6} K^{-1}, 298~728 K).[86] For (1-*x*)PT-*x*$Pb(Fe_{0.5}Nb_{0.5})O_3$, the thermal expansion can be tailored by the substitution of $Pb(Fe_{0.5}Nb_{0.5})O_3$ ferroelectric relaxor. Intrinsic linear CTE changes from α_l = -8.2×10^{-6} K^{-1} (300~763 K) for *x* = 0.0 to 2.0×10^{-6} K^{-1} (300~393 K) for *x* = 1.0.[89]

Since most chemical substitutions reduce the NTE of PT-based ferroelectrics, over substitution certainly will transform NTE to PTE. Here the value of CTE for the PTE in the tetragonal PT-based ferroelectrics is positive but still lower than that of paraelectric phase (*i.e.*, α_V = 3.72×10^{-5} K^{-1} for cubic phase PT).[59] For example, $(Pb_{0.5}Ba_{0.5})TiO_3$ exhibits a relative small PTE (α_V = 1.15×10^{-5} K^{-1}, 298~603 K).[61] Similar PTE behaviour is in 0.4PT-0.6Bi$(Mg_{1/2}Ti_{1/2})O_3$ (α_V = 1.2×10^{-5} K^{-1}, 298~773 K),[71] $Pb(Ti_{0.5}Zr_{0.5})O_3$ (α_l = 2.3×10^{-6} K^{-1}, RT~651 K),[86] 0.7PT-0.3Bi$(Ni_{1/2}Ti_{1/2})O_3$ (α_V = 8.46×10^{-6} K^{-1}, 298~723 K),[70] and 0.45PT-0.3Bi$(Ni_{1/2}Ti_{1/2})O_3$-0.25$BiFeO_3$ (α_l = 6.41×10^{-6} K^{-1}, 298~723 K).[72]

One of interesting topics is to achieve CTE as close as possible to zero, which is termed as ZTE. ZTE is not only interesting for fundamental studies but also important for industrial applications. The practical application of ZTE has a long history, which can be traced back to the discovery of Invar alloys by Guillaume in 1897.[8,19] However, ZTE materials are rare. Our previous studies on thermal expansion of PT exhibit that PT has a flexible ability to achieve ZTE over a wide temperature range by selecting suitable chemical modifications. The crossover from NTE to PTE offers an opportunity to achieve ZTE by carefully adjusting chemical composition. For example, ZTE is in $(Pb_{0.8}La_{0.2})TiO_3$ (α_V = -1.1×10^{-6} K^{-1}, 298~403 K),[59] 0.6PT-0.3Bi$(Zn_{1/2}Ti_{1/2})O_3$-0.1$BiFeO_3$ (α_V = -3.1×10^{-6} K^{-1}, 298~773 K, Fig. 13),[69] 0.6PT-0.4Bi$(Mg_{1/2}Ti_{1/2})O_3$ (α_V = 8.3×10^{-7} K^{-1}, 298~798 K),[71] and 0.8PT-0.2Bi$(Ni_{1/2}Ti_{1/2})O_3$ (α_V = 1.21×10^{-6} K^{-1}, 298~798 K, Fig. 14).[70] One good feature of the PT-based ZTE materials is that ZTE can reach to high temperature, *e.g.*, 773 K in 0.6PT-0.3Bi$(Zn_{1/2}Ti_{1/2})O_3$-0.1$BiFeO_3$.

It is known that most ZTE materials can be obtained below room temperature due to low contribution from lattice vibration. High temperature ZTE is much rarer and more difficult to get. Another good feature of the PT-based ZTE material is that they show good mechanical properties. For example, ZTE oxide ceramics of 0.8PT-0.2Bi$(Ni_{1/2}Ti_{1/2})O_3$ have the Vickers' hardness (H_V = 2.74 GPa) and the fracture toughness (K_{IC} = 11.5 MPa·m$^{1/2}$).[70] The mechanical properties are comparable to α-Al_2O_3 structural ceramics (H_V = 15 GPa, and K_{IC} = 3.5 MPa·m$^{1/2}$).[11] The advantages of high temperature ZTE, good thermal stability, and high mechanical properties allow good potential applications for the PT-based ZTE materials.

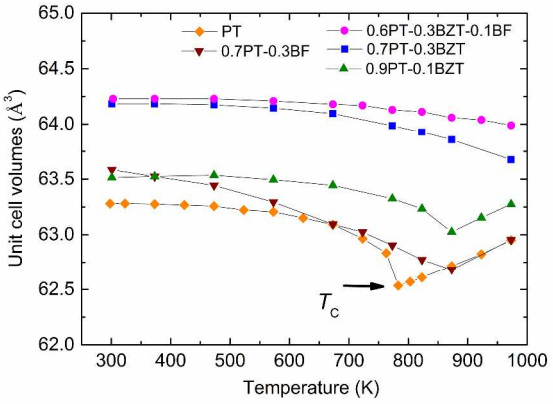

Fig. 13 Temperature dependence of unit cell volume of PT-Bi$(Zn_{1/2}Ti_{1/2})O_3$-$BiFeO_3$. (Reprinted with permission from ref. 69. Copyright 2008, American Chemical Society.)

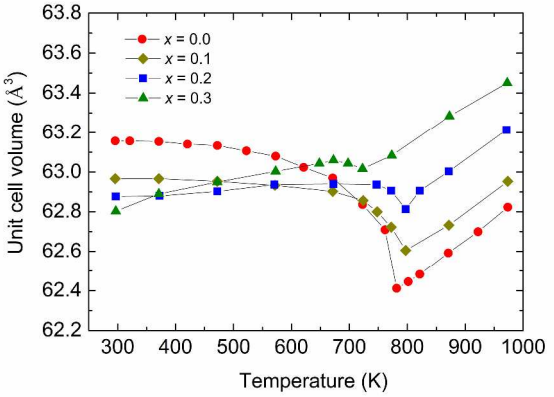

Fig. 14 Temperature dependence of unit cell volume of (1-*x*)PT-*x*Bi$(Ni_{1/2}Ti_{1/2})O_3$. (Reprinted with permission from ref. 70. Copyright 2010, American Chemical Society.)

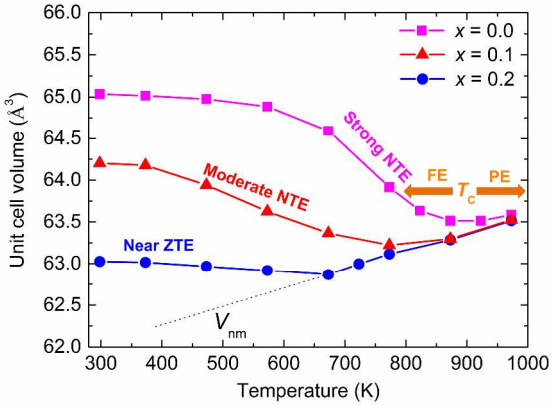

Fig. 15 Temperature dependence of unit cell volume of 0.5PT-0.5($Bi_{1-x}La_x$)FeO_3. The dash line is nominal unit cell volume (V_{nm}). (Reprinted with permission from ref. 73. Copyright 2013, Nature Publishing Group.)

For the control of thermal expansion of PT-based ferroelectrics by chemical substitutions, there is an interesting system of 0.5PT-0.5($Bi_{1-x}La_x$)FeO_3 in which an effective control of thermal expansion over a giant range can be simply achieved by adjusting La content (Fig. 15).[73] For x = 0.0, large NTE occurs in 573~873 K (α_V = -7.0×10^{-5} K^{-1}). However, NTE is much weakened by the La substitution. For x = 0.1, the NTE becomes linear below T_C with a CTE of α_V = -3.55×10^{-5} K^{-1} (298~773 K). With further La substitution (x = 0.2), a very low thermal expansion is achieved in a wide temperature range (RT~673 K, α_V = -7.1×10^{-6} K^{-1}). The adjustable CTE includes a giant range from -7.0 to -0.71×10^{-5} K^{-1}, which contains the CTE range of most known NTE materials.[2,3,73]

Apart from the control of NTE from chemical substitution, the thermal expansion of PT-based ferroelectrics can be effectively controlled by the effect of particle size.[67] The particle size effect can transform the strong NTE to PTE in 0.7PT-0.3$BiFeO_3$ ferroelectrics (Fig. 16). Such transformation is unusual, since most studies show that there could be a common phenomenon that the grain size effect can transform PTE to NTE.[67] For bulk state of 0.7PT-0.3$BiFeO_3$, it has a strong NTE (-2.39×10^{-5} K^{-1}, RT~823 K). However, as particle size decreases from the bulk state to 160 nm, the NTE is considerably weakened (-9.2×10^{-6} K^{-1}, 303~813 K). With further decreases in particle size, a striking change takes place in the thermal expansion of 0.7PT-0.3$BiFeO_3$. ZTE was found below its T_C for the particle size of 140 nm (-4.6×10^{-6} K^{-1}, 303~793 K), and PTE was found for the smaller particle size of 110 nm (9.6×10^{-6} K^{-1}, 303~773 K). The transformation of strong negative to positive thermal expansion is a new phenomenon. The particle size controllable CTE varies in a very large content from -2.38 to 0.96×10^{-5} K^{-1}, which covers almost all NTE oxides.[2,3,73]

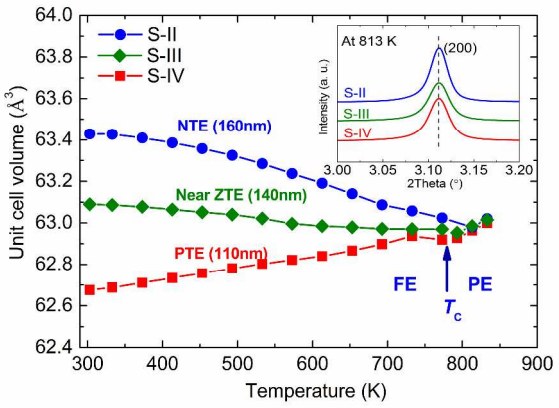

Fig. 16 Temperature dependence of unit cell volume of 0.7PT-0.3$BiFeO_3$ with various particle size. The inset pattern is the singlet profile (200) of cubic phase at 813 K. FE and PE mean ferroelectric and paraelectric, respectively. (Reprinted with permission from ref. 67. Copyright 2013, American Physical Society.)

The unusual transformation from strong negative to positive thermal expansion is highly correlated with ferroelectricity weakening. With decreasing particle size, the P_S displacements at room temperature are gradually reduced and cannot maintain at high level anymore, which means that ferroelectricity is weakened. The polar directions of A and B sites P_S are aligned parallel along the c axis in the 0.7PT-0.3$BiFeO_3$ perovskite. The large value of the c axis is originated from the high P_S. As the P_S reduces, the c axis shrinks. As a result, the unit cell volume at RT is decreased. Above T_C the unit cell volume is nearly identical for various grain particles (Fig. 16). Here the perovskite of 0.7PT-0.3$BiFeO_3$ is in a cubic phase with a close-packed structure, and the unit cell volume is actually dominated by the radius of atoms, due to the loss of ferroelectricity.[68] Therefore, the unusual transformation from strong negative to positive thermal expansion in 0.7PT-0.3$BiFeO_3$ ferroelectric is resulted from weakened ferroelectricity.[67] This work further supports the mechanism of PT-based ferroelectrics, which will be reviewed in the next section 2.4 in details.

Apart from the control of NTE of PT compound by the chemical modification and particle size effect, the thermal expansion can be adjusted by physical route of applying pressure.[139, 140] At room temperature, PT transforms from tetragonal ferroelectric phase to cubic paraelectric phase by applying pressure at 11.2 GPa. Such tetragonal-to-cubic transition induced by pressure is reduced upon heating.[139] At ambient pressure, PT exhibits strong NTE over a wide temperature range (α_V = -1.99×10^{-5} K^{-1}, 298~763 K).[59] However, by applying pressure thermal expansion of PT changes apparently (Fig. 17). One point is that NTE disappears while PTE occurs at the critical pressure of 0.9 GPa. For example, PT exhibits PTE with an α_V = 1.4×10^{-5} K^{-1} (300~730 K) at 1.2 GPa. At higher pressure, tetragonal PT exhibits a stronger PTE with an α_V = 3.2×10^{-5} K^{-1} which is normal to the PTE of paraelectric phase.[139] The other point is that at pressures below the critical one (0.9 GPa) the turnover from positive to negative thermal expansion is raised to higher temperatures (Fig. 17). The turnover temperature is RT at ambient pressure while increases to 447 K at 0.3 GPa.[58,140]

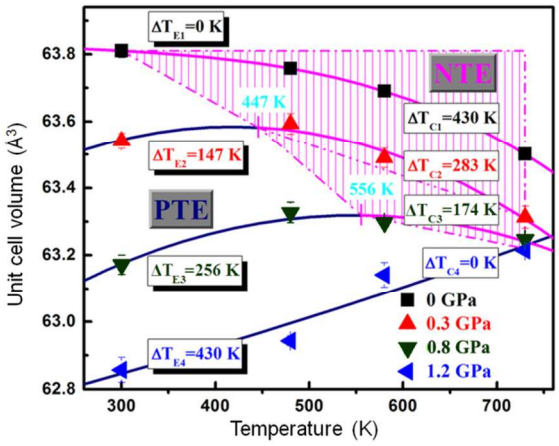

Fig. 17 Unit cell volume of $PbTiO_3$ as function of temperature and pressure. The shadow area indicates the region of NTE, while the reset one donates the region of PTE. (Reprinted with permission from ref. 140. Copyright 2014, Nature Publishing Group.)

2.4 NTE mechanism

The NTE of PT was ever discussed to be correlated with tetragonal-to-cubic phase transition at 763 K, based on the crystallographic character of TiO_6 octahedra distortion with increasing temperature.[2,3] At room temperature, the structure of PT contains highly distorted TiO_6, where Ti-O bond lengths are 1.766, 4×1.979, and 2.390 Å; while at high temperature (823 K), it is in isotropic structure where six Ti-O bonds are 1.983 Å.[141] TiO_6 octahedra changes from being distorted to being more regular at T_C, and the average bond length of Ti-O contracts from 2.012 to 1.983 Å. The NTE of PT was thought to be correlated with the release in the distortion. However, there are many perovskites with distorted octahedron which do not exhibit NTE. Even for tetragonal PT-based solid solutions, there are some compositions showing PTE not NTE. The transformation of distorted-to-undistorted TiO_6 octahedron with increasing temperature could be the result not the reason for NTE. The mechanism of NTE in PT-based ferroelectrics should be due to those underlying physical factors which dominate the change in chemical bonds of Ti-O and Pb-O.

The NTE mechanism in PT-based ferroelectrics have been studied by high temperature neutron powder diffraction and Raman lattice dynamics of the A_1(1TO) soft mode.[69,142] Two representative compositions were selected to comparatively study the role of P_S in the nature of NTE. They are 0.7PT-0.3Bi($Zn_{1/2}Ti_{1/2}$)O_3 and 0.7PT-0.3BiFeO_3, which have a similar enhanced c/a (c/a = 1.091 for 0.7PT-0.3BiFeO_3, and c/a = 1.092 for 0.7PT-0.3Bi($Zn_{1/2}Ti_{1/2}$)O_3), but oppositely NTE properties (Fig. 18). It is enhanced NTE for 0.7PT-0.3BiFeO_3 (α_V = -2.5×10^{-5} K^{-1}, 298~773 K), but much reduced NTE for 0.7PT-0.3Bi($Zn_{1/2}Ti_{1/2}$)O_3 (α_V = -6.0×10^{-6} K^{-1}, 298~773 K). Since for both compositions the a(b) axes display a similar temperature-dependent behaviour while only c axis is different. The c/a ratio exhibits the same trend with the unit cell volume as function of temperature. Therefore, the c/a ratio was adopted to show how unit cell volume changes in 0.7PT-0.3Bi($Zn_{1/2}Ti_{1/2}$)O_3 and 0.7PT-0.3BiFeO_3 (Fig. 19). It is interesting to observe that with increasing temperature P_S decreases relatively slightly in the 0.7PT-0.3Bi($Zn_{1/2}Ti_{1/2}$)O_3 which has the weak NTE, however, decreases rapidly in the 0.7PT-0.3BiFeO_3 which has the strong NTE. The A-site P_S displacement is similar at room temperature ($\delta z_{Pb/Bi}$ = 0.534 Å for 0.7PT-0.3BiFeO_3, and 0.525 Å for 0.7PT-0.3Bi($Zn_{1/2}Ti_{1/2}$)O_3), while it gradually separates with increasing temperature (at 773 K $\delta z_{Pb/Bi}$ = 0.259 Å for 0.7PT-0.3BiFeO_3, and 0.362 Å for 0.7PT-0.3Bi($Zn_{1/2}Ti_{1/2}$)O_3).[142] As shown in Fig. 19b, there is a good linear correlation between c/a-1 and $\delta z^2_{Pb/Bi}$, which gives a direct experimental evidence for the role of P_S in NTE. The temperature dependent behaviour of P_S directly determines the change of unit cell volume. With increasing temperature, if P_S decreases rapidly, the unit cell volume decreases faster resulting in a strong NTE such as in the 0.7PT-0.3BiFeO_3; however, if P_S can be well maintained, the unit cell volume decreases slowly resulting in a low NTE such as in the 0.7PT-0.3Bi($Zn_{1/2}Ti_{1/2}$)O_3. Another example is the tetragonal $PbTi_{0.8}Hf_{0.2}O_3$ which shows NTE (α_V = -5.1×10^{-6} K^{-1}, 300~705 K). It is interesting to note that the unit cell volume of $PbTi_{0.8}Hf_{0.2}O_3$ shows a similar decreasing slope as function of temperature to its P_S, which also indicates that the probable coupling role in NTE and P_S.[87] The trend in Fig. 19b can guide the design and control of NTE for PT-based ferroelectrics. For enhanced NTE, P_S should change with temperature in a large scale, while for a low thermal expansion P_S should change in a small scale.

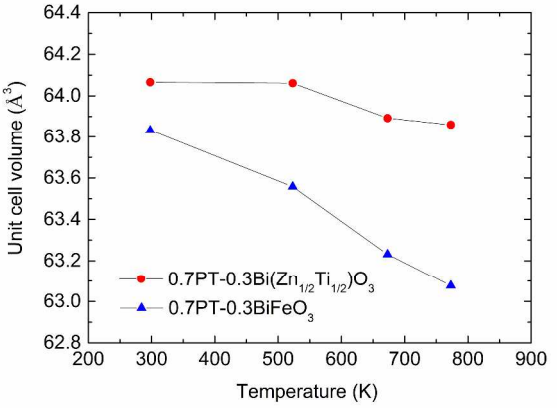

Fig. 18 Temperature dependence of unit cell volume of 0.7PT-0.3Bi($Zn_{1/2}Ti_{1/2}$)O_3 and 0.7PT-0.3BiFeO_3. (Reprinted with permission from ref. 142. Copyright 2011, American Chemical Society.)

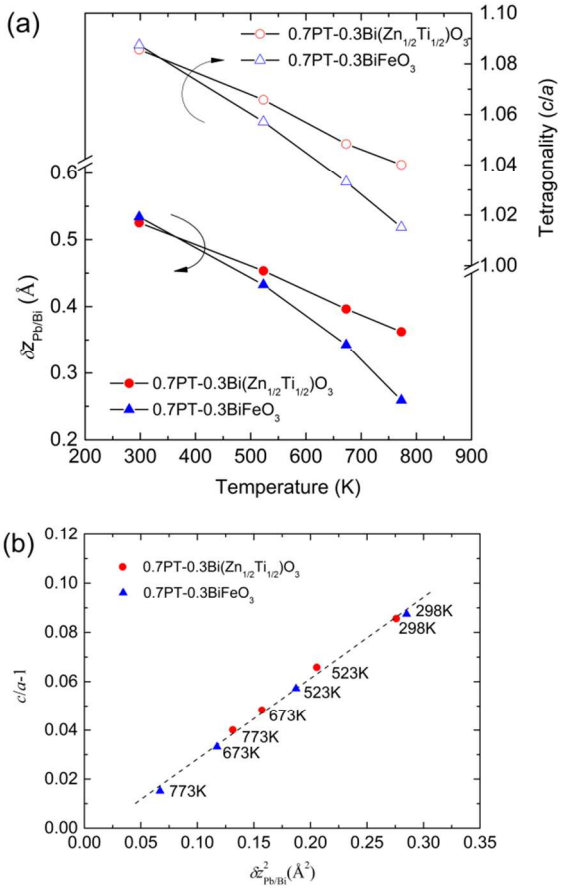

Fig. 19 (a) Temperature dependence of c/a and $\delta z_{Pb/Bi}$, and (b) the relationship between (c/a-1) and $\delta z^2_{Pb/Bi}$ of 0.7PT-0.3Bi($Zn_{1/2}Ti_{1/2}$)O_3 and 0.7PT-0.3BiFeO_3 in 298~773 K. (Reprinted with permission from ref. 142. Copyright 2011, American Chemical Society.)

In other ferroelectrics, there is a similar role of P_S in NTE. For example, NTE was observed in ferroelectric phase of high temperature rhombohedral phase F_{RH} ($R3m$) (α_V = -1.0×10^{-5} K^{-1}, 410~515 K) and PTE in the low temperature rhombohedral phase F_{RL} ($R3c$) in $PbHf_{0.8}Ti_{0.2}O_3$ (α_V = 1.7×10^{-5} K^{-1}, 300~400 K).[88] The polar c axis length shrinks in both phases but with a different slope as function of temperature. With increasing temperature, the polar c axis decreases slightly in the F_{RL} phase, but shrinks strongly in the F_{RH} phase. Simultaneously, P_S reduces slightly in the F_{RL} phase and can maintain at a high level (*e.g.*, 39 μC cm^{-2} at 10 K to 30 μC cm^{-2} at 410 K); however, rapidly vanishes in the F_{RH} phase (*e.g.*, 30 μC cm^{-2} at 410 K to zero at T_C of 525 K).[88] The temperature dependent behaviour of P_S determines the variation of polar c axis and thus determines the transformation of PTE-to-NTE at the F_{RL}-to-F_{RH} phase transition.

In tungsten bronze ferroelectrics, we can also find the coupling between ferroelectricity and NTE. NTE is often observed along the polar direction. For example, NTE occurs along the polar c axis in tetragonal ferroelectric $Rb_5Nb_3OF_{18}$ below its T_C (600 K),[77] and (Ba,Sr)Nb_2O_6.[79] In orthorhombic $Pb_2KNb_5O_{15}$ ($Cm2m$, T_C = 733 K), NTE occurs in the b axis where P_S aligns (α_l = -1.6×10^{-6} K^{-1}), while the other axes show PTE. Pb is hybridized with surrounding oxygens, and P_S is strongly correlated to the hybridization of Pb-O.[80] Tetragonal ($Ba_{1-x}Sr_x$)Nb_2O_6:($Na_{1-y}K_y$)NbO_3 shows NTE in the polar c axis. The composition of 2($Ba_{0.25}Sr_{0.75}$)Nb_2O_6:($Na_{0.5}K_{0.5}$)NbO_3 which has large polarization simultaneously exhibits a relatively stronger NTE along the polar c axis; while the composition of 2($Ba_{0.4}Sr_{0.6}$)Nb_2O_6:($Na_{0.6}K_{0.4}$)NbO_3 which has a small polarization simultaneously exhibits a smaller NTE of the polar c axis. For a further evidence, adding more content of Na/K ions reduces both polarization and NTE of the polar c axis, since Na/K are non-ferroelectricity and pure ionic property.[76]

It is known that ferroelectricity is related to the balance of short-range repulsion favouring cubic phase and long range Coulomb force favouring ferroelectric order. The equilibrium lattice parameters are dictated by such balance.[110] With decreasing temperature from paraelectric to ferroelectric phase, two factors contribute to unit cell volume of ferroelectric phase: anharmonic lattice phonon vibration and ferroelectric order. With decreasing temperature, the contribution from the factor of anharmonic lattice phonon vibration decreases. Thus the nominal unit cell volume (V_{nm}) should normally contract, which can be described by the Debye-Grüneisen equation 3. As shown in Fig. 2, the V_{nm} below T_C which is only determined by anharmonic lattice phonon vibration should be the extrapolation from high-temperature cubic paraelectric phase to low-temperature ferroelectric one. However, below T_C the experimental unit cell volume (V_{exp}) of PT actually shows an abnormal increase with decreasing temperature. In ferroelectric state the deviation of unit cell volume from V_{nm} to V_{exp} is given rise from the ferroelectrovolume effect (FVE). The value of FVE can be quantitatively described by the spontaneous volume ferroelectrostriction (SVFS) using the equation:

$$\omega_S = (V_{\mathrm{exp}} - V_{\mathrm{nm}})/V_{nm} \times 100\% \qquad (7)$$

The SVFS is a new physical quantity in ferroelectrics, which was proposed recently.[73] As shown in Fig. 2, the value of SVFS for PT gradually decreases with increasing temperature, and reaches to zero at T_C (763 K).

In order to study SVFS, a ternary system of PT-based compositions were designed, that is 0.5PT-0.5($Bi_{1-x}La_x$)FeO_3 (x = 0.0, 0.1, and 0.2). In the composition of 0.5PT-0.5($Bi_{1-x}La_x$)FeO_3, Bi and La have essentially the same ionic radius (1.34 Å for Bi^{3+}, and 1.36 Å for La^{3+}) however with much different ferroelectric activity. Bi^{3+} has the strong ferroelectric activity (0.8 Å), while La^{3+} has weak one (0.05 Å). As shown in Fig. 15, a slightly chemical substitution of La for Bi, the NTE of 0.5PT-0.5($Bi_{1-x}La_x$)FeO_3 is much changed from the strong NTE for x = 0.0 (-4.06×10^{-5} K^{-1}, RT~873 K) to the nearly ZTE for x = 0.2 (-7.1×10^{-6} K^{-1}, RT~673 K). The SVFS value at RT is much reduced from 4.8% for the x = 0.0 to 1.6% for the x = 0.2. Due to the similar radius of Bi^{3+} and La^{3+}, the unit cell volume in paraelectric phase is similar for three compositions in 0.5PT-0.5($Bi_{1-x}La_x$)FeO_3. However, the unit cell volume in ferroelectric phase is much different. It is highly correlated with the change in ferroelectricity.

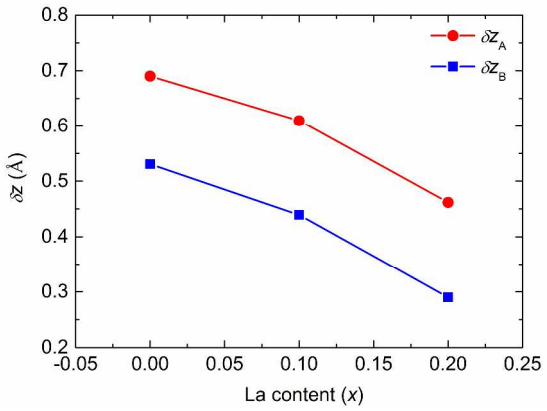

Fig. 20 P_S displacements at *A*-site (δz_A) and *B*-site (δz_B) of 0.5PT-0.5($Bi_{1-x}La_x$)FeO_3 as function of La content (*x*). (Reprinted with permission from ref. 73. Copyright 2013, Nature Publishing Group.)

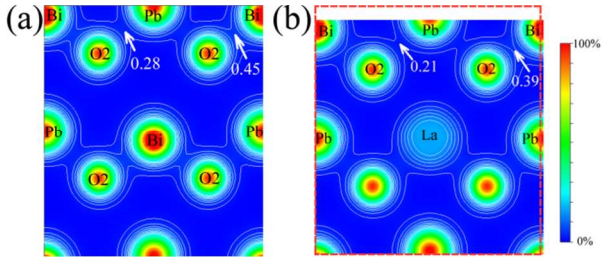

Fig. 21 Valence electron-density distributions on the *bc* plane at *x* = 1/2 of supercell. (a) (Pb_4Bi_4)(Ti_4Fe_4)O_{24}, and (b) ($Pb_4Bi_3La_1$)(Ti_4Fe_4)O_{24}, which, respectively, corresponds to *x* = 0.0, and *x* = 0.25 in 0.5$PbTiO_3$-0.5($Bi_{1-x}La_x$)FeO_3 through first-principle calculations. The dash line frame indicates the original lattice without La substitution. The 0% and 100% in colour scale corresponds to 0.2 and 8 $Å^{-3}$, respectively, and contours are from 0.2 to 4 $Å^{-3}$ by step of 0.2 $Å^{-3}$. (Reprinted with permission from ref. 73. Copyright 2013, Nature Publishing Group.)

In the solid solutions of 0.5PT-0.5($Bi_{1-x}La_x$)FeO_3, the P_S displacements are much reduced by the La substitution (Fig. 20), indicating weakened ferroelectricity. For example, the $\delta z_{Pb/Bi}$ is reduced from 0.6903 Å for the *x* = 0.0 to 0.4619 Å for the *x* = 0.2. Such weaken ferroelectrcity can be further supported by the valence electron-density distribution calculated based on density function theory. The hybridization between Pb-O2 and Bi-O2 bonds is weakened by the substitution of La for Bi (Fig. 21).

Using the equation 7, we can adopt SVFS to quantitatively describe the correlation between NTE and ferroelectricity. Similar to the Landau theory,[136] we can observe a good relationship for three compositions of 0.5PT-0.5($Bi_{1-x}La_x$)FeO_3:

$$\omega_s \sim \alpha \delta z_A^2 \qquad (8)$$

where α is the coupling coefficient between ω_s and P_S. As shown in Fig. 22, there is good linear correlation between ω_s and P_S. Other available NTE PT-based compositions are also plotted in Fig. 22. The correlation is not only good agreement for 0.5PT-0.5($Bi_{1-x}La_x$)FeO_3, but also for other PT-based compositions. It means that the P_S determines the ω_s. On one hand, strong ferroelectric property induces a large value of ω_s and thus produces a strong NTE such as for the composition of *x* = 0.0 in 0.5PT-0.5($Bi_{1-x}La_x$)FeO_3. On the other hand, weakened ferroelectric property induces a small value of ω_s and produces a low thermal expansion such as for the composition of *x* = 0.2 in 0.5PT-0.5($Bi_{1-x}La_x$)FeO_3. Additionally, the sign of the coupling coefficient α of the equation 8 indicates whether thermal expansion is negative or positive. For example of Pb(Zr,Sn,Ti)O_3 antiferroelectrics, NTE is in the phase transitions of FE→AFE and FE→PE, which means positive value of α, while strong PTE for the phase transitions of AFE_O→AFE_T, FE_L→FE_H, AFE→FE, and AFE→PE, which means negative value of α (Fig. 4).[98,99] The role of SVFS in ferroelectrics, antiferroelectric, and relaxors should be studied in detail.

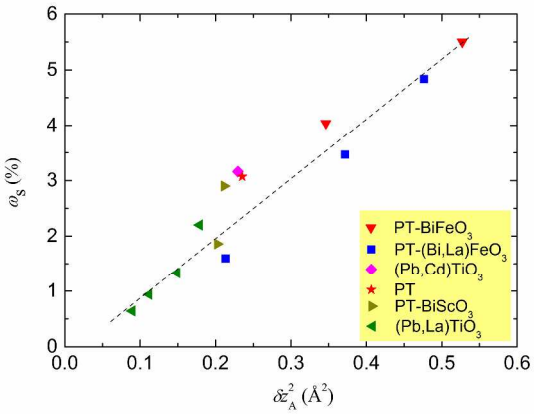

Fig. 22 The correlation between the spontaneous volume ferroelectrostriction (ω_s) and square of P_S displacement (δz_A^2) for PT-based tetragonal NTE ferroelectrics.

The physical quantity of SVFS can be helpful for understanding the ZTE nature below T_B in relaxor ferroelectrics.[74,75,89,91,92] As temperature cooling down from T_B, the effect of SVFS is produced due to the frozen PNRs. Thermal expansion induced from lattice phonon vibration is counteracted by the effect of SVFS, and thus near ZTE appears. Good examples can be seen in thermal expansion in complex perovskites of $A(Mg_{1/3}Ta_{2/3})O_3$ (*A* = Pb and Ba) which gives a good evidence for such suggestion (Fig. 23).[91] In compositions of $A(Mg_{1/3}Ta_{2/3})O_3$ (*A* = Pb and Ba), Pb is ion with strong ferroelectric activity while Ba weak one. Both compositions of $A(Mg_{1/3}Ta_{2/3})O_3$ (*A* = Pb and Ba) remain in cubic phase in 1.5~730 K. However, the thermal expansion is apparently different (Fig. 23a). The unit cell parameter of $Pb(Mg_{1/3}Ta_{2/3})O_3$ begin to deviate from linear thermal expansion at *T* = 420 K, and nearly does not change below *T* = 180 K on cooling. ZTE occurs below 180 K with CTE of α_l = 8.8×10^{-7} K^{-1}. However, the similar composition of $Ba(Mg_{1/3}Ta_{2/3})O_3$ does not show any anomalous thermal expansion (Fig. 23a). The structure refinement was performed on $Pb(Mg_{1/3}Ta_{2/3})O_3$ and $Ba(Mg_{1/3}Ta_{2/3})O_3$ based on cubic symmetry ($Pm\bar{3}m$). As for $Ba(Mg_{1/3}Ta_{2/3})O_3$, there was no anomalous in refined parameters including temperature factors of Ba, Mg/Ta, and O. However, thermal displacement of Pb along <110> direction was observed in $Pb(Mg_{1/3}Ta_{2/3})O_3$. The deviation from linear thermal expansion in $Pb(Mg_{1/3}Ta_{2/3})O_3$

occurs at the similar temperature where diffuse scattering appears (Fig. 23b). The occurrence of diffuse scattering in $Pb(Mg_{1/3}Ta_{2/3})O_3$ was thought to result from the increased and correlated Pb displacements. In other words, the thermal expansion of $Pb(Mg_{1/3}Ta_{2/3})O_3$ becomes anomalous simultaneously when the displacements of Pb become correlated. The effect of SVFS is produced due to the frozen PNRs, and thus results in ZTE in $Pb(Mg_{1/3}Ta_{2/3})O_3$. However, no PNRs occur in $Ba(Mg_{1/3}Ta_{2/3})O_3$, and thermal expansion obeys the theoretical Debye-Grüneisen one (equation 3).

Additionally, there is a physical concept of electrostriction which should be distinguished from SVFS. The exact concept of electrostriction is originated from the electromechanical coupling property. Electrostriction is the basic electromechanical coupling property for all dielectrics including polar and non-polar compounds. However, SVFS only occurs in those ferroelectrics which have anomalous thermal expansion property. For example, $SrTiO_3$ exhibits a relatively large electrostriction coefficient ($Q_h = 4.7\times10^{-2}$ m^4 C^{-2}) compared with that of PT (2.2×10^{-2} m^4 C^{-2}); However, $SrTiO_3$ shows normal thermal expansion instead of NTE.[13,45] The physical quantity for anomalous thermal expansion in ferroelectrics should be exactly defined using SVFS which presents the FVE.

Fig. 24 illuminates the NTE mechanism schematic for ferroelectrics. In the high-temperature paraelectric phase, it is in positive thermal expansion which can be described by the Debye-Grüneisen equation 3. However, with decreasing temperature from T_C, the ferroelectric order is established, which will have negative contribution to thermal expansion. Here, the overall thermal expansion in ferroelectric phase is a result of balance between two competitive factors: anharmonic lattice phonon vibration and ferroelectric order. If the contribution from ferroelectric order is smaller than that from lattice phonon vibration, the overall thermal expansion is weakened but still positive. For example, some PT-based ferroelectrics such as PT-$Bi(Ni_{1/2}Ti_{1/2})O_3$, PT-$Bi(Mg_{1/2}Ti_{1/2})O_3$, and $(Pb,Ba)TiO_3$, show smaller PTE than that of paraelectric phase.[61,70,71] Thermal expansion of $BaTiO_3$ in ferroelectric phase ($\alpha_l = 6\times10^{-6}$ K^{-1}) is much lower than that of paraelectric phase ($\alpha_l = 1.2\times10^{-5}$ K^{-1}). [143] If the contribution from ferroelectric order overwhelms that from lattice phonon vibration, NTE is produced. If the contribution from ferroelectricity is equal to that of lattice phonon vibration, ZTE appears.

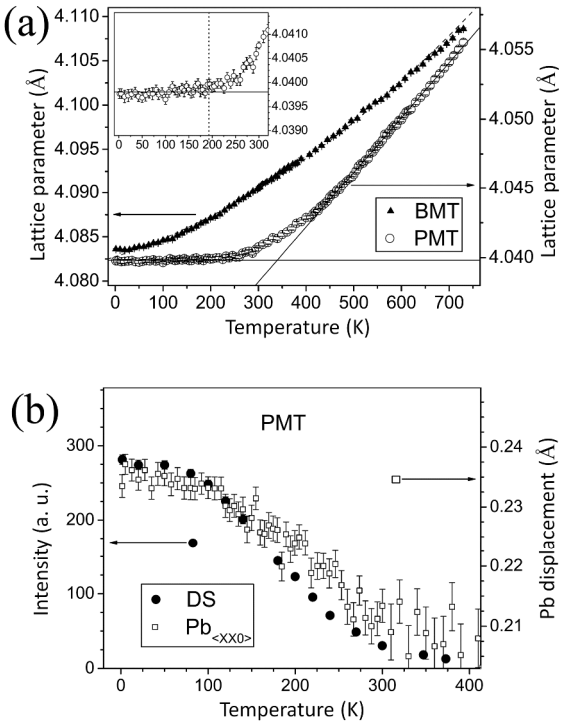

Fig. 23 (a) Temperature dependence of lattice parameter a of $Pb(Mg_{1/3}Ta_{2/3})O_3$ and $Ba(Mg_{1/3}Ta_{2/3})O_3$, and (b) temperature dependence of the integrated intensity of diffuse scattering and the Pb displacement along <110> direction in $Pb(Mg_{1/3}Ta_{2/3})O_3$. (Reprinted with permission from ref. 91. Copyright 2004, Springer.)

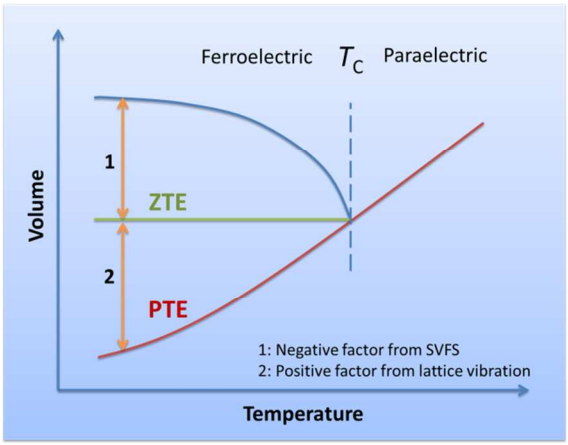

Fig. 24 The NTE mechanism schematic for ferroelectrics. The thermal expansion of ferroelectric is a result from the balance between two competitive factors of ferroelectric order for negative contribution and lattice phonon vibration for positive one.

The correlation between ferroelectricity and NTE provides us a guideline to control thermal expansion of ferroelectrics. The thermal expansion of ferroelectrics can be controlled through tailoring ferroelectricity. Those methods which can affect ferroelectricity would be utilized to control thermal expansion of ferroelectrics, such as chemical modification, size effect, and pressure.[59-73,139,140] As for the commonly used method of chemical modification, we can modulate the ferroelectric activity of cations to adjust the value of ω_s and thus control the

thermal expansion of PT-based ferroelectrics. Strong NTE can be achieved by the substitutions of those cations with strong ferroelectric activity, such as Bi (0.8 Å), Ti (0.25 Å), Fe (0.17 Å), Zn (0.25 Å), and Cd (0.35 Å), while low thermal expansion by the substitution of cations with weak ferroelectric activity, such as La (0.05 Å), Mg (0.08 Å), Ni (0.08 Å), and Zr (0.13 Å).The examples can be referred to Table 1 and the section 2.3. In NTE ferroelectric of $(NH_4)_2SO_4$, its NTE loses by substituting non-ferroelectric activity alkali ion of Rb.[97] The control of thermal expansion of ferroelectrics via methods of particle size and pressure effects actually takes effect through the correlation between ferroelectricity and NTE, which have been discussed in the previous paragraph.[67,140]

Theoretical calculations have been carried out to understand the NTE mechanism of PT.[144-147] From the view of first-principles calculation, the thermal expansion of PT has studied, and can be further understood from the role of electron interaction and atoms' vibration.[145,146] The temperature dependence of unit cell volume of PT was estimated by calculating the Helmholtz free energy F(T) as follows: [145]

$$F(T) = E_s + \int g(\omega)\left(\frac{h\omega}{2} + k_B T \ln\{1 - e^{-h\omega/(k_B T)}\}\right) d\omega \quad (9)$$

where E_s is the static energy, which is the total energy of the crystal at its equilibrium state; the next term is the lattice vibrational free energy for which ω is the phonon frequency and $g(\omega)$ is the phonon density of states.

The calculated temperature dependence of unit cell volume for PT displayed PTE below 120 K, and NTE from 120 to 520 K. There was a crossover from positive to negative thermal expansion at 120 K.[145] The thermal expansion of PT in ferroelectric phase can be understood by the decomposition of the total Helmholtz free energy into two aspects contributions: Vibrational free energy and static energy (Fig. 25). Vibrational free energy is contributed from thermal vibration, while the static energy comes from electronic interaction without considering temperature. Without consideration of temperature influence, the electronic contribution keeps PT with higher *c*/*a*, which favours ferroelectricity (Fig. 25e). However, the vibrational free energy shows a temperature dependent behaviour (Fig. 25a-d). At lower temperature, *i.e.*, 20 K, vibrational free energy brings lattice expansion in both *a*(*b*) and *c* axes. However, at higher temperature, *i.e.*, 520 K, it brings longer *a*(*b*) axes and shorter *c* axis (Fig. 25d). The equilibrium lattice parameters are determined by the balance of thermal vibration favouring cubic phase and electronic interaction favouring ferroelectric phase.[145]

The role of vibrational free energy for individual atom of Pb, Ti, and O to thermal expansion is shown in Fig. 26. At low temperature, *i.e.*, 20 K, the energy descent direction of three atoms of Pb, Ti, and O is accordant, expanding the lattice. However, at high temperature, i.e. 520 K, the energy descent direction from the vibrational free energy of Pb and O atoms changes, which forces *c* axis to be shorter. The role of Ti remains unchanged. Therefore, the vibration of Ti atoms drive lattice expansion at the whole temperature, while the thermal vibration of Pb and O atoms causes PT favouring cubic phase with increasing temperature.

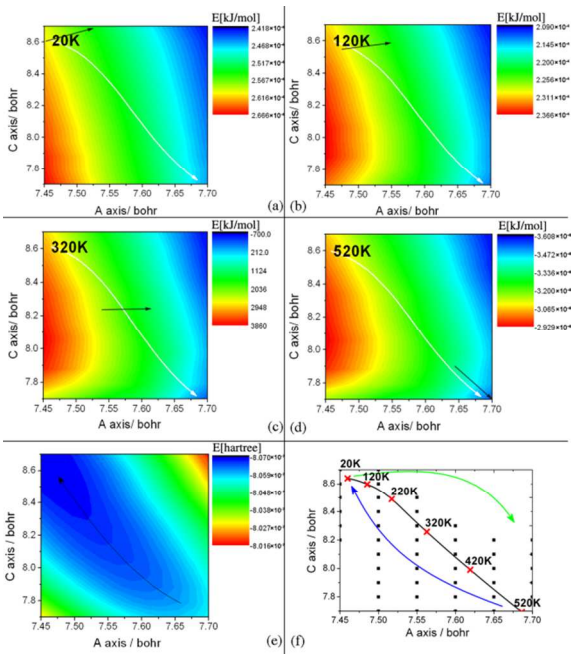

Fig. 25 The contour maps of vibrational free energy at *T* = 20 K (a), 120 K (b), 320 K (c), and 520 K (d). White line in a-d represents the tendency of lattice parameters of PT. The contour map of the static energy is shown in (e). The continuous trends of the static energy (blue line), vibrational free (green line), and total free energy (black line) with different temperatures is shown in (f). Red and blue regions indicate areas of high energy and low energy, respectively. The black arrow denotes the energy gradient descent direction. (Reprinted with permission from ref. 145. Copyright 2013, American Institute of Physics.)

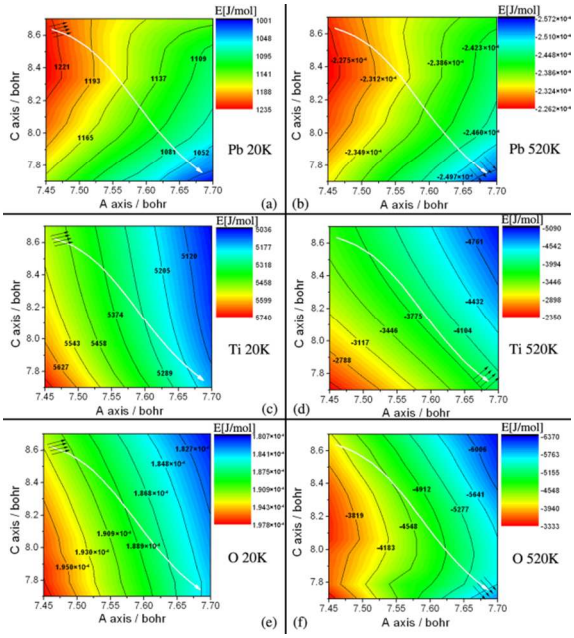

Fig. 26 The contour maps of vibrational free energy of various atoms at T = 20 K and 520 K. White line represents the tendency of lattice parameters of PT. Red and blue regions indicate areas of high energy and low energy, respectively. The black arrow denotes the energy gradient descent direction. (Reprinted with permission from ref. 145. Copyright 2013, American Institute of Physics.)

PT is *A*-site driven ferroelectricity. The electronic contribution is attributed to the strong hybridization of Pb6*s* and O2*p*, which stabilizes the large tetragonal distortion. As temperature increases, the thermal vibration of Pb and O atoms plays an important role which destroys the hybridization between Pb-O bonds, since the thermal vibration of Pb and O atoms favors cubic phase (Fig. 26b and f). The first-principles calculations are in agreement with those experimental results. The NTE of PT is originated from the contribution of ferroelectrcity, while the vibration of atoms modulates ferroelectricity. Furthermore, the crossover from positive to negative thermal expansion at RT in PT as shown in Fig. 3 is due to the combined actions between the thermal vibration of Ti-O and Pb-O bonds.[145]

The nature of NTE can be further understood in $(Pb_{1-x}Cd_x)TiO_3$ solid solutions by first-principles calculations.[148] The enhancement of NTE in $(Pb_{1-x}Cd_x)TiO_3$ by Cd substitution for Pb is highly correlated to the stronger hybridization between Cd-O orbitals. Cd substitution promotes directly the stronger orbital hybridization of Pb/Cd-O, gives rise to a significant increase in P_S, and thus enhances the NTE. As a comparison, the substitution of Ca with weak ferroelectric activity to Cd with strong ferroelectric activity weakens the NTE.[64]63 With increasing Ca content, the ionic character of A-O is enhanced, and the hybridization is weakened.[148]

3. NTE in magnetic materials

Magnetic functional materials consist of a large number of NTE materials. There are many magnetic materials which have been found to exhibit NTE, such as alloys, oxides, nitrides, sulfides, and fluorides. The anomalous thermal expansion is a result of magnetovolume effect (MVE) which is a change in volume resulted from the amplitude variation of magnetic moment. The first observation of MVE was discovered by Guillaume in 1897 in Invar alloys of $Fe_{0.65}Ni_{0.35}$ which has a very small CTE (α_l = 1.2×10^{-6} K^{-1} at 300K) below its T_C (500 K).[19] A general explanation of NTE caused by MVE is that the appearance of a magnetic moment in a magnetic material is favoured by increased volume. In the early stage of studies on low thermal expansion of Fe-Ni Invar alloys, MVE was theoretically explained by the concept of the 2γ model.[149] It is true for magnetic materials whose unit cell volume below magnetic ordering temperature is higher than that of non-magnetic system.

The MVE can be quantitatively described by the physical variable of spontaneous volume magnetostriction (SVMS), ω_s, which presents the effect of magnetism on unit cell volume. The SVMS is as function of the amplitude of magnetic moment *M*, according to the following equation,[150]

$$\omega_s(T) = 3\int \alpha_m(T)dT = kC_{\mathrm{mv}}\{M(T)^2 + \xi(T)^2\} \quad (10)$$

where $\alpha_m(T)$ is the magnetic contribution to linear CTE at temperature *T*, *k* and C_{mv} are the compressibility and the magnetovolume coupling parameter, and $M(T)$ and $\xi(T)$ are the amplitudes of local magnetic moment and spin fluctuations, respectively. ω_s can be simply described to the square of magnetism, M^2. For the first-order transition, there is sharp change in unit cell volume, because $M(T)$ discontinuously disappears at T_C; While for the second-order transition, unit cell volume gradually changes due to continuous changes in $M(T)$ and $\xi(T)$. The value of ω_s can be calculated by subtracting the contribution of anharmonic phonon vibration from the experimental data using the Debye-Grüneisen equation 3.[151]

MVE is commonly observed in many kinds of magnetic compounds, such as Invar alloys of $Fe_{0.65}Ni_{0.35}$, Laves phase intermetallics of YMn_2,[152] Th_2Zn_{17}-type compounds of $Tm_2Fe_{16}Cr$,[153] Er_2Fe_{17},[154] and $Y_2Fe_{17}C_x$,[155,156] antiperovskite of Mn_3AX,[172-177] CuO nanoparticles,[186] $NaZn_{13}$-type intermetallics of $La(Fe,Si)_{13}$,[150, 157, 158] $Nd_2Fe_{14}B$,[159, 160] and perovskite of $SrRuO_3$.[161,162]

In magnetic materials, there is a similar equation to Landau theory to determine T_C of magnetics:

$$T_c = \Gamma M_{loc}^2/(3k_B) \quad (11)$$

where M_{loc} is the value of the magnetic local moment for the paramagnetic disordered local moment state. An example is shown in disordered f.c.c. Fe-Pt alloys,[163] and Y-Co binary intermetallics.[155] Since the NTE of magnetic compounds also occurs below T_C, the NTE temperature range of magnetic compounds can be adjusted by controlling T_C.

In this section, we focus on those magnetic materials which have NTE property, because there are plenty of magnetic materials exhibiting anomalous thermal expansion below magnetic ordering temperature. Table 3 lists some representative NTE magnetic materials.

3.1 Invar and NTE alloys

The term of "Invar effect" was originated from the investigation by Guillaume in 1897, on ferromagnetic $Fe_{0.65}Ni_{0.35}$ alloy showing *invar*iant length over a wide temperature range around room temperature.[19] The linear CTE of $Fe_{0.65}Ni_{0.35}$ is as low as 1.2×10^{-6} K^{-1} at 300 K (Fig. 27),[165] which is an order of magnitude smaller than in the pure end members of Fe and Ni. The term of Invar effect originally presented the meaning of low or zero thermal expansion property for alloys. Later studies also extended the term of Invar effect to generally describe the anomalous thermal expansion in magnetic materials. The discovery of ZTE in Invar alloys was found to the practical applications of precision instruments and electronic devices such as seismograph, surveying tape, shadow mask for television, and computer screen. In addition to the applications as rather small devices, Invar alloys are utilized as structural components, for instance, container of liquefied natural gas, and core wires of long-distance power cables. Because of contribution to the discovery of Invar alloys, Guillaume was honored with the Nobel Prize in 1920.

Fig. 27 shows details of thermal expansion of $Fe_{0.65}Ni_{0.35}$ Invar alloy.[165] The physical quantity of SVMS (ω_s) is used to quantitatively describe the contribution of MVE to anomalous thermal expansion. Taking Invar alloy as an example, ω_{exp} is

the experimental data for the relative volume thermal expansion $\omega_{exp} = 3\Delta l/l$. ω_{nm} is the reference thermal expansion of nonmagnetic, which is extrapolated from high temperature paramagnetic phase based on the Debye-Grüneisen equation 3. Therefore, the magnetic contribution to thermal expansion, is described by ω_s ($\omega_s = \omega_{exp}-\omega_{nm}$). The maximum value of ω_s (0 K) is 1.9 % for the $Fe_{0.65}Ni_{0.35}$ Invar alloy. Based on the thermal expansion as shown in Fig. 27a, CTEs of α_{exp}, α_{nm}, and α_m are estimated according to ω_{exp}, ω_{nm}, ω_s, respectively. Here, we can see that the CTE of α_m, contributed from SVMS, is negative below its T_C. It compensates the thermal expansion from lattice thermal vibration, corresponding for the ZTE property of Invar alloys. The increase in the value of SVMS will reduce the transition of CTE from positive to negative. The data of SVMS and CTE for some typical Invar alloys are listed in Table 3.

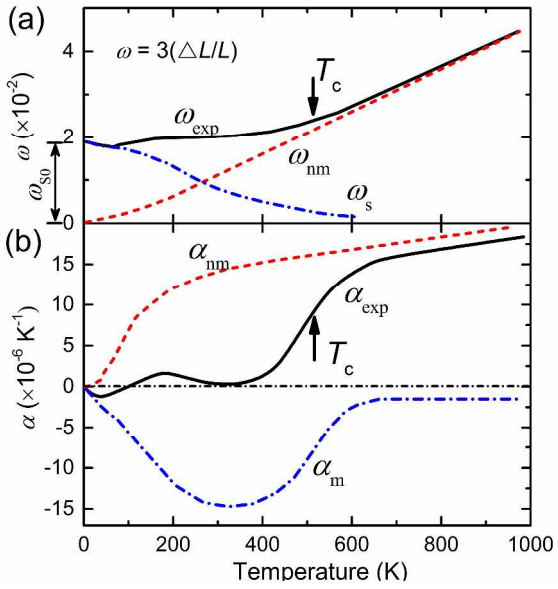

Fig. 27 Thermal expansion properties in Invar alloy of $Fe_{0.65}Ni_{0.35}$. (a) ω_{exp} is the experimental thermal expansion, ω_{nm} is the thermal expansion in a nonmagnetic reference, which is calculated according to the Debye-Grüneisen relationship, and ω_s is the spontaneous volume magnetostriction (SVMS) contributed from magnetic property. (b) CTE calculated from thermal expansion. α_{exp}, α_{nm}, and α_m are derived from thermal expansion of ω_{exp}, ω_{nm}, and ω_m, respectively. $\omega_{exp}=\omega_{nm}+\omega_m$. (Reprinted with permission from ref. 165. Copyright 1990, Elsevier.)

Invar effect has been attracted much attention not only from engineers but also from physicists. Even though Invar effect was found for more than one century, and seems to an old question, the studies on Invar continue to be interesting for physicists because of the difficulty in the understanding the origin of anomalous thermal expansion which is entangled in the complex magnetism.[8] The understanding of the Invar anomaly has remained a challenging problem for more than one century. To celebrate one century of studies on Invar, a symposium was held in 1997 to review the progress in Invar research.[164] As for the mechanism of Invar effect, there are a number of proposed models which can be classified into two

Table 3 Thermal expansion data in magnetic functional materials

Materials	CTE ($\times 10^{-5}$ K^{-1})	Temp. range (K)	Method	Ref.
$Fe_{0.65}Ni_{0.35}$	0.12 (α_l)	T = 300	Dilto.	165
Y_2Fe_{17}	-0.56	5~320	XRD	156
$Y_2Fe_{17}C_{0.6}$	0.24	5~460	XRD	156
$Nd_2Fe_{17}N_x$	-6.3 (α_l)	300~730	Dilto.	166
Gd_2Fe_{17}	-1.1	293~534	XRD	167
$Gd_2Fe_{16}Cr$	-0.61	294~572	XRD	168
Tb_2Fe_{17}	-0.42	5~400	XRD	156
$Dy_2Fe_{17}B$	-0.42 (α_l)	4.2~635	Dilto.	159
Er_2Fe_{17}	-1.3	5~320	XRD	154
$(Zr_{0.65}Nb_{0.35})Fe_2$	0.7	155-300	Dilto.	169
$Mn_{0.9}Co_{0.1}B$	-0.74 (α_l)	447-580	Dilto.	170
$Mn_{0.5}Co_{0.5}B$	-0.016 (α_l)	70-440	Dilto.	170
$Nb_2Fe_{14}B$	-1.0	300~600	SPD	160
$LaFe_{11.5}Si_{1.5}$	-5.0 (α_l)	170~240	Dilto.	157
$LaFe_{10.5}Co_{1.0}Si_{1.5}$	-2.6 (α_l)	240~360	Dilto.	157
GdAgMg	-2.8 (α_l)	2~85	Dilto.	171
$Mn_3Cu_{0.5}Ge_{0.5}N$	-1.2 (α_l)	280~365	Dilto.	172
$Mn_3Cu_{0.5}Sn_{0.5}N$	-2.8 (α_l)	296~332	Dilto.	173
$Mn_3Zn_{0.5}Sn_{0.5}N$	-45 (α_l)	381~428	XRD	174
$Mn_3Cu_{0.6}Si_{0.15}Ge_{0.25}N$	-1.6 (α_l)	120~184	Dilto.	175
$Mn_3Zn_{0.4}Sn_{0.6}N_{0.85}C_{0.15}$	-2.3 (α_l)	270~336	XRD	176
$Mn_3(Ga_{0.5}Ge_{0.4}Mn_{0.1})(N_{0.9}C_{0.1})$	<0.05 ($\lvert\alpha_l\rvert$)	190~272	Dilto.	177
$Mn_3Zn_{0.93}N$	0.0583 (α_l)	10~185	NPD	178
Nano $Mn_3Cu_{0.5}Ge_{0.5}N$	0.0118 (α_l) (12 nm)	12~230	NPD	179
$SrRuO_3$	0.16	12~160	XRD	161
$Pb(Fe_{1/2}Nb_{1/2})O_3$	-0.464	12~150	XRD	180
$Ca(Ru_{0.85}Fe_{0.15})O_3$	-1.4	10~80	NPD	162
$(La_{0.8}Ba_{0.2})MnO_3$	-7.8 (α_l)	150~175	Dilto.	181
$(La_{0.6}Y_{0.15}Ca_{0.25})MnO_3$	-1.2	1.5~110	XRD	182
$(Tb_{0.911}Mn_{0.063})MnO_3$	-0.23	3.5~37	NPD	183
$AlFeO_3$	-1.1	5~150	NPD	184
$CaMn_7O_{12}$	-0.054 (α_l)	49~89	Dilto.	185
Nano CuO	-11	20~170	SPD	
$CdCr_2O_4$	-0.14 (α_l)	45~140	Dilto.	187
$ZnCr_2Se_4$	-0.36 (α_l)	21~40	Dilto.	188
$CdCr_2S_4$	-0.18 (α_l)	4.2~120	Dilto.	189
MnF_3	-9.5	5~43	NPD	190
$(Sc_{0.85}Ga_{0.05}Fe_{0.1})F_3$	0.023 (α_l)	300~900	XRD	38
Nano Au	-2.5 (α_l)	150~400	XRD	191

different approaches. One is based on the localized electron picture in which each atom has its own permanent and temperature independent moment, and the other is based on the itinerant picture of magnetism for the understanding of the composition dependence of the average moment.[164] Among these models important and popular one is the phenomenological "2γ-sate model" which is widely known and also debated.[192] It was assumed that there are two different magnetically ordered states, a ferromagnetic ground and high volume state γ_1 with parallel aligned magnetic spins, and an antiferromagnetic and smaller volume state γ_2 with antiparallel aligned magnetic spins. With increasing temperature, the state γ_2 becomes thermally excited, so that the induced contraction of volume can compensate the thermal expansion of lattice thermal vibration, giving rise to the low or zero thermal expansion of Invar alloys. Recently, the microscopic nature of Invar effect in the most typical Fe-Ni system has been revealed by *ab initio* calculations of the volume dependences of magnetic and thermodynamic properties (Fig. 28).[193] The special aspect of this calculation is the fact that non-collinear

spin ordering has been included in the simulations, that is spins can be titled at arbitrary angles to each other if such configuration can lowers the energy of total spins system. The calculations showed that at large volume corresponding to low temperature the ground state is in the ferromagnetic configuration with aligned spins, however, with decreasing volume corresponding to high temperature the spins gradually depart from the parallel alignment to because disordered. At temperature higher than T_C, the spins become disordered completely, resulting in no net magnetic moment. Therefore, the increasing disorder of spins reduces the volume, and thus compensates the lattice thermal expansion.[193]

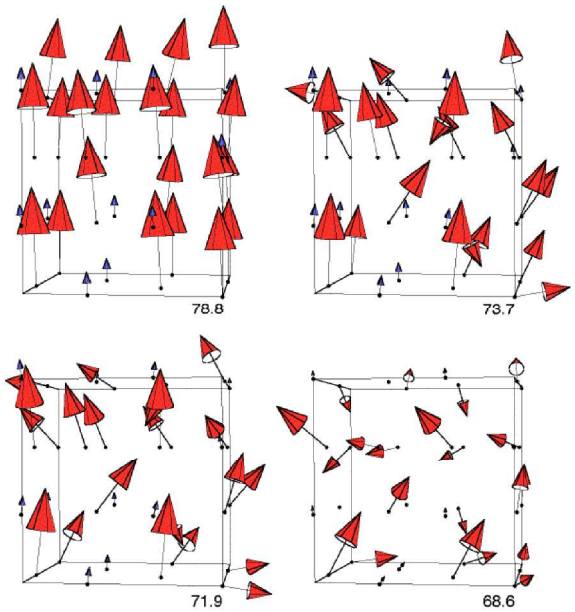

Fig. 28 Self-consistent magnetic spin configurations of the f.c.c. Fe-Ni alloy at four different volumes. Red and blue arrows show moments on Fe and Ni atoms, respectively. Arrow sizes reflect local moment amplitudes. (Reprinted with permission from ref. 193. Copyright 1999, Nature Publishing Group.)

The term of Invar is actually broad physical concept. Even though the Invar effect was originated from the anomalous thermal expansion, there are a broad variety of physical anomalies which are considered to be Invar anomalies such as elastic constants, heat capacity, and forced volume magnetostriction. These Invar anomalies are as function of composition and variable external parameters like temperature, pressure, and magnetic field. More information of Invar problem can be referred to the excellent reviews.[165,194,195]

The Invar effect, which was not bound to Fe-Ni alloys, has been widely accepted to be a well-known property in many ferromagnetic alloys, such as $Fe_{1-x}Pt_x$, $Fe_{1-x}Mn_x$, $Ni_{1-x}Mn_x$, $Co_{1-x}Mn_x$, $Co_{1-x}Fe_x$, $Cr_{1-x}Fe_x$, and $Cr_{1-x}Mn_x$, and many Fe-based ternary systems like Fe-Ni-Co, Fe-Co-Cr, and Fe-Ni-Mn.[163,165,164] Many intermetallic compounds show the Invar effect, including $ZrFe_2$,[169] MnB,[170] $RECo_2$ (RE: Gd, Tb, Dy, Ho, Er), permanent magnet $RE_2Fe_{14}B$ (RE: all except Eu),[159,160] permanent magnet RE_2Fe_{17} (RE: Y, Dy, Lu).[196,197] The Invar effect is neither restricted by lattice structure. It can even observed in Fe-rich amorphous magnetic materials such as $Y_{1-x}Fe_x$, $Fe_{1-x}ET_x$ (ET: Sc, Y, Zr, Hf, La), $Fe_{1-x}B_x$, and $Fe_{1-x}P_x$.[165, 198, 199] Invar effect has also been found in antiferromagnetic compounds, which was studied in the purpose that the dimension of non-magnetic Invar alloys is not sensitive to magnetic field. Some Mn-based compounds exhibit anomalous thermal expansion by antiferromagnetic spin ordering. Cr-Fe-Mn alloys show ZTE property at RT.[200] Thermal expansion in antiferromagnetic Mn-Ge alloys can be chemically controlled by Ge content. For instance, near ZTE at RT was found in the 23at% Ge alloy.[201] Laves phases of RMn_2 have MVE. Among then, antiferromagnetic YMn_2 exhibits a giant volume contraction of about 5% at Neél temperature (T_N = 100 K).[202] In the following paragraphs of this section, we will review those magnetic NTE systems which have been studied in structure and NTE properties in details.

R_2Fe_{17} (R is rare-earth) intermetallic and its solid solutions exhibit anomalous thermal expansion, *i.e.*, NTE or relatively low thermal expansion, below the magnetic ordering temperature.[154-156,203,204] NTE of R_2Fe_{17} is normally dominated by the stronger linear NTE along the *c* axis (Fig. 29), such as Y_2Fe_{17},[155,156] Ce_2Fe_{17},[203] Pr_2Fe_{17},[204] Tb_2Fe_{17},[156] Tm_2Fe_{17},[156] and Er_2Fe_{17}.[154] R_2Fe_{17} generally crystalize in rhombohedral structure (Th_2Zn_{17}-type, space group $R\bar{3}m$) for light R elements, and in hexagonal one (Th_2Ni_{17} type, space group $P6_3/mmc$) for heavy R elements. Below the magnetic ordering temperature, the R_2Fe_{17} compounds are generally ferromagnetic. The large SVMS is due to the short bond lengths of Fe sites, and dominated by the Fe sublattice. The exchange interactions between neighbouring sites are modified by the rare-earth atoms, which correspondingly results in adjusting thermal expansion by various rare-earth atoms. The magnetostrain calculations for different bonds in the structure of R_2Fe_{17} reveals that all the bonds associated with Fe(4f) and Fe(6c) have relatively larger values, which is related to the largest magnetic moment at those sites.[205] The MVE in R_2Fe_{17} is dominated by the Fe sublattice,[205, 206] similar to other magnetic compounds like $Nd_2Fe_{14}B$.[160] The large contribution of the *c* axis to the NTE in R_2Fe_{17} has been attributed to the dumb-bell pairs of Fe atoms, which is aligned along the *c* axis.[155]

For example, the NTE and magnetic structure have been studied in Er_2Fe_{17} in details by temperature dependence of neutron powder diffraction.[154] The Curie temperature is estimated to be T_C = 303 K. As shown in Fig. 29a and b, on heating from 2 K up to T_C, the *c* axis contracts, while the basal-plane unit cell parameters slightly increase. Unit cell volume exhibits NTE below 320 K ($\alpha_V = -1.3\times10^{-5}$ K^{-1}), relatively low thermal expansion in the intermediate region in 320~450 K ($\alpha_V = 1.4\times10^{-5}$ K^{-1}), and then follows Grüneisen-like normally PTE of paramagnetic phase above 450 K ($1.5\cdot T_C$, $\alpha_V = 4.2\times10^{-5}$ K^{-1}).[154] Other R_2Fe_{17} compounds show a similar NTE mechanism to Er_2Fe_{17} in which NTE is ascribed to the magnetic coupling in the Fe sublattice.[155,156,205] Fig. 29c shows SVMS, $\omega_s(T)/\omega_s(5\text{ K})$, compared with that of the square of the magnetic moment, $\left(\mu_{Fe}^{Total}\right)^2(T)/\left(\mu_{Fe}^{Total}\right)^2(5\text{ K})$, as function of reduced temperature (T/T_C). Both curves overlap up to $T\sim0.8\cdot T_C$. At higher

temperature, the $\omega_s(T)$ curve deviates from the $\left(\mu_{Fe}^{Total}\right)^2(T)$ one. It suggests that the presence of short-range magnetic correlations (described in the equation 10), which disappear for $T > 450$ K ($T/T_C \sim 1.5$). The local magnetic property is similar to the PNRs in Pb-based relaxor ferroelectrics in which unit cell volume becomes to deviate from linear thermal expansion at T_B.[91]

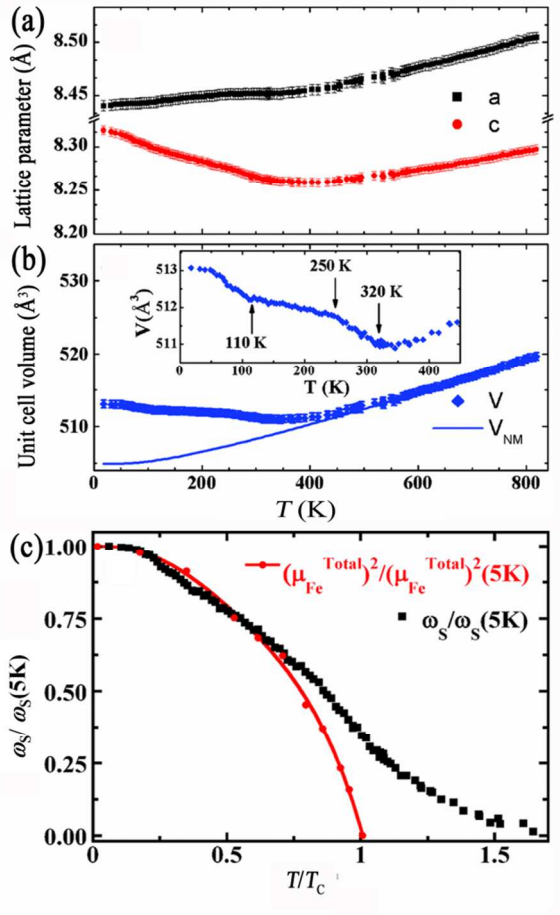

Fig. 29 Temperature dependence of (a) the lattice parameters, and (b) unit cell volume for Er_2Fe_{17}. The solid line shown in (b) represents the non-magnetic contribution to unit cell volume using the Debye-Grüneisen equation. (c) The spontaneous volume magnetostriction, $\omega_s(T)/\omega_s(5\text{ K})$, as function of reduced temperature (T/T_C), compared with that of the square of the total magnetic moment $(\mu_{Fe}^{Total})^2$ for Fe the sublattice for Er_2Fe_{17}. The value of $\omega_s(5\text{ K})$ is 1.6% and $\mu_{Fe}^{Total}(5\text{ K})$ is 14.7 μ_B, respectively. (Reprinted with permission from ref. 154. Copyright 1999, American Physical Society.)

Since NTE of R_2Fe_{17} occurs with its magnetic ordering temperature, the NTE temperature range can be controlled by adjusting the magnetic ordering temperature. The NTE temperature range can be increased by those chemical substitutions which can enhance the magnetic ordering temperature, such as the substitution of Al, Ga, Cr, Si for Fe[153,168,196,206-208] or interstitial atoms such as C or N.[156,166] Or the NTE temperature range can be reduced by the chemical substitutions such as Mn in $Dy_2Fe_{17-x}Mn_x$, [209] and $Dy_2AlFe_{10}Mn_6$.[210] For example, by formation of interstitial compounds with C, T_C is increased from 327 K for Y_2Fe_{17} to 470 K for $Y_2Fe_{17}C_{0.6}$ (Fig. 30). As a result, a wider temperature of ZTE can be achieved in $Y_2Fe_{17}C_{0.6}$ ($\alpha_V = 2.4\times10^{-6}$ K^{-1}, 5~460 K), compared with undoped Y_2Fe_{17} exhibiting NTE over a narrow temperature range (α_V = -5.6×10^{-6} K^{-1}, 5~320 K).[155,156,196] By chemically nitriding in Nd_2Fe_{17}, a strong NTE was found in the temperature range of 300~730 K in $Nd_2Fe_{17}N_x$ intermetallic with a linear CTE $\alpha_l = -6.3\times10^{-5}$ K^{-1}.[166] The NTE of $Tb_2Fe_{17-x}Cr_x$ can be chemically adjusted by the substitution of Cr. The undoped Tb_2Fe_{17} exhibits a relatively smaller NTE (α_V = -4.2×10^{-6} K^{-1}, 5~400 K).[156] By a small amount of Cr substitution, the NTE magnitude and temperature range of $Tb_2Fe_{16.5}Cr_{0.5}$ are enhanced ($\alpha_V = -1.6\times10^{-5}$ K^{-1}, 293~522 K).[208] Chemical substitution of non-magnetic ions in Y_2Fe_{17} can transform NTE to PTE. For example, $Y_2Fe_{15.3}Si_{1.7}$ and $Y_2Fe_{15.3}Al_{1.7}$ both show PTE below T_C. The CTE of $Y_2Fe_{15.3}Si_{1.7}$ is α_V = 1.1×10^{-5} K^{-1} (80~388 K), and that of $Y_2Fe_{15.3}Al_{1.7}$ is $\alpha_V = 1.7\times10^{-5}$ K^{-1} (80~430 K).[196]

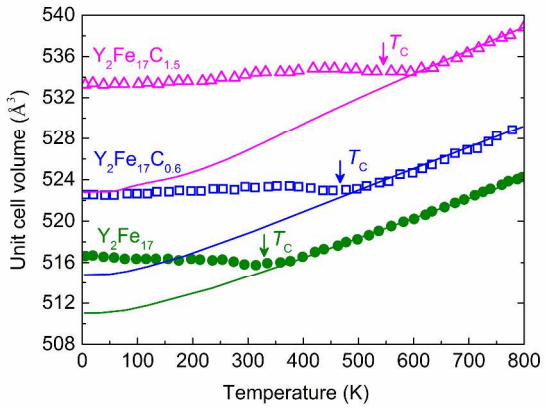

Fig. 30 Temperature dependence of unit cell volumes for Y_2Fe_{17}, $Y_2Fe_{17}C_{0.6}$, and $Y_2Fe_{17}C_{1.5}$. The arrows indicate T_C. (Reprinted with permission from ref. 156. Copyright 1991, Elsevier.)

Intermetallics of $LaFe_{13-x}Si_x$ with an isotropic structure show a giant NTE at the ferromagnetic-to-paramagnetic phase transition.[150,157,211] The magnitude of SVMS or NTE can be chemically adjusted by varying Si content. For example, ω_s (0 K) is decreased from 0.72 % for $x = 1.2$ to 0.43 % for $x = 2.0$.[211] At the same time, NTE of $LaFe_{13-x}Si_x$ is much weakened by the Si chemical substitution ($LaFe_{11.5}Si_{1.5}$: α_l = -5.0×10^{-5} K^{-1} (170~240 K), $LaFe_{10.6}Si_{2.4}$: $\alpha_l = -1.1\times10^{-5}$ K^{-1} (160~270 K)).[157] The sudden unit cell volume contraction at the first-order magnetic transition can be converted to a continuous change of volume at the second-order transition over a broader temperature range. Interesting, the giant NTE of $LaFe_{13-x}Si_x$ can be extended to room temperature by Co chemical substitution for Fe. Since the temperature range of NTE is well consistent with the magnetic transition temperature T_C, the increase in T_C will broaden temperature range of NTE. For instance, T_C is increased in $LaFe_{11.5-x}Co_xSi_{1.5}$ due to the increase of 3d electron number by the Co substitution for Fe. $LaFe_{10.5}Co_{1.0}Si_{1.5}$ exhibits a giant NTE (α_l = -2.6×10^{-5} K^{-1}, 240~350 K), which is three times larger than that of the conventional NTE material of ZrW_2O_8 ($\alpha_V = -2.73\times10^{-5}$ K^{-1}, 0~300 K).[2] The NTE mechanism of $LaFe_{13-x}Si_x$ is well correlated to the MVE, where the

correlation between ω_s and magnetization can be well established as function of temperature, and the temperature dependent volume is highly coupled with magnetization.[157,211] Magnetic NTE materials of $LaFe_{10.5}Co_{1.0}Si_{1.5}$ exhibit several advantages for NTE materials' applications: Isotropic NTE, high thermal conductivity, machinability, and high conductivity.

Anomalous thermal expansion has been observed in magnetically ordering intermetallics of *RT*Mg (*R* = Eu, Gd and *T* = Ag, Au).[171] Very strong NTE was observed in ferromagnetic compounds of EuAuMg (α_l = -2.2×10^{-5} K^{-1}, 2~35 K) and GdAgMg (α_l = -2.8×10^{-5} K^{-1}, 2~85 K). Interestingly, their NTE is highly sensitive to an external magnetic field, where NTE becomes smeared with increasing magnetic field. For example, with increasing magnetic field from 0T to 14T, the CTE of ferromagnetic GdAgMg increases pronouncedly from α_l = -2.8×10^{-5} K^{-1} (2~85 K) to -1.3×10^{-5} K^{-1} (2~125 K).[171] According to thermal expansion and temperature dependence of specific heat data, the presence of a large coupling of spin-lattice was confirmed. Additionally, in both materials of EuAuMg and GdAgMg the ferromagnetic order can be expected to be completely suppressed by hydrostatic pressure of a few GPa, and at the same time NTE becomes much smeared.[171]

$R_2Fe_{14}B$ compounds (*R* = rare earth, space group $P4_2/mnm$) with excellent rare-earth permanent magnetic properties exhibit NTE below T_C.[159,160] As shown in Fig. 31, both *a*(*b*) and *c* axes have NTE property below T_C in tetragonal $R_2Fe_{14}B$. The *a*(*b*) axes show a stronger NTE than the *c* axis. The stronger NTE in the *a*(*b*) axes is consistent with the higher spin moment density distributed in the (110) basal plane than along the *c* axis.[160,212] The NTE of $R_2Fe_{14}B$ compounds is originated from the magnetic contributions of rare earth and Fe. The contributions of different element to SVFS are roughly proportional to the magnetic moments.[160] As shown in Fig. 32, direct experimental evidence is the good linear correlation of ω_s vs. M^2 described in the equation 10 as function of temperature for $Ce_2Fe_{14}B$.[159] The NTE is mainly contributed from the Fe sublattice, and the contribution from rare-earth is smaller and various in different rare-earth elements.[159,160] Those Fe sites in sublattice having larger magnetic moments have larger contributions to the NTE.[160]

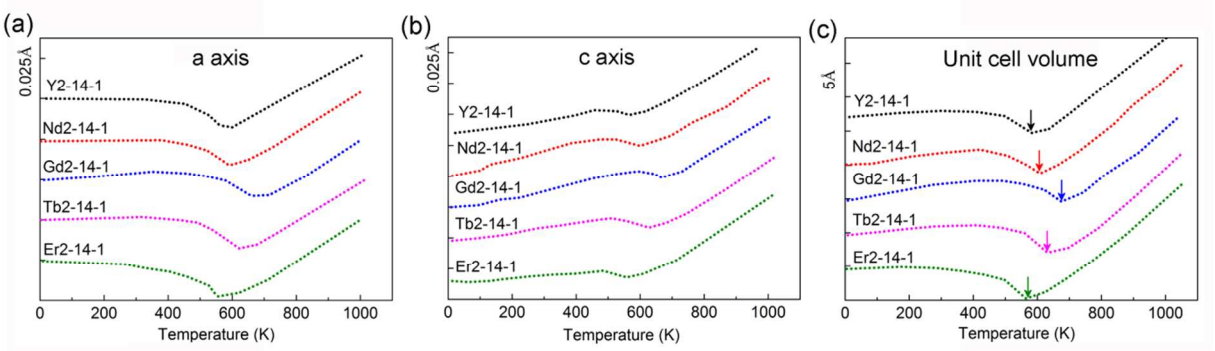

Fig. 31 Temperature dependence of (a) *a* axis, (b) *c* axis, and (c) unit cell volume of $R_2Fe_{14}B$ compounds. (Reprinted with permission from ref. 160. Copyright 2005, Elsevier.)

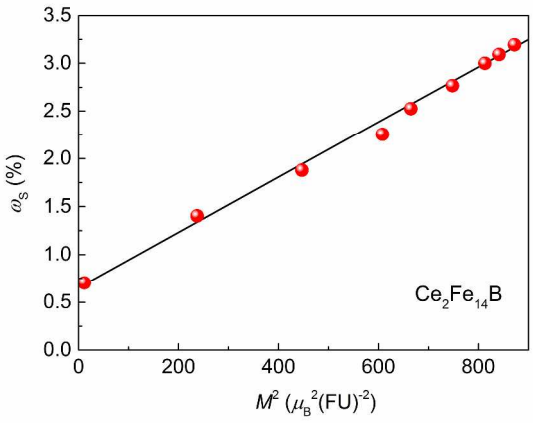

Fig. 32 Spontaneous volume magnetostriction (ω_s) vs. the square of magnetization (M^2) of $Ce_2Fe_{14}B$ as function of temperature. (Reprinted with permission from ref. 159. Copyright 1987, Elsevier.)

NTE or relative low thermal expasnion is also observed in the following magnetic alloys. The thermal expansion of $ZrFe_2$ can be chemically adjusted by substituting Zr with Nb, and CTE becomes smaller or even negative depending upon Zr content.[169] The CTE of α_V is 1.1×10^{-5} K^{-1} (4.2-630 K) and 7.0×10^{-6} K^{-1} (155-300K) for $ZrFe_2$ and $(Zr_{0.65}Nb_{0.35})Fe_2$, respectively.[169] The solid solution of $Mn_{1-x}Co_xB$ shows an adjustable thermal expansion by chemical substitution of Co. NTE occurs at *x* = 0.1 in a narrow temperature range of 447-580 K below its T_C (580 K) with α_l = -7.4×10^{-6} K^{-1}, while in $Mn_{0.5}Co_{0.5}B$ a ZTE occurs in the broader temperature range with a CTE of α_l = -1.6×10^{-7} K^{-1} (70-440 K).[170] Y_6Fe_{23} with a cubic Th_6Mn_{23}-type structure exhibits a relative low PTE below T_C (390 K) with a smaller α_l = 8.5×10^{-6} K^{-1} (< 390 K) compared with that in paramagnetic phase (α_l = 2.2×10^{-5} K^{-1}).[213] NTE is observed in $CeInCu_2$[214], CeNiSn,[215] rare earth metal Holmium.[216]

3.2 Antiperovskite of Mn_3AN

NTE was recently found in antiperovskite Mn_3AN (*A* = Ga, Zn, Cu, Sn, etc.), in which the magnetic Mn atoms are located at the face-centered positions and the non-metal atom *A* is at the

body-centered positions.[172] The discovery of antiperovskite Mn_3AN can be traced back to 1950's.[217] The antiperovskite occasionally shows abrupt lattice contraction accompanied with the magnetic transition from ferromagnetic (FM) or antiferromagnetic (AFM) to paramagnetic (PM). Due to the sharp change of lattice volume, NTE properties of antiperovskite Mn_3AN compounds didn't attract any attention at that time. In 2005, Takenaka *et al.* reported that the sharp lattice contraction in $Mn_3Cu_{1-x}Ge_xN$ could be broadened by doping Ge at the *A* site.[172] As show in Fig. 33, the NTE is gradually broadened with increasing Ge content. For x = 0.47 and 0.5 compositions of $Mn_3Cu_{1-x}Ge_xN$, CTE is α_l = -1.6×10^{-5} K^{-1} (267~342 K), and α_l = -1.2×10^{-5} K^{-1} (280~365 K), respectively. This provides an opportunity to produce a suitable negative or near ZTE in different temperature ranges for practical applications. The study of NTE on Mn_3AN compounds regains interests because of features of metallic property and controllable isotropic NTE behaviours. Compared with other NTE materials, Mn_3AN magnetic compounds show the following advantages: Controllable and isotropic NTE properties, and metallic characters with high performances of mechanical strength, hardness, electrical or thermal conductivity.[172] The present section gives a briefly review on the progress of NTE studies on Mn_3AN antiperovskites, including the NTE control and mechanism. One can refer to excellent reviews for more information.[7,218,220]

Recently, many studies have been carried out on the NTE of Mn_3AX compounds. By substitution of Ge into Zn site in Mn_3ZnN, NTE can be obtained from 348 K to 448 K (α_l = -7.2×10^{-6} K^{-1}).[219] NTE of Mn_3AN compounds can be modified by Sn-doping, such as $Mn_3Cu_{0.5}Sn_{0.5}N$ (α_l = -2.8×10^{-5} K^{-1}, 296~332K),[173] and $Mn_3Zn_{0.5}Sn_{0.5}N$ (α_l = -4.5×10^{-4} K^{-1}, 381~428K).[174] The NTE temperature range is, however, not wide in Ge-substituted antiperovskites. Successively, the NTE temperature range can be broadened in $Mn_3Cu_{0.6}Si_xGe_{0.4-x}N$ by the Si substitution, *e.g.*, $Mn_3Cu_{0.6}Si_{0.15}Ge_{0.25}N$ (α_l = -1.6×10^{-5} K^{-1}, 120-184 K).[175] In addition, the width of NTE temperature range of Mn_3AN could be further broadened by codoping at N site. For example, $Mn_3Zn_{0.4}Sn_{0.6}N_{0.85}C_{0.15}$ shows NTE (α_l = −2.3×10^{-5} K^{-1}) over a broader temperature range (270~336 K), while $Mn_3Zn_{0.4}Sn_{0.6}N$ shows NTE (α_l = -3.8×10^{-5} K^{-1}) over a narrow temperature range (410~440 K).[176] ZTE behaviour was achieved in ultra-nanocrystalline $Mn_{3-x}Cu_{0.5}Ge_{0.5}N$ compounds, due to the fact of broadening effect induced by partial Mn vancancy.[179] ZTE can be much broadened by the introduction of vacancies at Zn site of Mn_3Zn_xN (x = 0.93, α_l = 5.83×10^{-7} K^{-1}, 10~185 K, Fig. 34c).[178] For a brief summary, the NTE of Mn_3AN could be controlled and modified over a relatively wide temperature range by chemical substitution or introduction of vacancy.

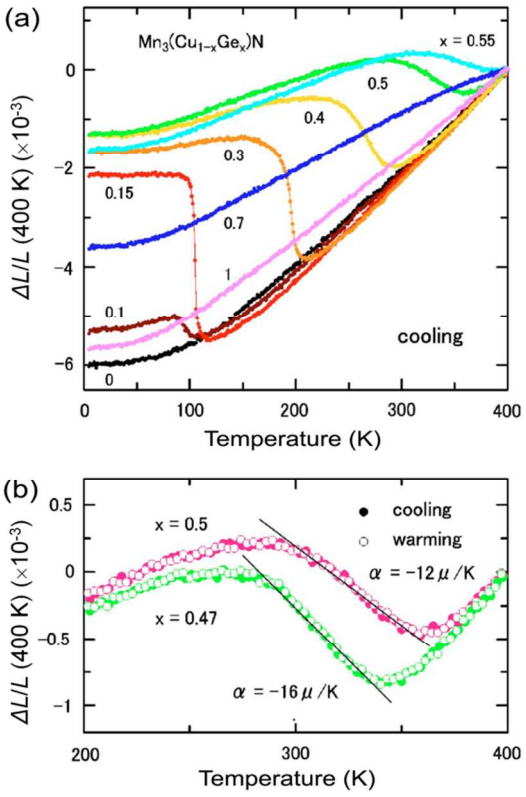

Fig. 33 (a) Linear thermal expansion of anti-perovskite $Mn_3(Cu_{1-x}Ge_x)N$, and (b) NTE for x = 0.47 and 0.5. (Reprinted with permission from ref. 172. Copyright 2005, American Institute of Physics.)

The strong spin-lattice coupling plays important roles in giving rise to the NTE of Mn_3AN compounds based on plenty of experimental facts.[172,177, 220 - 223] The cubic triangular antiferromagnetic (Γ^{5g}, Fig. 34a) phase supports the occurrence of abrupt lattice contraction in Mn_3AN, such as Mn_3ZnN, Mn_3GaN, and $Mn_3Cu_{0.9}Ge_{0.1}N$.[172,177,221,222,223] On the other hand, the origin of the broadening effect mostly arises from the local distortion induced by element doping or substitution. The existence of local lattice distortion in $Mn_3Cu_{1-x}Ge_xN$ has been confirmed using neutron pair distribution function.[224] By using the same method, the distribution of Cu/Sn-Mn in the local structure of $Mn_3Cu_{1-x}Sn_xN$ (x = 0.1 and 0.5) have investigated.[225] The study of x-ray absorption fine-structure on local structure of $Mn_3Cu_{0.7}Ge_{0.3}N$ indicated that the introduction of Ge causes the intense local strain and the local disorder around it.[226] Nevertheless, only partial elements, such as Ge, Sn, Si, and Co, are effective to broaden the NTE temperature range as "relaxant". The codoping of C at N site could be expected to result in the broadening effect; however, this requires the coexistence of "relaxant" elements. Therefore, structural instability induced by local distortion plays an important role in the broadening effect rather than chemical disorder. Furthermore, Mn_3AN compounds are strongly electron-correlated materials. The broadening effect in Mn_3AN may also imply their peculiar electronic states after the introduction of "relaxant" elements.[227]

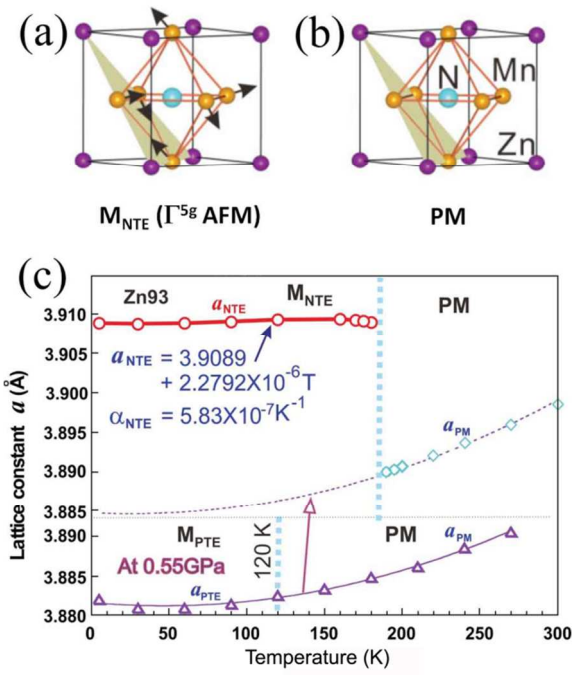

Fig. 34 (a) and (b) Crystal structure and magnetic phases for Mn_3Zn_xN. (c) Temperature dependence of lattice parameter of $Mn_3Zn_{0.93}N$ with Zn vacancies. ZTE is in the M_{NTE} phase, while PTE in the paramagnetic phase (PM). An external pressure of 0.55 GPa (Δ) converts M_{NTE} to M_{PTE}, or M_{PM} at higher temperature. (Reprinted with permission from ref. 178. Copyright 2012, American Physical Society.)

In addition to NTE or ZTE effect around magnetic transition, the ZTE effect was also observed in the AFM region of Mn_3AN antiperovskites. Wang *et al*. reported that $Mn_3Zn_{0.93}N$ exhibits near ZTE effect below 185 K according to the Γ^{5g} AFM phase, which was supported by Zn vacancies (Fig. 34).[178] Based on the neutron diffraction results, a quantitative relationship between the ordered magnetic moment and lattice variation was found. The ZTE behaviour of this phase may originate from a competition between the usual thermal expansion and lattice contraction due to the gradual decrease of magnetic moment in the AFM region.[178,179] The development of Γ^{5g} AFM moment is responsible the gradual lattice expansion of $Mn_3Cu_{1-x}Ge_xN$ (x~0.5) with decreasing temperature.[228]

3.3 NTE magnetic oxides and other materials

Apart from the NTE alloys and antiperovskites of Mn_3AX, there are some magnetic oxides and other materials which have been found to exhibit NTE, such as perovskite-type oxides of $LaMnO_3$,[182, 229 - 232] $SrRuO_3$,[161,162, 233] and $(Tb_{0.911}Mn_{0.063})MnO_3$,[183] orthorhombic antiferromagnetic $CuCl_2H_2O$,[234] molecule-based magnets of $M[N(CN)_2]_2$ (M = Co, Ni),[235] ferromagnetic $AlFeO_3$,[184] ReO_3-type MnF_3,[190] and spinels with the formula ACr_2X_4 (X = O, S, and Se).[187-189,236-238] NTE or anomalous thermal expansion generally occurs below the temperature of magnetic ordering.

NTE was found in the parent compound $LaMnO_3$[229] and its hole-doped colossal magnetoresistance compounds of $La_{1-x}A_xMnO_3$ (A = Ca, Sr, Ba) in a narrow temperature range below the Jahn-Teller transition (T_{JT}).[230-232] The NTE is correlated with the T_{JT}. For $LaMnO_3$, unit cell volume collapse undergoes at T_{JT} (750 K) with a volume contraction of 0.36 %. At the same time the average Mn-O bond distances show an abrupt contraction of 0.45% at the T_{JT}. The NTE of $LaMnO_3$ is connected with the orbital order-disorder transition, where the orbital disordered state allows a more efficient packing of the MnO_6 octahedra.[230] In $La_{0.85-x}Y_{0.15}Ca_xMnO_3$, its orthorhombic symmetry (*Pbnm*) shows ferromagnetic ordering with the Mn moments parallel to c axis. Simultaneously c axis becomes NTE below T_C, which means a coupled role with Mn moment. For the composition of x = 0.25, NTE was found below the magnetrostructural transition at T = 110 K (α_V = -1.2×10^{-5} K^{-1}).[182]

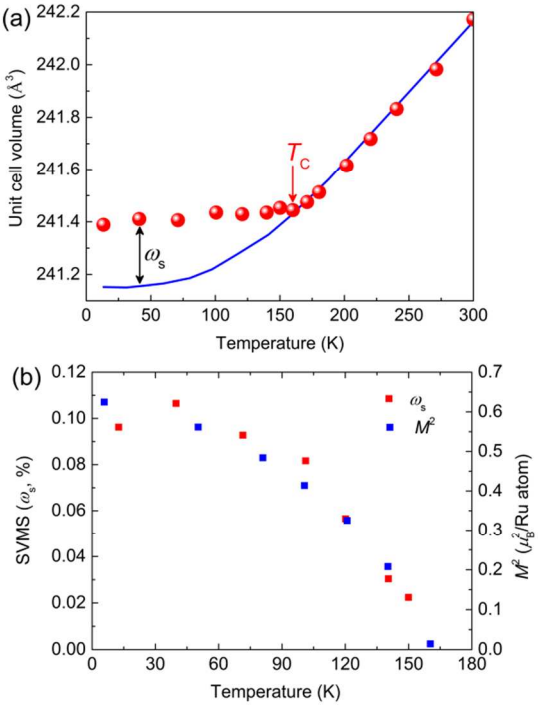

Fig. 35 (a) Temperature dependence of unit cell volume of perovskite-type ferromagnetic $SrRuO_3$. T_C is 160 K. The solid line represents the anharmonic phonon contribution to thermal expansion. (b) Temperature dependence of spontaneous volume magnetostriction, ω_s, and the square of spontaneous magnetization, M^2, of $SrRuO_3$. (Reprinted with permission from ref. 161. Copyright 1996, American Physical Society.)

Magnetic $SrRuO_3$ exhibits anomalous thermal expansion below T_C.[161,162,233] As shown in Fig. 35a, $SrRuO_3$ exhibits a near ZTE below its T_C (α_V = 1.6×10^{-6} K^{-1}, 12~160 K).[161] The nature of near ZTE is originated from the fact that SVMS compensate the PTE from anharmonic phonon vibration. As shown in Fig. 35b, the SVFS (ω_s) shows a good correlation to the square of spontaneous magnetization M^2 as function of temperature,[161] as described by equation 10. As a comparison, paramagnetic $CaRuO_3$ does not show any anomalous thermal expansion. Thermal expansion of $SrRuO_3$ can be modified by the introduction of defects in Ru sites. With increasing content of Ru defects in $SrRu_{1-x}O_3$, the spontaneous magnetization is

weakened, resulting in the reduced T_C. Accordingly the temperature range of near ZTE is shifted to lower temperature.[233] NTE can be introduced in paramagnetic and PTE oxide of $CaRuO_3$ by substitution of magnetic element of Fe in the Ru site.[162] For example, $Ca(Ru_{0.85}Fe_{0.15})O_3$ shows NTE below its T_C (T_C = 85 K, α_V = -1.4×10^{-5} K^{-1}, 10~80 K). Here, the correlation of $\omega_s \sim M^2$ is similar to the behaviour of $SrRuO_3$ (Fig. 35b).

MnF_3 magnetic fluoride crystalizes in monoclinic $C2/c$ symmetry, and has a simple ReO_3-type open-framework structure which consists of corner-shared MnF_6 octahedra. Below its T_N = 43 K, lattice parameters show NTE along three axis directions, resulting in a strong NTE (α_V = -9.5×10^{-5} K^{-1}, 5~43 K).[190] Its NTE shows a coupling result from antiferromagnetic ordering, not from polyhedral coupled rotation. The absence of the framework contribution to NTE is due to large distorted framework. The angle of linkage F-Mn-F is about 145-148° which much deviates from the straight angle of 180°.

NTE was found in magnetic chromium-based spinels with the formula ACr_2X_4 (X = O, S, and Se), such as $ZnCr_2Se_4$,[188,236,237] $CdCr_2S_4$,[189,238] and $CdCr_2O_4$.[187] These cubic spinels have being studied as magnetic frustrated systems and multifunctional solid compounds such as multiferroicity.[239] Those properties are attributed to the cooperativity and competition between charge, spin, and orbital degrees of freedom, all of which are interestingly strongly coupled with lattice. NTE has been found in those magnetic frustrated spinels due to the strong spin-lattice coupling. Such coupling has been explained in terms of strong competition between ferromagnetic and antiferromagnetic interactions. Due to this competition, NTE behaviour occurs at temperatures above T_N where such competition coexists in $ZnCr_2Se_4$ (α_l = -3.6×10^{-6} K^{-1}, 21~40 K),[236,237,188] and $CdCr_2O_4$ (α_l = -1.4×10^{-6} K^{-1}, 45~140 K),[187] or in ferromagnetic phase with relative lower T_C such as $CdCr_2S_4$ (α_l = -1.8×10^{-6} K^{-1}, 4.2~120 K).[189,238,239] Note that for those ferromagnetic spinels with higher T_C, such as $CdCr_2Se_4$ and $HgCr_2Se_4$, antiferromagnetic interaction is weaker, which implies weaker spin-lattice coupling. Accordingly, these spinels show PTE.[238] For example of NTE in $ZnCr_2Se_4$ spinel, the contribution of spin-lattice coupling and the coexistence of AFM and FM to NTE have been well supported by experimental studies of infrared-spectroscopy lattice dynamics and temperature dependence of neutron diffraction.[188,236,237] On cooling below T_1~ 68 K the cubic lattice constant exhibits NTE until T_N (21 K). Note that there is no structural transformation observed at T_1. The specific-heat and magnetization measurement suggest strong spin fluctuations below T_1. Indeed, in the NTE temperature range broad diffuse scattering contributions centered on the (0,0,δ) magnetic reflections were observed, which corresponds to magnetic fluctuation. The NTE occurs with the growth of the FM clusters.[236,237] Such NTE behaviour in frustrated magnetic $ZnCr_2Se_4$ is similar to the ZTE in Pb-based ferroelectric relaxor in which thermal expansion deviates from normal one accompanying by the occurrence of PNRs in paraelectric matrix.

Furthermore, due to the competition and balance between AFM and FM states in frustrated magnetic spinels, thermal expansion behaviour can be easily affected by applying external magnetic field which can stabilize the FM state.[188,189,237] For example in $ZnCr_2Se_4$, the dominant magnetic coupling mechanism is superexchange, which includes FM Cr-Se-Cr and AFM Cr-Se-Zn-Se-Cr or Cr-Se-Se-Cr exchange interactions. An external magnetic field changes balance between FM and AFM interactions enhancing ferromagnetic correlations. As a result, the NTE of $ZnCr_2Se_4$ can be extended down to lower temperature with decreasing T_N by applying external magnetic field (Fig. 36).[188] As shown in Fig. 36, at zero magnetic field NTE appears above T_N (21 K) with a linear CTE α_l = -3.6×10^{-6} K^{-1} (21~40 K), while by applying magnetic field of 30 kOe the NTE appears above T_N (17 K) with a linear CTE α_l = -4.8×10^{-6} K^{-1} (17~40 K). As magnetic field is enhanced to 70 kOe, antiferromagnetic phase is completely suppressed and NTE is well maintained down to the measured lowest temperature 4.3 K (α_l = -5.2×10^{-6} K^{-1}, 4.3~40 K). Another example is $ZnCr_2S_4$ which shows two antiferromagnetic transitions (T_{N1} = 15 K and T_{N2} = 8 K) and PTE (α_l = 1.31×10^{-5} K^{-1}, 2~16 K) at zero magnetic field. By applying magnetic field, the magnetic field starts to break the delicate balance between AFM and FM interactions and enhances the FM interactions. By applying 5T external magnetic field NTE is induced (α_l = -2.14×10^{-5} K^{-1}, 2~16 K).[237]

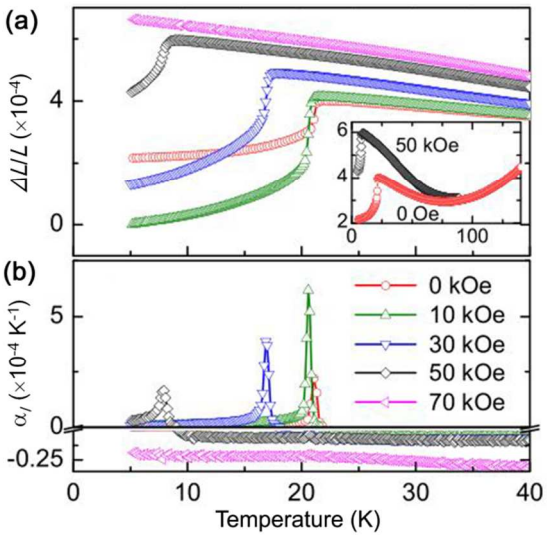

Fig. 36 (a) Relative linear thermal expansion, ΔL(T)/L$_0$ and (b) linear CTE α_l of $ZnCr_2Se_4$ at different magnetic field. The inset of (a) shows an extended temperature range illustrating the NTE between T_N (21 K) and 75 K in H = 0 and 50 kOe. (Reprinted with permission from ref. 188. Copyright 2007, American Physical Society.)

3.4 Size effect in magnetic materials

Thermal expansion is generally studied in the bulk state of materials. It is common sense that physical and chemical properties of materials are affected by size effect. It is also true for the size effect on thermal expansion properties of materials. The study on the effect of particle size on thermal expansion

provides on important issue that the effect of particle size should be paid much attention for applications such as films and nano devices, because thermal expansion could change much at nanoscale range. Accordingly, physical properties of functional materials at nanoscale range could be greatly affected due to change in thermal expansion or mismatched CTE at interface of thin film or heterostructure. Some progress has been made in the issue of the particle size effect on thermal expansion.[67,179,186,191,240-244] The issue of size effect on thermal expansion will be one of interesting topics for future studies. According to the available literatures, size effect on thermal expansion of magnetic materials has shown interesting phenomena. The size effect on thermal expansion is worth further study not only on magnetic materials but also other functional materials.

In this section, the size effect on magnetic materials is reviewed. For example, giant NTE can be introduced in magnetic nanocrystals such as CuO and MnF_2 which originally show a PTE in the bulk state.[186] As shown in Fig. 37, the bulk state of CuO exhibits a slight PTE below its T_N ($\alpha_V = 2.1\times10^{-6}$ K^{-1}, 20~210 K). As particle size is decreased to 5 nm, a giant NTE appears ($\alpha_V = -1.1\times10^{-4}$ K^{-1}, 20~170 K). The magnitude of NTE in nano CuO is four times larger than that observed in ZrW_2O_8 ($\alpha_V = -2.73\times10^{-5}$ K^{-1}, 0~300 K).[2] Above T_N thermal expansion is almost the same in either bulk or nano state. The same phenomenon was observed in antiferromagnetic nano MnF_2 below T_N (67 K) but not in nano NiO. The size effect introduced giant NTE was proposed to correlate with the strong magneto-lattice coupling, *i.e.*, MVE. The detailed mechanism could be clarified by further studying the size effect on crystal and magnetic structure, phonon, and their correlations.

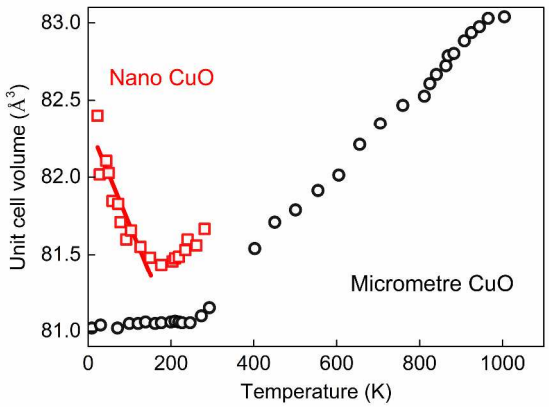

Fig. 37 Temperature dependence of unit cell volume in nano and micrometre CuO. (Reprinted with permission from ref. 186. Copyright 2008, Nature Publishing Group.)

NTE was observed in Au nano particles whose bulk state exhibits PTE and diamagnetic properties.[191] As shown in Fig. 38, with increasing temperature Au nanoparticles (4 nm) shows a crossover from PTE ($\alpha_l = 3.2\times10^{-5}$ K^{-1}, 15~100 K) to NTE ($\alpha_l = -2.5\times10^{-5}$ K^{-1}, 150~400 K). No structure phase transition exists. The PTE in nanoparticles is 2.3 times larger than that of the bulk Au ($\alpha_l = 1.4\times10^{-5}$ K^{-1}).[191] The anomalous thermal expansion was interpreted by accounting for the effects of the valence electron potential on the equilibrium lattice separations, with a weakly temperature dependent level spacing. For a bulk state system, the electronic contribution to the total energy results slowly varies with temperature, while for a nanostate the presence of electronic discrete energy levels separated by only few meV implies a relevant variation of the electronic energy with temperature. The intrinsic ferromagnetic property of Au nanoparticles has been observed by means of technologies of x-ray magnetic circular dichroism (XMCD) and neutron diffraction measurements.[245] The ferromagnetism is associated with the Au atoms on the surface, which is created by localized 5d holes, while the core atoms remain diamagnetic. The anomalous thermal expansion could also be entangled with size introduced magnetism, and the anomalies with crossover were also observed in the magnetic response.[191]

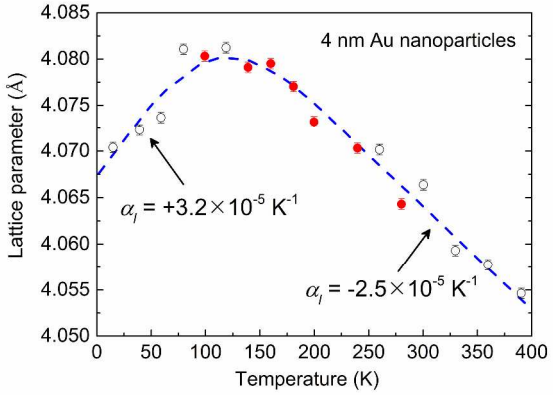

Fig. 38 Temperature dependence of lattice parameter of the Au nanoparticles. A crossover from a PTE at low temperatures to a NTE at high temperatures is at about 125 K. (Reprinted with permission from ref. 191. Copyright 2002, American Physical Society.)

The size effect can transform NTE to ZTE in magnetic antiperovskite of $Mn_{3-x}Cu_{0.5}Ge_{0.5}N$ reported by Song *et al*.[179] As shown in Fig. 39a, NTE is observed in 260~340 K with $\alpha_l = -1.7\times10^{-5}$ K^{-1} in coarse-grained polycrystalline (mean grain size ~2.0 μm) of $Mn_{3-x}Cu_{0.5}Ge_{0.5}N$. With decreasing grain size, NTE is weakened and temperature range is extended to 160~260 K ($\alpha_l = -3.89\times10^{-6}$ K^{-1}) for the nanocrystalline sample (mean grain size ~30 nm). Interestingly, ZTE occurs over a wide temperature range ($\alpha_l = 1.18\times10^{-7}$ K^{-1}, 12~230 K) for the ultra-nanocrystalline sample (mean grain size ~12 nm). The mechanism of size effect on thermal expansion of $Mn_{3-x}Cu_{0.5}Ge_{0.5}N$ is due to the coupling of the thermal expansion with the magnetic ordering process, in which the rate of change of the lattice parameter with respect to temperature (d*a*/d*T*) is mainly affected by the rate of change of the magnetic moment (d*M*/d*T*). Here, the grain size plays a role in determine the Mn occupancy in the lattice of $Mn_{3-x}Cu_{0.5}Ge_{0.5}N$. With decreasing grain size, the Mn occupancy is decreased. The lower Mn occupancy in ultra-nanocrystalline leads to a low magnetic ordering transition temperature, a small magnetic moment, and a low rate of decreasing in the magnetic moment upon heating.

As a result, ZTE takes place over a wide temperature. The role of magnetic moment in thermal expansion of magnetic antiperovskite is similar to that of P_S in NTE of PT-based ferroelectrics.[142]

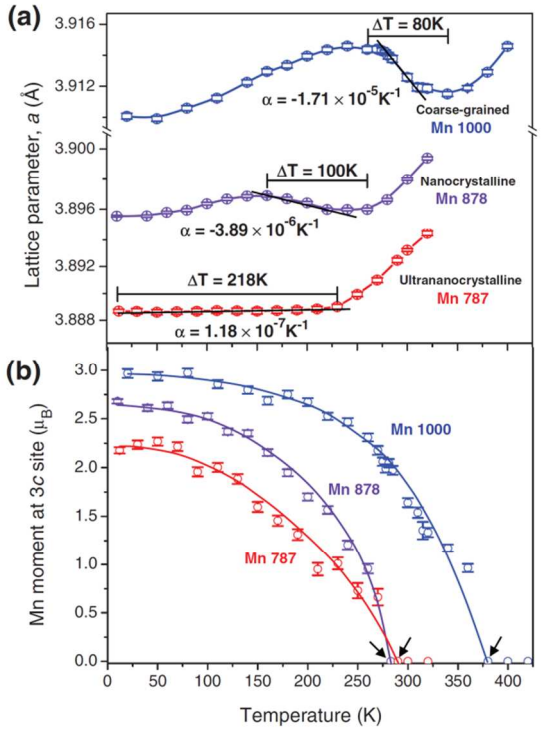

Fig. 39 Temperature dependence of (a) lattice parameter and (b) Mn magnetic moment of $Mn_{3-x}Cu_{0.5}Ge_{0.5}N$ of three materials having different microstructural length scales. The arrows indicate the magnetic ordering transition temperatures. (Reprinted with permission from ref. 179. Copyright 2011, American Physical Society.)

4. NTE in multiferroic materials

Multiferroics materials, which simultaneously behave two or more kinds of fundamental ferroicities, such as (ferro)magnetic and ferroelectric, have been intensively studied in the last decade.[56] Since there has been established the coupling role between NTE with ferroelectric or magnetic order. NTE could be expected to exist in multiferroic materials. There are several available multiferroic systems which have been reported to exhibit NTE. For example, NTE or near ZTE were observed in Pb-based multiferroic perovskites of $Pb(Fe_{1/2}Nb_{1/2})O_3$[180] and $Pb(Fe_{2/3}W_{1/3})O_3$.[92] In multiferroic perovskite of $Pb(Fe_{1/2}Nb_{1/2})O_3$ it has ferroelectric-to-paraelectric and G-type antiferromagnetic-to-paramagnetic at 385 K and 143 K, respectively. Its structure remains monoclinic (*Cm*) in the temperature range 12-300 K without any phase transition. As shown in Fig. 40, NTE occurs at antiferromagnetic phase transition (T_N = 143 K, α_V = -4.64×10^{-6} K^{-1}, 12~150 K).[180] The NTE of $Pb(Fe_{1/2}Nb_{1/2})O_3$ exhibit the coupling role with antiferromagnetic order however not with ferroelectric order. For multiferroic relaxor of $Pb(Fe_{2/3}W_{1/3})O_3$, its near ZTE also occurs below its antiferromagnetic phase transition (T_N = 340 K) not at the T_m (443~463 K). The CTE of $Pb(Fe_{2/3}W_{1/3})O_3$ is α_V = 4.5×10^{-6} K^{-1} (< 300 K).[92] For multiferroic $BiFeO_3$, the contraction of unit cell volume was observed in a narrow temperature range of 598~617 K at T_N.[246]

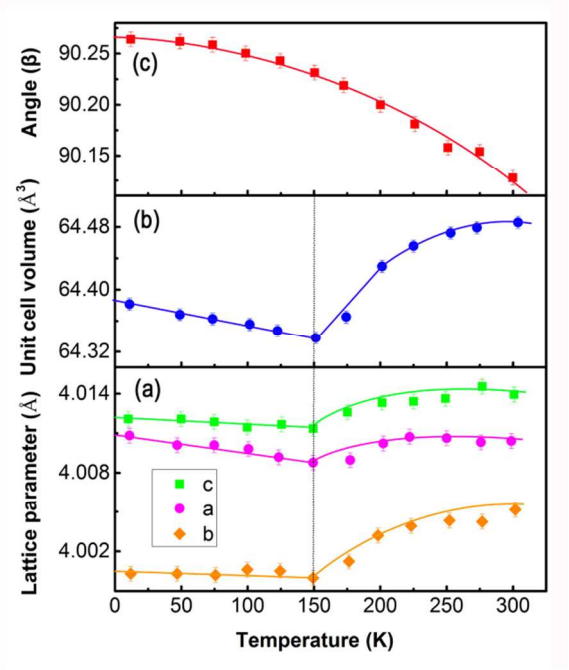

Fig. 40 Temperature dependence of (a) lattice parameters of perovskite ($a = a_m/\sqrt{2}$, $b = b_m/\sqrt{2}$b, and c = c_m), (b) unit cell volume, and (c) the monoclinic distortion angle (β) for $Pb(Fe_{1/2}Nb_{1/2})O_3$. (Reprinted with permission from ref. 180. Copyright 2007, American Institute of Physics.)

$CdCr_2S_4$ multiferroic with spinel structure exhibits the coexistence of ferromagnetism and proper ferroelectricity below T_C of 85 K. It has colossal magnetocapacitive effect and strong coupling of ferroelectric polarization to external magnetic field. Its ferromagnetism and ferroelectricity develop independently, and are driven by electronic superexchange and soft-mode behaviour, respectively. Its multiferroic property is associated with the Cr^{3+} ions. $CdCr_2S_4$ shows NTE below the ferromagnetic transition temperature (T_C = 85 K). Its CTE is α_l = -3.7×10^{-6} K^{-1} (6~90 K). The experimental results showed that NTE seems to couple with magnetic order, not with ferroelectric order. At temperature higher than magnetic T_C, ferroelectricity exists however with normal PTE.[239]

Multiferroic perovskites of PT-$Bi(Ni_{1/2}Ti_{1/2})O_3$ exhibit controllable thermal expansion for different chemical composition (Fig. 14).[70] For example, ZTE compound of 0.8PT-0.2$Bi(Ni_{1/2}Ti_{1/2})O_3$ has ferroelectric remanent polarization (P_r = 9.4 μC cm^{-2}), ferromagnetic remanent magnetization (M_r = 1.2×10^{-7} emu g^{-1}), and α_V = 1.21×10^{-6} K^{-1}. All compositions of PT-$Bi(Ni_{1/2}Ti_{1/2})O_3$ show NTE or anomalous thermal expansion below ferroelectric T_C. The NTE mechanism of PT-based ferroelectrics has been discussed in the section 2.4. There is no evidence for the effect of magnetic property on NTE.

In the above reviewed multiferroics, NTE is coupled either with magnetic order or ferroelectric one. So far we cannot find a multiferroic material in which NTE is coupled simultaneously with magnetism and ferroelectricity. In the available multiferroic systems showing NTE, the absence of simultaneous coupling between lattice and multiferroicity could be related to either much weak ferroelectricity or magnetism. For example, the remanent polarization of multiferroic $CdCr_2S_4$ is as low as $P_r \sim 0.3$ μC cm^{-2} at 25 K,[239] which is in an order magnitude smaller than common ferroelectrics. In the multiferroic PT-Bi($Ni_{1/2}Ti_{1/2}$)O_3, ferromagnetic remanent magnetization is too weak ($M_r = 1.2\times10^{-7}$ emu g^{-1}).[70] If ferroelectrcity and magnetism could be simultaneously enhanced, we could expect that NTE would be really tunable in multiferroics. In future study, thermal expansion could be focused on those multiferroics which have simultaneously enhanced ferroelectricity and magnetism. New multiferroic NTE functional materials could be found.

5. NTE in functional materials induced by electron configuration change

The change of electron configuration can bring NTE or anomalous thermal expansion in functional materials, such as semiconductors of Si, Ge, and GaAs,[247,248] Mott insulators of Ca_2RuO_4 based compounds,[249,250] charge transfer in perovskites of $LaCu_3Fe_4O_{12}$ [251] and $BiNiO_3$,[252] and superconductors of MgB_2 [253,254] and $Ba(Fe_{0.926}Co_{0.074})_2As_2$.[255] The NTE data of those functional materials with change of charge configuration are tabulated in Table 4.

Table 4 Negative thermal expansion of functional materials with change of electron configuration

Materials	α_V (10^{-5} K^{-1})	Temp. range (K)	Method	Ref.
$Ca_2(Ru_{0.9}Mn_{0.1})O_4$	-3.2	150~400	XRD	250
$Ca_2(Ru_{0.75}Mn_{0.25})O_4$	-0.43	90~410	XRD	250
$Ca_2Ru_{0.933}Cr_{0.067}O_4$	-8.0	90~210	XRD	249
NpFeAsO	-2.9	20~60	XRD	256
PrFeAsO	-0.26	2~30	NPD	257
$(Ca_{0.85}La_{0.15})Fe_2As_2$	-4.7	5~300	Dilto.	258
$Ba(Fe_{0.962}Co_{0.038})_2As_2$	-0.21	<7	Dilto.	255
$Ba(Fe_{0.926}Co_{0.074})_2As_2$	-0.11	<22	Dilto.	255
$SrCo_2As_2$	-0.39	8~80	XRD	259
$Bi_{2.2}Sr_{1.8}CaCu_2O_x$	-1.2	2~85	XRD	260
$Bi_2Sr_2CaCu_2O_{8+x}$	-26	110~250	XRD	261
MgB_2	-1.5	12~42	NPD	262
$Sm_{0.67}Y_{0.33}S$	-3.0 (α_l)	10~255	XRD	263
$Sm_{2.75}C_{60}$	-40	≤32	SPD	264
$Yb_8Ge_3Sb_5$	-155	5~15	SPD	265
$(Bi_{0.95}La_{0.05})NiO_3$	-41.3	300~370	SPD	252
$Ba_3BiIr_2O_9$	1%[a]	T = 70	NPD	266

[a]There is 1% sharp volume contraction at T = 70 K.

5.1 Semiconductors

NTE has been observed in low temperature in many tetrahedral semiconductors such as Si, Ge, and GaAs.[247,248] It has been suggested that free electrons of semiconductors could soften lattice, which could produce that free electrons change the range and magnitude of NTE.[247] For example, the magnitude and temperature range of NTE can be enhanced in Te-doped GaAs with an enhanced free-electron concentration (1.2×10^{19}cm^{-3}), compared with the undoped, n-type GaAs with a relatively lower free-electron concentration (2×10^{17}cm^{-3}). Also thermal expansion of Te-doped $Al_{0.32}Ga_{0.68}As$ semiconductor is near zero below 60 K in dark condition, while it is transferred to negative under strong illumination with white light.[247] It needs to mention that the NTE mechanism in semiconductors should distinguish from the contribution of phonon. It is also true for the studies on NTE mechanism in other functional materials.

5.2 Mott insulator

Large NTE has been observed in the classical Mott insulators of Ca_2RuO_4 based compounds below the metal-insulator transition (T_{MI}).[249,250] $Ca_2(Ru_{1-x}M_x)O_4$ (M = Cr, Mn, and Fe) exhibits NTE below T_{MI} for various content of chemical substitution M with examples of $Ca_2(Ru_{0.933}Cr_{0.067})O_4$ (α_V = -8.0×10^{-5} K^{-1}, 90~210 K), $Ca_2(Ru_{0.9}Mn_{0.1})O_4$ (α_V = -3.2×10^{-5} K^{-1}, 150~400 K), and $Ca_2(Ru_{0.92}Fe_{0.08})O_4$ (α_V = -3.7×10^{-5} K^{-1}, 150~390 K).[249,250] The NTE was ascribed to strong coupling with orbital order at the metal-insulator transition. As shown in Fig. 41, for the composition of $Ca_2(Ru_{0.9}Mn_{0.1})O_4$ with a sharp T_{MI}, the dramatic NTE occurs on cooling with an onset in close proximity to the T_{MI} (380 K) with α_V = -3.2×10^{-5} K^{-1} (150~400 K). However, for the composition substituted with more Mn content, $Ca_2(Ru_{0.75}Mn_{0.25})O_4$, the metal-insulator transition becomes broader and cannot be well defined. Simultaneously the strong NTE diminishes with nearly ZTE (-4.3×10^{-6} K^{-1}, 90~410 K).[250] Interestingly, the magnitude of NTE decreases as the atomic number of M increases. This trend may be associated with the fact that with increasing nuclear charge the 3d orbitals become more contracted, and the 3d band progressively fills and downshifts away from the Fermi energy E_F, thus weakening the overlapping with 4d band. The NTE mechanism for Mott insulators shows an electron-lattice interaction similar to MVE. In a Mott insulator the occurrence of an orbital order is always accompanied by electron localization, which costs kinetic energy of electrons whereas lattice expansion reduces the kinetic energy. NTE can take place if the energy gain from the electron-electron interaction

and the lattice expansion can overcome the energy cost from the electron-lattice interaction and the electron localization.[250]

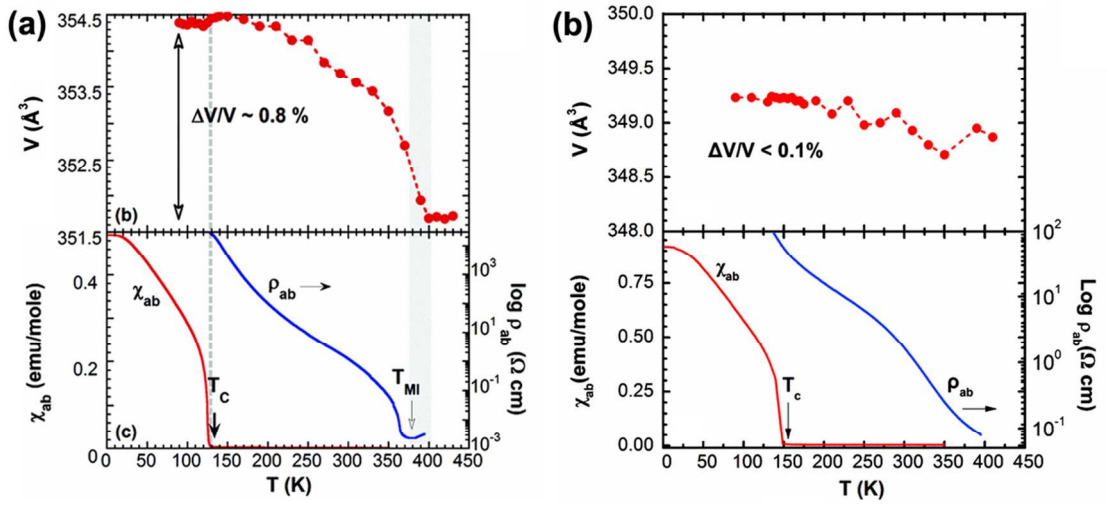

Fig. 41 Temperature dependence of unit cell volume (V), and ab-plane resistivity ρ_{ab} and magnetic susceptibility χ_{ab} at $\mu_0 H$ = 0.5T for $Ca_2(Ru_{1-x}Mn_x)O_4$, (a) x = 0.1, and (b) x = 0.25. (Reprinted with permission from ref. 250. Copyright 2012, American Physical Society.)

5.3 Charge transfer

Temperature-induced intersite charge transfer can give rise to the contraction of ionic radius upon heating, resulting in NTE. Some NTE materials have been found due to this effect, such as YbCuAl, [267] $LaCu_3Fe_4O_{12}$,[251] $BiNiO_3$,[252] $Yb_8Ge_3Sb_5$,[265] and $Sm_{2.75}C_{60}$.[264] The NTE mechanism of temperature-induced charge transfer can be traced back to the studies on rare earths in early years of 1980s, such as the charge change of rare earth Yb in YbCuAl[267] and $YbInCu_4$,[268] and Sm in $(Sm_{1-x}Y_x)S$ (x = 0.33, $\alpha_l = -3.0\times10^{-5}$ K^{-1}, 10~255 K)[263,269] and $(Sm_{1-x}Gd_x)S$.[270] The large NTE was observed in $A'Cu_3Fe_4O_{12}$ (A' = larger rare earth elements La to Tb, Sr and Bi) which has an A-site ordered double perovskites ($Im\bar{3}$) of $A'A_3B_4O_{12}$ (Fig. 42a). The NTE mechanism is due to the isostructural phase transition induced by the A-B intersite charge transfer.[251,271-274] Such A-B intersite charge transfer leads to paramagnetism-to-antiferromagnetism and metal-to-insulator phase transition. For example, a sharp unit cell volume contracts at the isostructural phase transition for $LaCu_3Fe_4O_{12}$ (~1%, Fig. 42b).[251] Similar sharp NTE was observed in other $A'Cu_3Fe_4O_{12}$ with A' = larger rare earth elements La to Tb and Bi,[273,274] but gradually NTE in $SrCu_3Fe_4O_{12}$.[271] The NTE mechanism was assigned to the temperature-induced intersite charge transfer transitions. With increasing temperature there is the charge transfer transition of $3Cu^{3+} + 4Fe^{3+} \rightarrow 3Cu^{2+} + 4Fe^{3.75+}$, which also means an isomorphic phase transition from the low-temperature $LaCu^{3+}{}_3Fe^{3+}{}_4O_{12}$ to the high-temperature $LaCu^{2+}{}_3Fe^{3.75+}{}_4O_{12}$.[251]

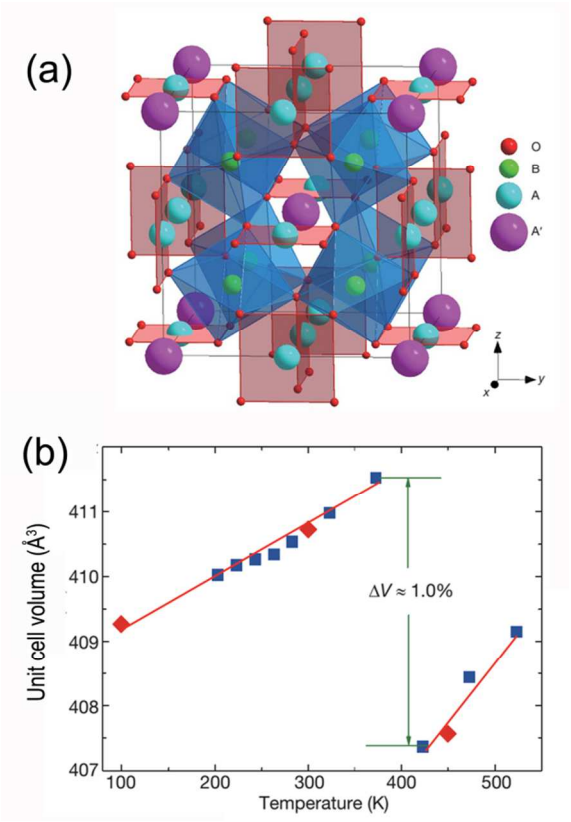

Fig. 42 (a) Crystal structure of the A-site-ordered $A'A_3B_4O_{12}$ double perovskites of $LaCu_3Fe_4O_{12}$. The A-site ions make square-planar coordinated and isolated AO_4 units, and the B-site ions form corner-sharing BO_6 octahedra. (b) Temperature dependence of unit cell volume of $LaCu_3Fe_4O_{12}$. (Reprinted with permission from ref. 251. Copyright 2009, Nature Publishing Group.)

Another experimental evidence for this mechanism is the fact that a sharp NTE taking place in $A'Cu_3Fe_4O_{12}$ (A' = larger rare earth elements La to Tb) is accompanied by a larger amount of

charge transfer, while a gradual NTE in $SrCu_3Fe_4O_{12}$ with a smaller amount of charge transfer.[271] It needs to note that those $A'Cu_3Fe_4O_{12}$ with smaller A′ rare earth elements Dy to Lu, and Y do not exhibit NTE but PTE during the phase transition. Here, the phase transition is caused by charge disproportionation ($8\ Fe^{3.75+} \rightarrow 5Fe^{3+} + 3Fe^{5+}$), and lower temperature phase is ferromagnetic.[271,275] The NTE mechanism of $A'Cu_3Fe_4O_{12}$ double perovskites should be noted that MVE could also play role in NTE, since there is magnetic ordering transition accompanying with NTE.

In 2011, Azuma *et al*. reported that under a constant pressure of 1.8 GPa, colossal NTE was observed in the Bi-based perovskites of $BiNiO_3$ during the phase transition from the high-temperature orthorhombic $Bi^{3+}Ni^{3+}O_3$ to the low-temperature triclinic phase $Bi^{3+}_{0.5}Bi^{5+}_{0.5}Ni^{2+}O_3$ (Fig. 43).[252,276] $BiNiO_3$ shows a 2.6% volume reduction at around 500 K under pressure due to intermetallic charge transfer between Bi^{5+} and Ni^{2+}. Chemical substitution of La for Bi can suppress the charge disproportionation in the $Bi^{3+}_{0.5}Bi^{5+}_{0.5}Bi^{2+}O_3$ phase thereby shifting the charge-transfer transition down to near room temperature at ambient pressure. It is interesting that the colossal NTE in $(Bi_{0.95}La_{0.05})NiO_3$ can be maintained at ambient pressure before the decomposition. The volume CTE α_V is -4.13×10^{-4} K^{-1} (300~370 K), and the maximum slope of dilatometric curve in 320~380 K corresponds to $\alpha_l = -8.2\times10^{-5}$ K^{-1} (Fig. 43b).[252,277] Additionally, the temperature range of the colossal NTE can be shifted by the chemical substitution of different lanthanide elements. The onset temperature of NTE is increased by substituting smaller lanthanide element due to the fact that the charge transfer transition is less affected.[278]

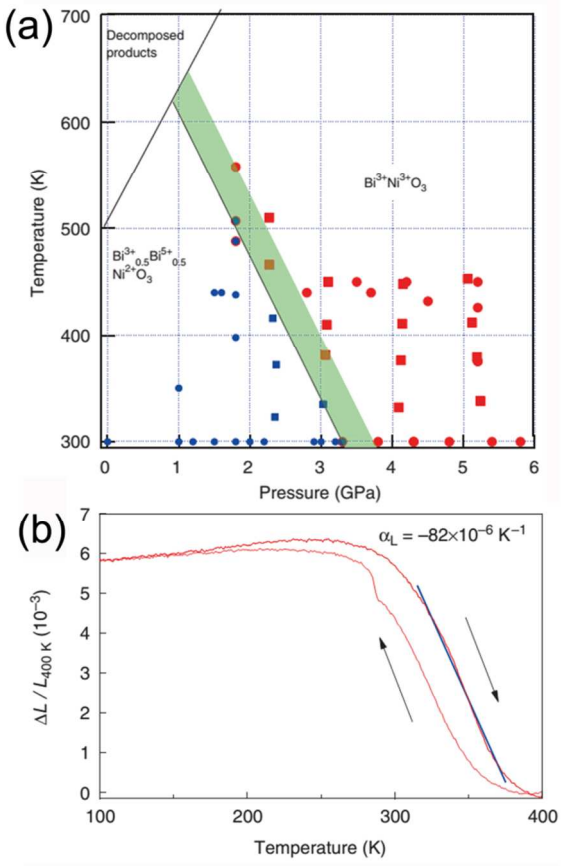

Fig. 43 (a) Pressure-temperature phase diagram of $BiNiO_3$. Blue symbols represent the low pressure and temperature phases corresponding to triclinic, antiferromagnetic and insulating $Bi^{3+}_{0.5}Bi^{5+}_{0.5}Bi^{2+}O_3$, while red ones represent the high pressure and temperature phases to orthorhombic, paramagnetic and metallic $Bi^{3+}Ni^{3+}O_3$. (b) The dilatometric linear thermal expansion for $Bi_{0.95}La_{0.05}NiO_3$ at ambient pressure. (Reprinted with permission from ref. 252. Copyright 2011, Nature Publishing Group.)

Large NTE was observed in rare earth fulleride of $RE_{2.75}C_{60}$ due to temperature-induced valence transition of rare earth.[264,279,280] The NTE occurs without any crystal structure change but originates from the temperature-induced differing radii of the rare earth $4f^n$ and $4f^{n-1}$ states. For example in $Sm_{2.75}C_{60}$, on heating a valence transition of Sm from nearly 2+ with a larger radius (Sm^{2+}, 1.14 Å) towards an intermediate value of 2.3+ with a smaller radius (Sm^{3+}, 0.96 Å) has a profound effect on lattice size and is responsible for its NTE (Fig. 44).[264] This valence change is driven by the coupling of the rare earth 4*f* band and the t_{1u} band of C_{60}.[279] As shown in Fig. 45, at high temperatures, 4*f* electrons can be thermally excited from the narrow 4*f* band into the C_{60} t_{1u} band; while at low temperatures, these electrons are taken back into the 4*f* band resulting in a $4f^{14}$ Yb electronic configuration and an expanded ionic radius.[279] NTE of $RE_{2.75}C_{60}$ can be adjusted by various rare earths. For example, $Sm_{2.75}C_{60}$ and $Yb_{2.75}C_{60}$ exhibit NTE with $\alpha_V = -4.0\times10^{-4}$ K^{-1} (≤ 32 K) and $\alpha_V = -5.5\times10^{-4}$ K^{-1} (≤ 32 K), respectively.[264,279] As a comparison, the NTE is absent when the electronically active 4*f* sublattice is missing in the related alkaline earth fulleride, $Ca_{2.75}C_{60}$.[279]

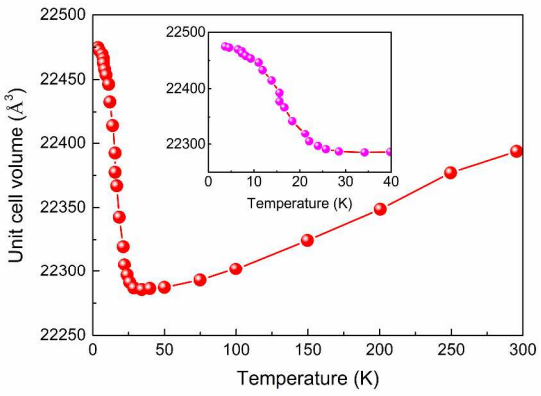

Fig. 44 Temperature dependence of unit cell volume of $Sm_{2.75}C_{60}$. The inset shows an expanded view of NTE between 4.2 and 40 K. (Reprinted with permission from ref. 264. Copyright 2003, Nature Publishing Group.)

NTE or ZTE was observed in Yb-based intermetallics which were ascribed to the change variation of Yb. In $Yb_8Ge_3Sb_5$, the NTE is due to temperature-induced charge change of Yb caused by the charge transfer from Yb 4*f* bands to Sb 5*p* and Ge 4*p* bands (-1.55×10^{-3} K^{-1}, 5~15 K).[265] The charge transfer mechanism was ever supposed to explain the ZTE in YbGaGe intermetallic compound in which Yb could change from 2+ with larger radius to 3+ with smaller radius on heating.[281] Yb

exhibits two energetically similar electronic configurations, magnetic Yb^{3+} ($4f^{13}$) and paramagnetic Yb^{2+} ($4f^{14}$). Since Yb^{2+} is much larger than Yb^{3+} (1.16 vs. 1.008 Å), the valence fluctuation of the transition from Yb^{2+} to Yb^{3+} can compensate for normal thermal expansion with increasing temperature. However, the ZTE in YbGaGe intermetallic could not be reproduced in following studies, where samples showed a normal PTE property in stoichiometric or non-stoichiometric compositions. [282 - 287] The charge variation of Yb was not observed and is nearly divalent in YbGaGe.[285-287] The low thermal expansion in YbGaGe could be resulted from the doping of carbon impurities.[285] The original growth of YbGaGe was performed in graphite crucibles.[281] The thermal expansion can be reduced by 47% with only 0.5 at.% carbon or boron included in starting materials. The near ZTE was suggested to be correlated with substitutional disorder.[285]

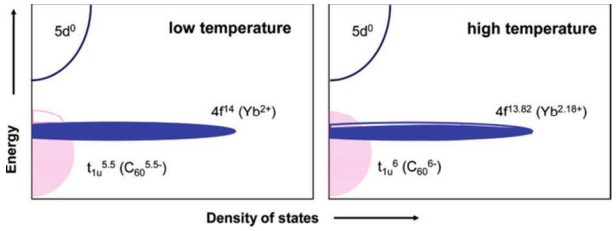

Fig. 45 Schematic representation of the electronic density of states in strong NTE $Yb_{2.75}C_{60}$ at low and high temperatures. The strong NTE results from the spilling over of electron density from the Yb 4*f* band to the t_{1u} band of C_{60} on heating. (Reprinted with permission from ref. 279. Copyright 2005, American Chemical Society.)

5.4 Superconductors

In superconductors or related materials, NTE has been observed below the superconducting T_C in systems such as Nb and Ta, [288] MgB_2,[253,254] $NdFeAsO_{0.89}F_{0.11}$, [289] $Ba(Fe_{0.926}Co_{0.074})_2As_2$,[255, 290] and $La_{1.85}Sr_{0.15}CuO_4$, [291] below magnetic phase transition of superconducting UCoGe,[284] and iron-based superconductors such as $AEFe_2As_2$ (AE = Ba, Sr, Ca)[292] and PrFeAsO,[257] or in non-superconducting iron-based layered compounds such as $Pr(Fe_{1-x}Ru_x)AsO$,[303] $(Ca_{1-x}La_x)Fe_2As_2$,[258] and $SrCo_2As_2$.[259] NTE is coupled with order parameter in superconducting phase for $NdFeAsO_{0.89}F_{0.11}$, [289] $Ba(Fe_{0.926}Co_{0.074})_2As_2$,[255] $La_{1.85}Sr_{0.15}CuO_4$,[291] and $Ba(Fe_{1-x}Co_x)_2As_2$,[255,290] magnetic order for NpFeAsO[256] and $AEFe_2As_2$ (AE = Ba, Sr, Ca),[292] or specific layer structure feature for $Pr(Fe_{1-x}Ru_x)AsO$,[303] $(Ca_{1-x}La_x)Fe_2As_2$,[258] and $SrCo_2As_2$.[259]

A change of volume in a superconducting phase can be thermodynamically described based on Gibbs free energy. The free energy G(Q, T) near the transition temperature T_C can be expressed using a Landau potential by the following equation:

$$G(Q,T) = G_0(T) + (1/2)A(T - T_c)Q^2 + (1/4)BQ^4 + (1/2)C|e|^2 - D|e|Q^2 \quad (12)$$

Where *A*, *B*, *C*, *D* are temperature independent positive constants, *e* is lattice strain, *Q* order parameter. From the equilibrium condition for the strain, there is a relation between *e* and *Q* as follows:

$$|e| = (D/C)Q^2 \quad (13)$$

It indicates the coupling between the lattice strain and order parameter in superconducting phase.[289] The lattice strain, *e*, is defined as $e = (a_{exp}\text{-}a_{nm})/a_{nm}$, where a_{exp} and a_{nm} are, respectively, the experimental lattice parameter, and the nominal one determined by extrapolation from high temperatures according to the Debye-Grüneisen equation 3. The superconducting order parameter is an energy gap $\Delta(T)$, *i.e.*, a Bardeen–Cooper–Schrieffer (BCS) gap, on a Fermi surface in the conventional superconductors. Positive *e* means NTE of lattice parameter, while negative one means PTE of lattice parameter. The value of *e* has been calculated in some superconductors, such as 7.0×10^{-5} (*c* axis) for $La_{1.85}Sr_{0.15}CuO_4$,[291] 2.4×10^{-5} (*a* axis) for $YBa_2Cu_3O_{6.5}$, [293] 1.4×10^{-5} (*a* axis) for MgB_2,[291] 1.3×10^{-4} (*c* axis) for $NdFeAsO_{0.89}F_{0.11}$ (Fig. 46),[289] 8×10^{-5} (*c* axis) $Ba(Fe_{0.926}Co_{0.074})_2As_2$,[255], and -5.1×10^{-5} (*a* axis) for $Ba_{0.6}K_{0.4}BiO_3$ (Fig. 47).[293] There is a correlation of $|e|\sim\Delta^2(T)$ which has been found in the above mentioned superconductors.[255,289,291,293] Please note that the above calculated *e* value presents one crystallographic direction.

The above phenomenological approach described in equations 12 and 13 can be physically understood based on the BCS theory.[289,294] The electronic contribution to CTE in isotropic superconducting state, β_{es}, is obtained based on the BCS theory in the limit of weak electron-phonon coupling.[294] β_{en} is the electronic contribution to CTE in normal state. The difference between β_{es} and β_{en} can be described as follows:

$$\beta_{es} - \beta_{en} = \frac{A}{\gamma}(S_{es} - C_{en}) + \frac{1}{T_cV}\left(\frac{\partial T_c}{\partial p}\right)(C_{es} - S_{es}) \quad (14)$$

Where β_{en} = AT, S_{es} and S_{en} are the entropies in the superconducting and normal states, respectively. C_{es} and C_{en} are electronic contributions to superconducting and normal states specific heat, respectively. γ and *p* are the coefficient of C_{en} and pressure, respectively. The sign of the second term of the equation is the same as the sign of $(\partial T_c/\partial p)$, which is dependent on the detailed mechanism of superconductivity. This term is positive or negative. Accordingly, the lattice parameters of superconductors have been observed to abnormally change to exhibit NTE in $NdFeAsO_{0.89}F_{0.11}$ (Fig. 46),[289] $La_{1.85}Sr_{0.15}CuO_4$, [291] $Ba(Fe_{0.926}Co_{0.074})_2As_2$,[255] MgB_2,[253,254,262] $YBa_2Cu_3O_{6.5}$,[293] and $PrOs_4Sb_{12}$ [295] or PTE in $Ba_{0.6}K_{0.4}BiO_3$ (Fig. 47),[293] and UCoGe.[296] Because the leading term in the equation 14 vanishes at T_C, the equation 14 reduces to the standard Ehrenfest equation. It also needs to note that there exist some superconductors in which the occurrence of NTE does not couple with the superconducting transition. The temperature ranges for NTE and superconductivity do not coincide. For example, $Bi_2Sr_2CaCu_2O_{8+x}$ begin NTE at 250 K which is much higher than its T_C (72~85 K).[261]

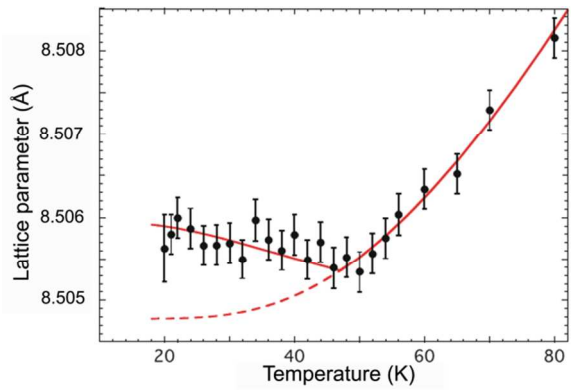

Fig. 46 Comparison between observed lattice parameter c (solid circles) and calculated one (solid line below T_C) of $NdFeAsO_{0.89}F_{0.11}$. The dash line below T_C is calculated based on the exploration from solid line above T_C according to the Debye-Grüneisen equation. (Reprinted with permission from ref. 289. Copyright 2012, Springer.)

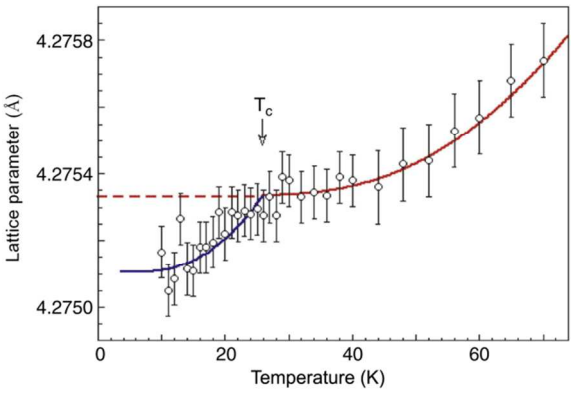

Fig. 47 Experimental lattice parameters (open circles) and calculated ones from the square of the BCS gap (blue solid line below TC) and from the Debye-Grüneisen equation (solid red line above T_C and dash line below T_C) for $Ba_{0.6}K_{0.4}BiO_3$. (Reprinted with permission from ref. 293. Copyright 2010, Elsevier.)

It is interesting to note that thermal expansion property can be utilized to adjust superconducting T_C. The effect of hydrostatic pressure on T_C has been studied in a number of groups of superconductors or parent compounds, which is useful for further increase in T_C. A large pressure dependence of T_C means that T_C can be optimized by introduction of chemical pressure or epitaxial strain in thin films. The pressure dependent T_C is highly correlated to the change in thermal expansion at T_C, which is described by the Ehrenfest relationship,

$$\frac{dT_c}{dp_i} = \frac{\Delta\alpha_i V_m}{\Delta C_p/T_c}, \quad (15)$$

Where $\Delta\alpha_i$ is the jump in the thermal expansion along the i direction, V_m is the molar volume, and ΔC_p is the specific heat jump. The pressure dependence of T_C can be understood according to the thermal property of expansion and specific heat. For example, $Ba(Fe_{0.92}Co_{0.08})_2As_2$ superconductor exhibits very anisotropic pressure dependence of T_C, where dT_c/dp_a = 3.1 K GPa^{-1} and dT_c/dp_c = -7.0 K GPa^{-1}, respectively. The volume pressure effect dT_c/dp_{vol} = -0.9 K GPa^{-1}, which agrees well with direct experimental measurements on single crystal.[297] These results imply that T_C of $Ba(Fe_{0.92}Co_{0.08})_2As_2$ can be increased significantly by increasing the c/a ratio. It is true for the cases that K-doping increases c/a while Co-doping decreases c/a. The difference in T_C for K-doped (39 K) and Co-doped (22 K) $BaFe_2As_2$ could be due to a chemical pressure effect upon c/a.[297]

The engineering of control of CTE matching has succeeded in enhancement of superconducting transition temperature T_C. According to the properties of uniaxial pressure dependence of T_C calculated on the base of the Ehrenfest relationship by means of measurements of high-resolution dilatometry thermal expansion on single crystals, T_C of $La_{2-x}Sr_xCuO_4$ could be enhanced by compressive strain in a-b plane, or by tensile strain along the c axis.[298] T_C of $La_{1.9}Sr_{0.1}CuO_4$ was doubled by introducing epitaxial strain.[52] Thin films of $La_{1.9}Sr_{0.1}CuO_4$ were grown on two substrates of $SrTiO_3$ and $SrLaAlO_4$. As shown in Fig. 48a, for $La_{1.9}Sr_{0.1}CuO_4$, $SrTiO_3$ and $SrLaAlO_4$, the lattice parameter a at RT, is 3.784, 3.905 and 3.754 Å, respectively; and their linear CTEs of α_l are 8.5×10^{-6} K^{-1}, 9×10^{-6} K^{-1}, and 1.1×10^{-5} K^{-1}, respectively. As shown in Fig. 48b, compared with T_C of bulk state (25 K), the $La_{1.9}Sr_{0.1}CuO_4$ thin film grown under compressive strain on the substrate of $SrLaAlO_4$ exhibits almost doubled T_C (49.1 K), while grown under tensile strain on the substrate of $SrTiO_3$ exhibits a much reduced T_C (10 K).[52]

The biaxial tensile strain MgB_2 films show enhanced T_C (41.8 K) to well beyond the bulk value by means of control of CTE between MgB_2 and substrates. Epitaxial MgB_2 thin films were deposited on (0001) 4H-SiC and (0001) sapphire substrates with different CTE of (0001) plane. The CTE in the (0001) plane at RT is 5.5×10^{-6} K^{-1} for MgB_2, 3.0×10^{-6} K^{-1} for SiC, and 6.7×10^{-6} K^{-1} for sapphire. Therefore, the mismatched CTE leads to large tensile strain in MgB_2 on SiC substrate, and compressive strain on sapphire one.[51]

Many superconductors and related compounds have layered structures. Due to the specific structure feature in layered material in which in-plane chemical bonding is strong whereas interlayer weak, materials with layered structure normally exhibit strong anisotropic thermal expansion properties with a typical example of layer material graphite or graphene.[299,300] It means that in-plane thermal expansion is small positive or negative, whereas out-of-plane is strongly positive. It is the case in layered structure superconductors and related compounds such as REFeAsO (RE is rare earth) based compounds, $AEFe_2As_2$ (AE = Ba, Sr, Ca) based compounds,[292,290] $YBaCuO_{7-x}$, [301] MgB_2, [253,254,262] and Na_xCoO_2.[302] For example, the parent $AEFe_2As_2$ (AE = Ba, Sr, Ca) exhibits typical anisotropic thermal expansion above the structural/antiferromagnetic transition, where the c axis CTE is about 3~4 times larger than that of the a axis.[255,292,290]

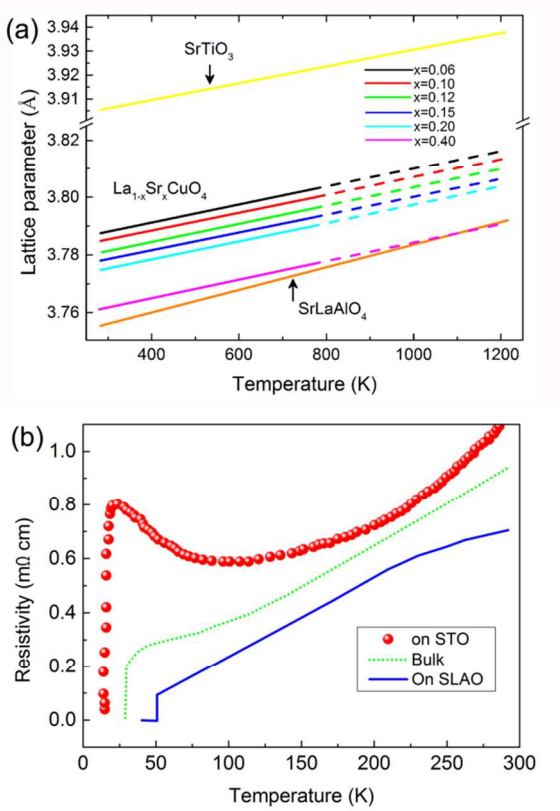

Fig. 48 (a) Extrapolated in-plane lattice parameters as function of temperature for $La_{2-x}Sr_xCuO_4$ as well as for substrates of $SrLaAlO_4$ and $SrTiO_3$. (b) Temperature dependence of resistivity of bulk state, thin films grown on substrates of $SrLaAlO_4$ and $SrTiO_3$ for $La_{1.9}Sr_{0.1}CuO_4$. (Reprinted with permission from ref. 52. Copyright 1998, Nature Publishing Group.)

Iron-based superconducting materials exhibit complex interplay between the lattice, superconductivity, phonons, and magnetism, which has become an interesting theme of research in iron-based superconductors. NTE occurs not only associating with superconducting T_C such as for $Ba(Fe_{1-x}Co_x)_2As_2$,[255,290] but also with antiferromagnetic phase for $AEFe_2As_2$ (AE = Ba, Sr, Ca),[292] and PrFeAsO.[257] NTE can even occur in non-magnetic and non-superconducting iron-based layered compounds such as $Pr(Fe_{1-x}Ru_x)AsO$,[303] $(Ca_{1-x}La_x)Fe_2As_2$,[258] and $SrCo_2As_2$.[259]

At superconducting T_C, NTE has been found in some iron-based layered superconductors, such as $Ba(Fe_{1-x}Co_x)_2As_2$,[255,290] $BaFe_2(As_{1-x}P_x)_2$,[304] and $NdFeAsO_{0.89}F_{0.11}$.[289] It needs to note that there is no specific crystallographic direction to display NTE, which could appear either in-plane (*a* or *b* axis) or out-of-plane (*c* axis). For example, NTE is out-of-plane along *c* axis in $Ba(Fe_{1-x}Co_x)_2As_2$ (x = 0.074, 0.16, and 0.23)[255,290] and $NdFeAsO_{0.89}F_{0.11}$,[289] while in-plane (*a* axis) in $Ba(Fe_{1-x}Co_x)_2As_2$ (x = 0.038),[255] and *b* axis $BaFe_2(As_{1-x}P_x)_2$.[304] According to the present available results, there could be a tendency that in-plane NTE occurs for orthorhombic-antiferromagnetic phases, whereas out-of-plane NTE for tetragonal ones.

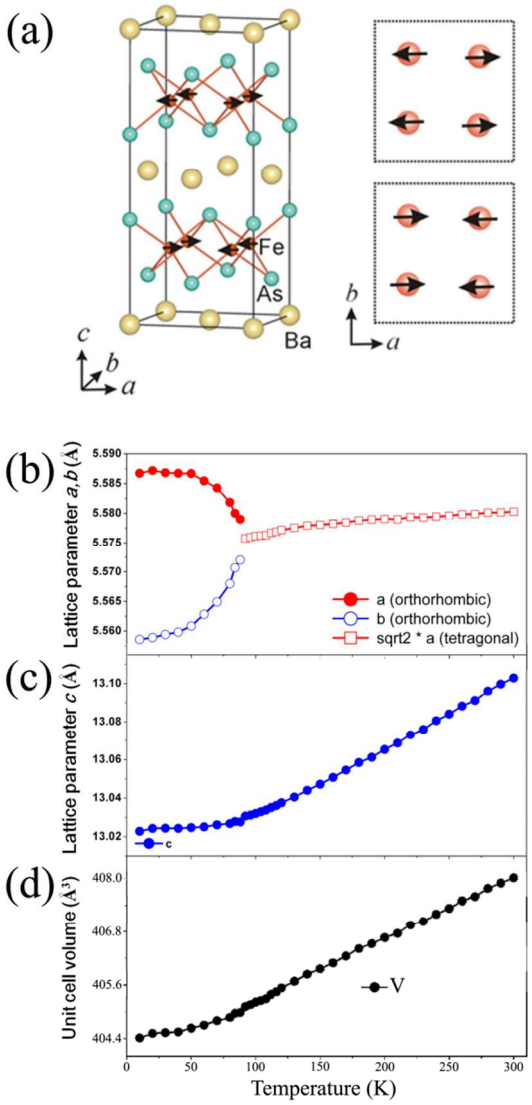

Fig. 49 (a) Magnetic and crystal structures of $BaFe_2As_2$. The Fe magnetic moments are aligned antiferromagnetically along the a and c axes, and ferromagnetically along the b axis. (Reprinted with permission from ref. 306. Copyright 2008, American Physical Society.) Temperature dependence of (b) lattice parameter *a* and *b*, (c) *c* axis, and (d) unit cell volume of $BaFe_2As_2$. (Reprinted with permission from ref. 307. Copyright 2008, arXiv.org.)

A good example is the solid solution of $Ba(Fe_{1-x}Co_x)_2As_2$, which has a orthorhombic-to-tetragonal phase boundary at x = 0.06.[255,290, 305] At the composition x = 0.038 in the orthorhombic-antiferromagnetic phase, *a* axis shows NTE below T_C of 7 K (α_l (*c* axis) = -1.3×10^{-6} K^{-1}, $\alpha_V = -2.1\times10^{-6}$ K^{-1}). However, at the composition x = 0.074 in the tetragonal phase, *c* axis shows NTE below T_C of 22 K (α_l (*c* axis) = -2.4×10^{-6} K^{-1}, $\alpha_V = -1.1\times10^{-6}$ K^{-1}).[255] It is also the same for the in-plane NTE (*b* axis) in orthorhombic $BaFe_2(As_{1-x}P_x)_2$ and out-of-plane NTE in tetragonal $NdFeAsO_{0.89}F_{0.11}$.[289,304]

In the parent compounds of iron-based superconductors, the coupling between lattice and magnetism below magnetostructural transition (T_{sm}) could produce NTE. The NTE in these non-superconducting iron-based parent

compounds should have been discussed in the section 3.3 for magnetic NTE materials, since the nature of NTE is the same. However, we organize the content here in order for a complete discussion between superconducting, magnetism, and lattice. The lattice contraction normally occurs in-plane for orthorhombic phases, which could be coupled with the in-plane antiferromagnetic ordering of Fe. For example, $BaFe_2As_2$ exhibits a tetragonal-to-orthorhombic transition at T_s = 140 K. Below T_s, Fe antiferromagnetic order occurs in the orthorhombic structure along *a* axis in the *a*-*b* plane with a saturation moment of 0.87 μ_B per Fe (Fig. 51a).[306] The NTE occurs along the *a* axis as shown in Fig. 51b,[307] which coincides with the direction of antiferromagnetic order. Note that the lattice contraction contributed from the *a* axis is compensated by the PTE from *b* and *c*-axes, resulting in overall PTE in unit cell volume (Fig. 51d). It is the same for $CaFe_2As_2$, where lattice contraction occurs below T_s along *a* axis along which the antiferromagnetic moment aligns.[308] Below T_s, $BaFe_2(As_{1-x}P_x)_2$ shows lattice contraction along the *a* axis (*i.e.*, x = 0.25, T_s = 48.5 K), and the *c* axis shows negative (*i.e.*, x = 0.25) or low thermal expansion (x = 0.18). The volume is, however, PTE, where the lattice contraction contributd from the *c* axis is compensated by the positive in-plane thermal expansion.[304]

Furthermore, the lattice contraction could also appear along *c* axis. In such cases, NTE will appear in unit cell volume with combined effect from both in-plane and out-of-plane contributions such as NpFeAsO.[256] NpFeAsO does not show any phase transition of tetragonal-to-orthorhombic, in contrast with other *R*FeAsO compounds. However, there are striking variations in lattice parameters as temperature crosses the antiferromagnetic-to-paramagnetic transition (T_N = 57 K). As shown in Fig. 50b, NTE was observed strongly in the *c* axis while weakly in the *a* axis, which results in the volume NTE (α_V = -2.9×10^{-5} K^{-1}, 20~60 K, ω_s = 0.2%).[256] The NTE in NpFeAsO gives further evidence for the coupling between lattice and magnetism, where the NTE occurs in the *c* axis which is the direction for the antiferromagnetic alignment of Np moments (Fig. 50a). The nature of NTE in NpFeAsO is the same to other magnetic NTE materials.

NTE was observed in the orthorhombic (*Cmma*) antiferromagnetic phase of PrFeAsO below 45 K, which is contributed from the NTE in the *c* axis. However, it needs to note that the onset temperature (45 K) of NTE does not exactly overlap with the Neél temperatures for Fe (T_N = 85 K) and P_r (T_N = 11 K).[257] It has a complex magnetic structure, where Fe moments antiferromagnetically align along the orthorhombic *a* axis, and P_r spins align along the *c* axis.[309] Such NTE is absent in superconducting F-doped PrFeAsO (*e.g.*, $PrFeAsO_{0.85}F_{0.15}$), consistent with suppresses of the structural and magnetic phase transition and the absence of Fe and P_r magnetic order.[257] The effect of Ru substitution on thermal expansion of nonsuperconducting $Pr(Fe_{1-x}Ru_x)AsO$ reveals a more complex nature of NTE.[303] The NTE remains in those compositions with x > 0.1 in which long-range magnetic order is absent. The *c* axis

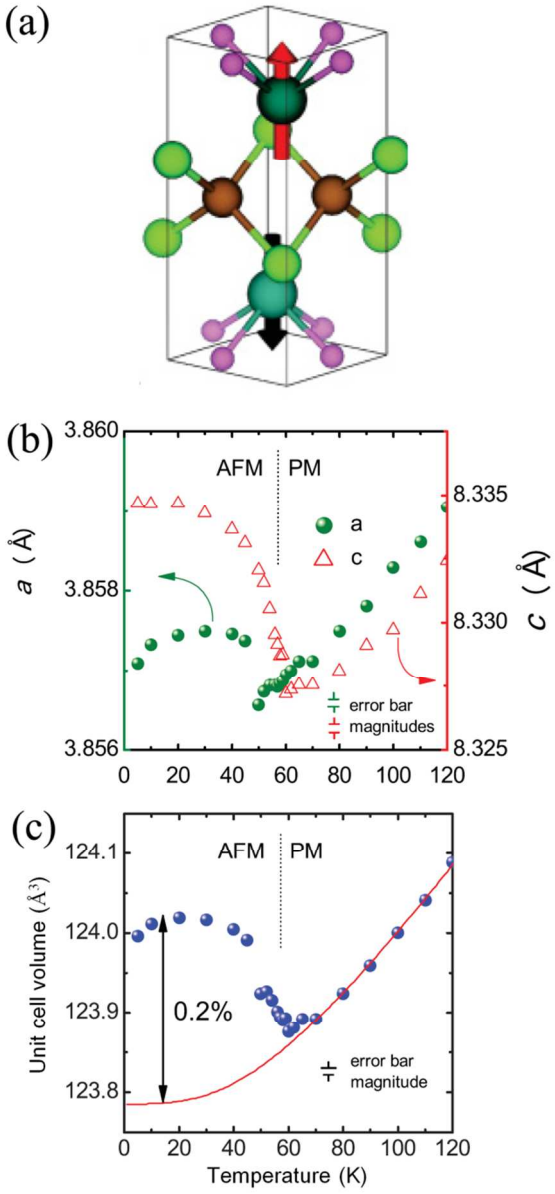

Fig. 50 (a) Crystal and antiferromagnetic structure of NpFeAsO. The Np moments align along the *c* axis. Temperature dependence of (b) lattice parameters, and (c) unit cell volume for tetragonal NpFeAsO. (Reprinted with permission from ref. 256. Copyright 2012, American Physical Society.)

shows a NTE property independent with Ru content, showing the minimum value at ~50 K. Its NTE stems neither from magnetism nor superconductivity. The nature of NTE could be correlated to the special feature of layered structure, since NTE has also been observed in other iron-based parent compounds of paramagnetism.[258,259]

Apart from the contributions from magnetic order and superconductivity, NTE has been also observed over a wide temperature range in other iron-based parent compounds.[258, 259] For example of $(Ca_{1-x}La_x)Fe_2As_2$, at x = 0.0 without La chemical modification, NTE occurs below T_s along *a* axis along which the antiferromagnetic moment aligns.[308] However, giant NTE was observed in $(Ca_{1-x}La_x)Fe_2As_2$ (x = 0.15, 0.20, and

0.25) which displays suppressed antiferromagnetic order and structure transition (Fig. 51).[258] $(Ca_{1-x}La_x)Fe_2As_2$ is not a bulk superconductor, and exhibits a broad transition to superconductivity due to an exceptionally small superconducting volume fraction (*e.g.*, 0.02% for $x = 0.15$). It is reasonable that no thermal expansion anomalous occurs at T_C. It is interesting phenomenon that the *a* axis shows a giant NTE over a large temperature range of RT-300 K, and the *c* axis also exhibits NTE in a temperature range. For example of $(Ca_{0.85}La_{0.15})Fe_2As_2$, with increasing temperature the *a* axis contracts between 5 and 300 K at a magnitude of $\Delta L/L_{300K} = 7.1\times10^{-3}$ ($\alpha_l = -2.4\times10^{-5}$ K^{-1}). The absolute CTE of *a* axis in $(Ca_{0.85}La_{0.15})Fe_2As_2$ is even larger than the that in metals of Mg, Al and Cu which have large PTE. $(Ca_{0.85}La_{0.15})Fe_2As_2$ also exhibit NTE along the *c* axis between 5 and 123 K. Its unit cell volume shows NTE in the temperature range of 5-300 K with $\alpha_V = -4.7\times10^{-5}$ K^{-1} (inset in Fig. 51b). The NTE occurs in the single tetragonal phase without any magnetic phase transition. The Grüneisen parameter is γ (45 K) = -22 and γ (300 K) = 1.0. Its large, negative Grüneisen parameter reflects the presence of anomalous phonon modes. Measurements and calculations of phonon dispersion of $CaFe_2As_2$ reveal unusual broadening, presumably due to the close proximity of $CaFe_2As_2$ to the collapsed-tetragonal phase.[310] In the AB_2X_2 family of materials, due to the presence or absence of interlayer X-X bonding, a segregation of occurs, which results in either a "collapsed" or "uncollapsed" tetragonal structure, respectively.[311] The anomalous behaviour in phonon dispersion could be enhanced since La substitution for Ca in $CaAs_2Fe_2$ could moves this system closer to the boundary of the collapsed-tetragonal phase. NTE was found in $SrCo_2As_2$ with a paramagnetic state in a temperature range of 8-80 K ($\alpha_V = -3.9\times10^{-6}$ K^{-1}).[259] There is no temperature-induced lattice distortion in $SrCo_2As_2$ which maintains in uncollapsed tetragonal symmetry below room temperature. However, for this composition its NTE is mainly contributed from the *c* axis, which differs that in $(Ca_{1-x}La_x)Fe_2As_2$. For a similar composition of $BaCo_2As_2$, Its *c* axis shows a similar NTE. However unit cell volume has PTE due to the compensation of PTE from the *a* axis.[312] The reason for NTE in $SrCo_2As_2$ could be similar to that of $(Ca_{1-x}La_x)Fe_2As_2$. $SrCo_2As_2$ is near the proximity of collapsed-tetragonal phase. However, in a collapsed-tetragonal phase NTE disappears such as the example of $CaCo_2As_2$.[313]

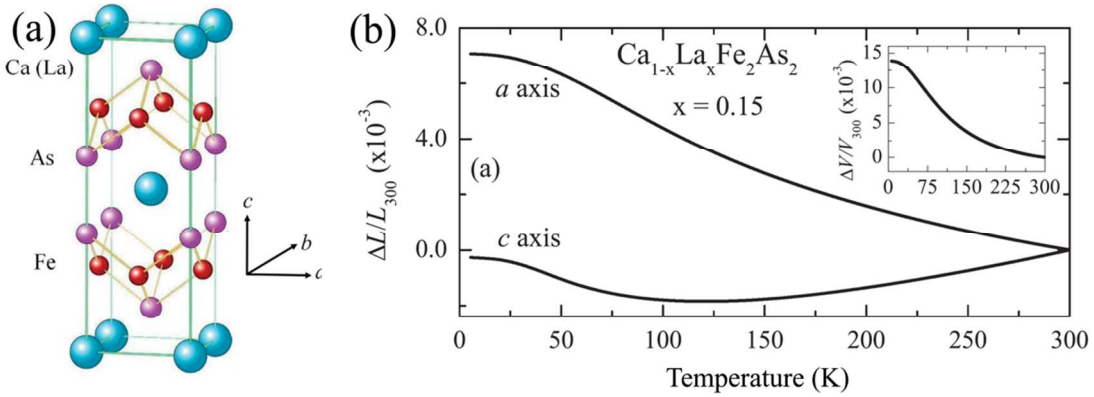

Fig. 51 (a) Crystal structure of tetragonal $(Ca,La)Fe_2As_2$. (b) Temperature dependence of length variation related to 300 K for tetragonal $(Ca_{0.85}La_{0.15})Fe_2As_2$. Inset shows relative volume variation as function of temperature. (Reprinted with permission from ref. 258. Copyright 2012, American Physical Society.)

In copper-based superconductors, there is also a coupling role between lattice and superconductivity. The structure of copper-based high-T_C superconductor can be considered as consisting of several layers stacked along the *c* axis. The in-plane chemical bonds are strong, while the interaction interlayer is weaker. Well above T_C such feature of layered structure exhibits a similar thermal expansion property to other layered materials, in which thermal expansion is large along *c* axis of out-of-plane while smaller one in-plane. For example, tetragonal $Bi_{2.2}Sr_{1.8}CaCu_2O_x$ has linear CTEs of $\alpha_c = 1.2\times10^{-5}$ K^{-1} and $\alpha_a = 5.5\times10^{-6}$ K^{-1} at 200 K,[260] and orthorhombic $YBa_2Cu_3O_{7-\delta}$ has $\alpha_c = 1.7\times10^{-5}$ K^{-1}, $\alpha_a = 8.9\times10^{-6}$ K^{-1} and $\alpha_b = 5.9\times10^{-6}$ K^{-1} at 200 K.[314]

The anomalous thermal expansion generally occurs in-plane below T_C,[260,301,315,316] which supports the coupling between lattice and superconductivity, due to the generally accepted fact that the Cu-O plane corresponds to the superconducting layers. For example, with decreasing temperature, the *a* and *b* axes deviate from the theoretical trend of phonon vibration at T_C (92.3 K) for high-T_C superconducting $YBa_2Cu_3O_{7-\delta}$. The *a* and *b* axes show contraction below 80 K and 35 K, respectively. The total volume exhibits relatively low thermal expansion due to more positive contribution from thermal expansion in *c* axis. The average α_V is 4.5×10^{-6} K^{-1} and 2.6×10^{-5} K^{-1}, respectively, below and above T_C.[301] Another example is $Bi_{2.2}Sr_{1.8}CaCu_2O_x$. NTE occurs in in-plane *a* axis below T_C (85 K), which coincides with superconductivity. The CTE is $\alpha_V = -1.2\times10^{-5}$ K^{-1} (2~85 K).[260] A strong NTE occurs in tetragonal $Bi_2Sr_2CaCu_2O_{8+x}$ in the temperature range 110~250 K, in which both *a* and *c* axes show NTE.[261] Its NTE is extremely strong with a CTE $\alpha_V = -2.6\times10^{-4}$ K^{-1} which is one order larger in magnitude than most NTE materials. Such giant NTE in $Bi_2Sr_2CaCu_2O_{8+x}$ should be re-examined.

5.5 Other electronic structure change

Giant NTE occurs in $Ba_3BiIr_2O_9$ due to a special electronic structure change, which is different to the mechanisms of long-range magnetic, charge, or orbital order as well as intermetallic charge transfer or disproportionation. In $Ba_3BiIr_2O_9$, a giant unit cell volume contraction of 1% takes place at $T = 70$ K (Fig. 52), coupled with the remarkable 4% changes in the length of the Ir-Ir bond and also Ir-O-Ir angle. The NTE is driven by a dramatic change in the interactions among Ir 5d orbitals, and represents a crossover between two very different, competing, ground states: One that optimizes direct Ir-Ir bonding above T, shortening that distance to maximize orbital overlap and resulting in electron delocalization; and the other that optimizes Ir-O-Ir magnetic superexchange below T, increasing the Ir-O-Ir bond angles toward 90° by lengthening Ir-Ir distances and resulting in electron localization and local moment formation.[266]

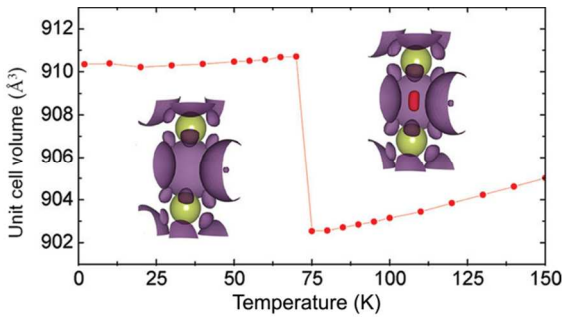

Fig. 52 Temperature dependence of unit cell volume of $Ba_3BiIr_2O_9$. Electron bonding function (ELF) from ab initio calculations of the electronic structure for the high-temperature and low-temperature states. (Reprinted with permission from ref. 266. Copyright 2012, American Chemical Society.)

6. ZTE in functional materials

ZTE is one of the most important issues for the studies of NTE. ZTE can be achieved by two methods. One is formation of composites with PTE and NTE materials. In this method, NTE materials are used as additives. The other is to achieve controllable ZTE in a single-phase material. Single-phase ZTE or low thermal expansion exhibit advantages of high mechanical performance, free of interface local stress, easy fabrication and so on. However, single-phase ZTE materials are rare, especially for cubic-phase ZTE materials.[19,32,38,177-179,318] According to the survey of CTE in 201 oxide ceramics, most oxide ceramics have a CTE between $\alpha_l = 6\sim12\times10^{-6}$ K^{-1}. There are only 25 oxides (~ 12%) which have low thermal expansion materials, and their CTEs distribute between $\alpha_l = -2.0\sim2.0\times10^{-6}$ K^{-1}.[4]

The ZTE materials have been applied in many fields, such as precision instruments and electronic devices of telescope, seismograph, surveying tape, container of liquefied natural gas, core wires of long-distance power cables, fire-resistant materials, and catalyst support. ZTE is important for the applications of functional materials. For example, the applications of electrostriction and magnetostriction actuators need to exclude the effect of temperature fluctuation on length change. ZTE ensures precise control of length by external electric or magnetic field.[45] For example, relaxor ferroelectrics like $Pb(Mg_{1/3}Nb_{2/3})O_3$-based ceramics exhibit not only large electrostrictive effect but also the advantage of ZTE. For ceramic of $0.9Pb(Mg_{1/3}Nb_{2/3})O_3$-0.1PT electric field induced strain is as high as 0.073% at 1 kV mm^{-1}. Due to the good feature of ZTE ($\alpha_l = 1\times10^{-6}$ K^{-1}, 173~373 K), the strain induced by thermal fluctuation is far smaller than the electrostrictive strain, which is advantageous for precise micropositioner applications. Near room temperature, a ten degree temperature fluctuation produces a strain about 5×10^{-6}, which could be eliminated by a small electric field of 14 V mm^{-1}.[45]

In NTE functional materials, ZTE can be achieved by adjusting NTE-related physical property, since there is coupling between physical property and NTE. ZTE functional materials have been relatively intensively studied in magnetic and ferroelectric materials. In other functional materials, there are also available investigations on ZTE.

In magnetic functional materials, there are a number of ZTE alloys and intermetallics.[165,195] The prototype ZTE is Invar alloys of $Fe_{0.65}Ni_{0.35}$ ($\alpha_l = 1.2\times10^{-6}$ K^{-1} at 300 K).[19,165] Other Invar alloys have been found to have ZTE, such as Cr-Fe-Mn alloys,[200] Mn-Ge alloys (23at% Ge),[201] and $Y_2Fe_{17}C_{0.6}$.[156] ZTE is found in magnetic oxides of $CdCr_2O_4$,[187] $CaMn_7O_{12}$,[185] and $SrRuO_3$,[161] and also in antiperovskite nitrides of $Mn_3(Ga_{0.5}Ge_{0.4}Mn_{0.1})(N_{0.9}C_{0.1})$,[177] $Mn_{3-x}Cu_{0.5}Ge_{0.5}N$ nanocrystallines,[179] and $Mn_3Zn_{0.93}N$.[178] Since there is the coupling of thermal expansion with magnetic order,[154,159,161,179,193] the ZTE property in magnetic materials can be achieved through those methods which can adjust the negative contribution of magnetic order for NTE to equally compensate the positive role of lattice thermal vibration for PTE. In the example of ZTE nanocrystalline $Mn_{3-x}Cu_{0.5}Ge_{0.5}N$ (Fig. 39), the Mn occupancy in $Mn_3Cu_{0.5}Ge_{0.5}N$ is decreased by decreasing grain size. The lower Mn occupancy in ultra-nanocrystalline leads to a small magnetic moment, and a low rate of decreasing in the magnetic moment upon heating. At the critical grain size, the low rate of decease in the magnetic moment upon heating just compensates the PTE from lattice thermal vibration. As a result, ZTE takes place over a relatively wide temperature from 12~230 K in the ultra-nanocrystalline $Mn_{3-x}Cu_{0.5}Ge_{0.5}N$ ($\alpha_l = 1.18\times10^{-7}$ K^{-1}).[179] ZTE can be extended to a broader temperature range in Mn_3Zn_xN antiperovskite by introduction of vacancies in Zn site (Fig. 34), which changes both the ordered magnetic moment and lattice parameters. For example, the temperature range of ZTE is extended from 135~185 K for $x = 0.99$ to 10~185 K for $x = 0.93$.[177]

In functional ferroelectric materials, our previous studies on thermal expansion of PT exhibit that PT has a flexible ability to achieve ZTE with tunable temperature range by chemical modifications,[59,67,69-71] Some ferroelectric functional materials have been found to exhibit ZTE property (Table 1), such as PT-based ferroelectrics of $(Pb_{0.8}La_{0.2})TiO_3$,[59] 0.6PT-$0.3Bi(Zn_{1/2}Ti_{1/2})O_3$-$0.1BiFeO_3$,[69] 0.6PT-$0.4Bi(Mg_{1/2}Ti_{1/2})O_3$,[71] 0.8PT-$0.2Bi(Ni_{1/2}Ti_{1/2})O_3$,[70] $Pb(Ti_{1-x}Zr_x)O_3$,[86] nano 0.7PT-

$0.3BiFeO_3$,[67] and Pb-based relaxor ferroelectrics of $Pb(Mg_{1/3}Nb_{2/3})O_3$.[75] As shown in Fig. 24, thermal expansion in ferroelectrics is a balance between two competitive factors of lattice thermal vibration and ferroelectricity. Lattice thermal vibration is a positive factor for PTE, while ferroelectricity is a negative factor. If the contribution from ferroelectrcity equally compensates the one from lattice thermal vibration, ZTE is produced. Therefore, any factor which can reduce ferroelectricity could be utilized to achieve ZTE in PT-based ferroelectric materials. For example, ZTE can be obtained by chemical substitution of ions with weak ferroelectric activity such as La, Ba, Sr, Mg, Ni, and Zr (Table 2).[59,70,71,86] Or ZTE can be obtained by decreasing particle size or applying pressure.[67,140]

NTE of Mott-insulator is correlated with the metal-insulator transition. Dramatic NTE occurs with a sharp metal-insulator transition in $Ca_2(Ru_{0.9}Mn_{0.1})O_4$. The strong NTE diminishes and ZTE appears, when the metal-insulator transition becomes broader and cannot be well defined by more chemical substitution of Mn in $Ca_2(Ru_{0.75}Mn_{0.25})O_4$.[250]

In the framework-structure materials, there are some compounds that exhibit ZTE property, such as $Ca_{0.25}Sr_{0.25}Zr_2(PO_4)_3$,[317] $Fe[Co(CN)_6]$,[28] $Zr_{0.4}Sn_{0.6}Mo_2O_8$,[32] and TaO_2F.[318] The NZP family has well been studied to exhibit adjustable thermal expansion from positive to negative. Some compounds display low or zero thermal expansion.[17] For example, ZTE can be achieved in solid solution of $Ca_{0.5-x}Sr_xZr_2(PO_4)_3$ (x = 0.25), in which α_a and α_b remain constantly in the temperature of RT to 773 K. The average α_V is -3.0×10^{-7} K^{-1} (RT~773 K). Due to the prominent feature of ZTE, the microcracks can be significantly reduced in its ceramics.[317] Other compositions have also been found to have ZTE property, such as $Ca_{0.5}Zr_2(PO_4)_3$ (-2.1×10^{-7} K^{-1}, 298~773 K).[17] ZTE can be obtained by specific structure feature in 3D framework of intermetallics RE_4TGe_8 (RE = Yb, Gd; T = Cr-Ni, Ag).[319] This flexible 3D framework creates a unique thermal expansion property that is ZTE in the *ac* plane while slightly PTE perpendicular to the *ac* plane (*i.e.*, *b* axis). The *ac* plane seems to more compressive which can compensate the thermal expansion form thermal vibration, resulting in ZTE in the *ac* plane. For example, for Yb_4NiGe_8 the CTE of *a* and *c* axis is $\alpha_l = -7.2\times10^{-6}$ K^{-1} and 5.1×10^{-7} K^{-1}, respectively, while that of *b* axis is $\alpha_l = 8.3\times10^{-6}$ K^{-1} in the temperature range of 10~160 K. The overall volume CTE is as low as $\alpha_V = 2.0\times10^{-6}$ K^{-1} (10~160 K).[319]

It has been known that it is not easy to obtain ZTE in those NTE materials with open-framework structure feature. Though it has been widely accepted that transverse thermal vibration can induce NTE, it is few documented for the control of NTE according to this mechanism.[32,38] For example, the NTE of ZrW_2O_8 can be only adjusted in a small magnitude (α_l = -7.3~-8.7×10^{-6} K^{-1}).[137] In 2013, Evans group reported that ZTE has been achieved in the cubic $(Zr_{1-x}Sn_x)Mo_2O_8$ solid solutions by adjusting the content of Sn.[32] The thermal expansion of $(Zr_{1-x}Sn_x)Mo_2O_8$ can be controlled over a large range α_l = -$5.9\sim7.9\times10^{-6}$ K^{-1} (12-500 K) by chemical modification of Sn. At x = 0.6, ZTE was achieved in the composition of $Zr_{0.4}Sn_{0.6}Mo_2O_8$ with an extremely low CTE ($\alpha_l = -6\times10^{-8}$ K^{-1}, 12-600 K). The ZTE and tunable thermal expansion in the $(Zr_{1-x}Sn_x)Mo_2O_8$ are benefited to both advantages: One is the isotropic PTE in $SnMo_2O_8$ which is unique among cubic AM_2O_8 materials; and the other is that the *A*-site solubility range is significantly higher than that observed in other AM_2O_8 systems.[32]

In 2014, there is a study managing to achieve the control of NTE by modulating local structure property, and an isotropic ZTE was found in cubic ReO_3-type ScF_3 based compounds over a wide temperature range. Moreover, ferromagnetic property can be introduced to the framework structure ScF_3-based ZTE materials. ScF_3 exhibits a cubic ReO_3-type structure and a large NTE over a wide temperature rage ($\alpha_l = -3.1\times10^{-6}$ K^{-1}, 300~900 K).[33,39] Its NTE mechanism is not different to other framework NTE compounds. That is upon heating the transverse vibration of F anion normal to the straight Sc···Sc axis, involving the cooperative rotation of ScF_6 octahedra rigid units, gives rise to the reduction in Sc···Sc separation and thus ensures NTE. With this well-known physical image, the NTE of ScF_3 could be adjusted if the contribution from the transverse thermal vibration can be weakened. A local distorted structure is introduced in the macroscopic cubic lattice by heterogeneous cation substitution of Fe and Ga for Sc to form solid solutions of $(Sc_{1-x}Ga_xFe_y)F_3$ in order to impede the contribution of transverse vibration.[38] NTE in $(Sc_{1-x}Ga_xFe_y)F_3$ is weakened with increasing content of Ga/Fe. Interestingly, isotropic ZTE is achieved in cubic $(Sc_{0.85}Ga_{0.05}Fe_{0.1})F_3$ over a wide temperature and can maintain to high temperature ($\alpha_l = 2.3\times10^{-7}$ K^{-1}, 300~900 K).[38] Such wide temperature ZTE in $(Sc_{0.85}Ga_{0.05}Fe_{0.1})F_3$ is unconventional, since most ZTE materials are restricted to a relatively low temperature or narrow temperature range. The ZTE mechanism was suggested to be correlated to the local distorted structure which was confirmed by pair distribution function (PDF) analysis of synchrotron radiation x-ray total scattering. As shown in Fig. 53, in undoped ScF_3, fluorine atoms locate exactly at the midpoint of the Sc-F-Sc linkages and the angle is 180°. However, $(Sc_{0.85}Ga_{0.05}Fe_{0.1})F_3$ exhibits a local rhombohedrally distorted structure in the cubic macroscopic lattice. Fluorine atoms depart from the original midpoint with a displacement of 0.117 Å, resulting in the bending Sc/M-F-Sc/M linkages with angle of 173.3°. Having higher substitutions content of Ga/Fe, the composition of $(Sc_{0.8}Ga_{0.05}Fe_{0.15})F_3$ shows more PTE. There is good correlation between angle of Sc/M-F-Sc/M linkages and CTE. For the compositions of ScF_3, $(Sc_{0.85}Ga_{0.05}Fe_{0.1})F_3$, and $(Sc_{0.8}Ga_{0.05}Fe_{0.15})F_3$ with increasing Ga/Fe content, the angle decreases from 180°, 175.8°, to 173.3°, and CTE changes from -3.1×10^{-6} K^{-1}, -1.3×10^{-6} K^{-1}, to 2.37×10^{-7} K^{-1}, respectively. It is not difficult to understand that most ReO_3-type metal trifluorides, such as AlF_3 and TiF_3, do not show NTE but strong PTE due to macroscopic distortion of rhombohedral symmetry ($R\bar{3}c$), featuring larger bending of M-F-M linkages (Al-F-Al: 157.6°, and Ti-F-Ti: 160.8°).[320,321]

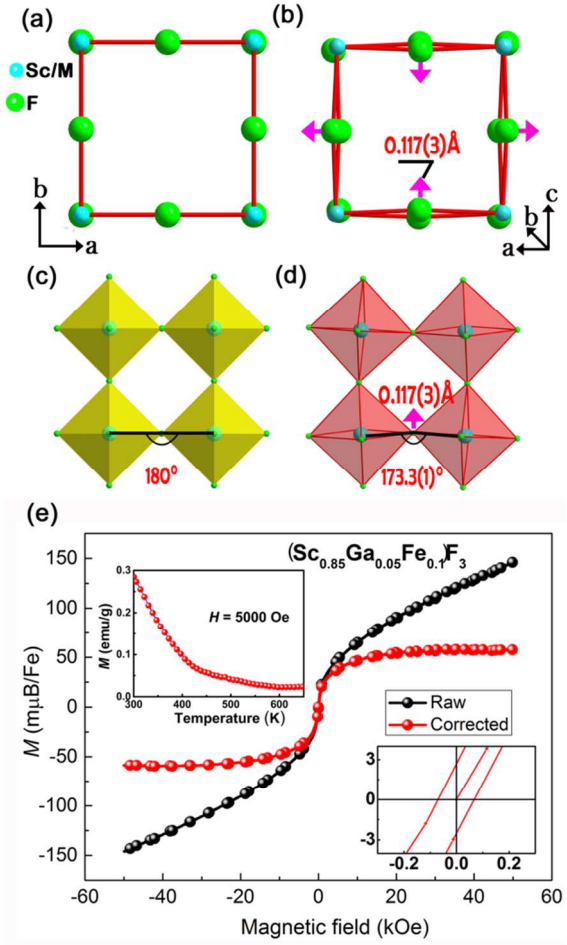

Fig. 53 (a) The cubic model, (b) the rhombohedral model in *cubic-like* form with purple arrows indicating static displacement of fluorine atoms, (c) ideal stacking (Sc,*M*)F_6 octahedra in the cubic model with the 180° angle of Sc/*M*-F-Sc/*M*, and (d) distorted stacking (Sc,*M*)F_6 octahedra in the rhombohedral model with the 173.3(1)° angle of Sc/*M*-F-Sc/*M* of $(Sc_{0.85}Ga_{0.05}Fe_{0.1})F_3$. (e) *M*–*H* curve of ZTE $(Sc_{0.85}Ga_{0.05}Fe_{0.1})F_3$ at room temperature. The inset at the top-left shows its *M*–*T* curve in *H* = 5000 Oe and the inset at the bottom-right displays H_c in the low magnetic region. The corrected *M*–*H* curve is calculated by the deduction of paramagnetic contribution. (Reprinted with permission from ref. 38. Copyright 2014, American Chemical Society.)

Additionally, it is interesting to note that ScF_3-based NTE materials can be functionalized to exhibit magnetic property due to the introduction of Fe ions. High-T_C ferromagnetic property was observed in $(Sc_{0.85}Ga_{0.05}Fe_{0.1})F_3$ (Fig. 53e), while those compositions without Fe, *e.g.*, ScF_3 and $(Sc_{0.95}Ga_{0.05})F_3$, show diamagnetic behaviour. The incorporation of Fe ions in $(Sc_{0.85}Ga_{0.05}Fe_{0.1})F_3$ demonstrates the introduction of magnetism. The magnetic moment decreases slowly and demonstrates a broader magnetic transition temperature span, leading to a T_C as high as ~435 K (the inset of Fig. 53f). In addition, considerable band gap narrowing also occurs in $(Sc_{0.85}Ga_{0.05}Fe_{0.1})F_3$ with a noticeable visible-light absorption and band gap value of ~1.88 eV, compared to the insulator ScF_3 (5.5~6.0 eV). [38]

7. Summary and outlook

After two decades studies on the topic of NTE, there has been good progress in aspects of finding new NTE materials, control of thermal expansion, and illuminating NTE mechanisms. A large amount of NTE materials have been found in various types of functional materials, such as ferroelectrics, magnetic materials, semiconductors, and superconductors. The NTE functional materials make up of an important branch of NTE family, which presents a general physical picture that there is a coupling role between physical properties and NTE. NTE in functional materials is a complex interplay between lattice, phonons, and electrons. In NTE ferroelectrics, NTE originates from ferroelectric order which occurs due to the strong hybridization between cations with oxygen. The behaviour of temperature-dependent P_S plays an important role in determining NTE of ferroelectrics. A new physical quantity of SVFS has been established, which is a linkage between ferroelectricity and NTE, and it can quantitatively describe the contribution of ferroelectricity to NTE. In NTE magnetics, the studies on NTE have a long history which traces back to the discovery of Invar alloys more than one century ago. There are a number of NTE magnetic solid compounds including alloys, oxides, nitrides, and sulfides. The underlying nature for NTE or anomalous thermal expansion in magnetics is the same, that is the coupling between magnetic order and lattice. The behaviour of temperature-dependent magnetic moment determines how NTE takes place. If we compare NTE behaviours in both ferroelectrics and magnetics, it is interesting to find that there is global nature which is valid for both ferroelectrics and magnetics. The NTE is determined by the order parameter of ferroelectric or magnetic transition. There are parallel physical parameters which are valid for NTE properties in both ferroelectrics and magnetics, like FVE in ferroelectrics vs. MVE in magnetics, and SVFS in ferroelectrics vs. SVMS in magnetics. In NTE functional materials with change of electron configuration, NTE has been found in semiconductors, Mott insulators, intersite charge transfer, superconductors and so on. All these NTE functional materials show a correlation between the specific physical properties with NTE. The NTE property of semiconductors could be adjusted by controlling free-electron concentration. The NTE property of Mott insulators could be controlled by modulating the metal-insulator transition. For those NTE functional materials induced from the temperature-induced intersite charge transfer, the NTE property can be controlled by modulating the amount of charge transfer. As for the NTE in superconductors, there is a coupling between the lattice strain and order parameter of the energy gap in the superconducting phase. Especially, iron-based superconducting materials exhibit a complex interplay between lattice, superconductivity, phonon, and magnetism. NTE occurs associated with various factors of superconducting T_C, magnetic phase, and specific layered structure. Thanks to the definite relationship between NTE and physical properties for these NTE functional materials, the thermal expansion can be well controlled by various chemical methods. Interestingly, a lot of materials have been found to exhibit the ZTE property, such as ZTE ferroelectrics, ZTE magnetics, and ZTE Mott-insulators.

Functional materials offer us a good opportunity to find new NTE compounds.

The control of thermal expansion is an important topic not only for fundamental studies but also practical applications of materials. According to the correlations between NTE and physical properties of functional materials, we can establish a multi-way to control thermal expansion (Fig. 54) through the coupling roles of ferroelectricity-NTE, magnetism-NTE, change of electron configuration-NTE, open-framework-NTE and so on. Any factor which can affect those physical properties could control the property of NTE. For example, the most commonly utilized method is by chemical substitution. The present progresses have proved that it is an effective method. The NTE of functional materials can be enhanced or weakened by the chemical substitution. For example, in PT-based ferroelectrics the NTE can be enhanced by selecting those ions with strong ferroelectric activity, or weakened by those ions with weak one. Other factors include particle size effect, defects, and external fields of pressure, magnetic and electric. For example, by applying pressure, NTE can be transformed to PTE in ferroelectric PT[140] and open-framework $(Sc,Y)F_3$,[38] ZTE to PTE in magnetic $Mn_{3-x}Cu_{0.5}Ge_{0.5}N$ nanocrystalline[179] and $Mn_3Zn_{0.93}N$,[177] and NTE becomes smeared in EuAuMg and GdAgMg ferromagnetic materials.[171] By applying magnetic field, the NTE temperature range of $ZnCr_2Se_4$ can be extended to lower temperature range. The effect of particle size can make a transformation between NTE and PTE through the coupling role as shown in Fig. 54, such as NTE-to-PTE in ferroelectric $0.7PT\text{-}0.3BiFeO_3$,[66] PTE-to-NTE in CuO[186] and Au,[191] and NTE-to-ZTE in magnetic $Mn_{3-x}Cu_{0.5}Ge_{0.5}N$.[179]

As shown in Fig. 54, it can be expected that NTE of functional materials could be simultaneously modulated by more coupling roles. For example, one can propose the control of NTE by both coupling roles of ferroelectrcity-NTE and magnetism-NTE in multiferroics. In principle, it could occur, since multiferroics simultaneously have ferroelectric and magnetic orders. However, in the available multiferroic systems, NTE is coupled either with ferroelectricity or magnetism, not really with multiferroic properties. The absence of coupling between NTE and multiferroic is due to the fact of either too weak ferroelectricity or magnetism. If ferroelectrcity and magnetism could be simultaneously enhanced, we could expect that NTE would be really tunable in multiferroics. The co-coupling role to NTE of functional materials is a new topic in future study, which would bring new phenomena and new mechanisms. It brings a challenge for chemists to find new compounds which have such co-coupling roles. The studies in this field will be important to not only solid state chemistry but also to solid state physics.

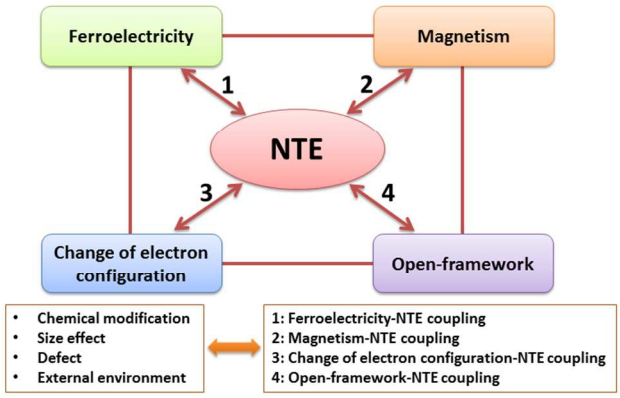

Fig. 54 Multi-way to control of NTE in functional materials.

For applications of NTE materials, one sometimes needs to functionalize NTE materials to have specific physical properties like electron conductivity, thermal conductivity, magnetism, and so on. Non-magnetic NTE materials can be functionalized to have magnetic properties by substitution of magnetic elements. For example, paramagnetic $CaRuO_3$ perovskite is transformed to NTE ferromagnetic $Ca(Ru_{0.85}Fe_{0.15})O_3$ by the substitution of Fe for Ru.[162] Ferromagnetic property exists in NTE or ZTE ferroelectric solids of $PT\text{-}Bi(Ni_{1/2}Ti_{1/2})O_3$ by the introduction of Ni into PT lattice.[70] After introduction of magnetic element of Fe into diamagnetic ScF_3, high-T_C ferromagnetic property is found in NTE or ZTE materials of $(Sc,Ga,Fe)F_3$.[38] Semiconductivity property occurs with a narrow band gap value of 1.88 eV for $(Sc,Ga,Fe)F_3$, while undoped ScF_3 shows insulator property (5.5−6.0 eV).[38] Furthermore, NTE material of ScF_3 is good potential candidate of matrix for phosphor due to the large indirect band gap. Lanthanide ions (Tb^{3+}, Eu^{3+}, Yb^{3+}, Tm^{3+}, Er^{3+} and Ho^{3+}) activated ScF_3 nanocrystals shows tunable luminescence properties, exhibiting multicolour ultraviolet, photoluminescence, cathodoluminescence, up-conversion luminescence.[322] Multifunctionalization in NTE materials is one of the important topic in future studies.

For future applications of NTE materials, there still exist some problems which have to be considered. For example, many Invar alloys with low or zero thermal expansion have been applied in various precise instruments. However, we must consider a negative factor of magnetostriction effect to the precision, if strong magnetic field exists. In such case, antiferromagnetic ZTE alloys are welcome and could extend the application of ZTE materials. One important purpose for the applications of NTE materials is proposed to be used as additive in composite. In such case, the pressure dependence of phase transition of NTE materials has to be considered. Most NTE materials with open-framework structure have structural instability under moderate pressure, resulting in undesirable phase transition. Such phase transition is detrimental to the NTE property of compensator, which commonly endure local pressure in composites. For example, ZrW_2O_8 shows irreversible phase transition at 0.2 GPa.[323] It is also true for

HfW_2O_8 (0.6 GPa), and $Zr_2WP_2O_{12}$ (1.4 GPa).[324,325] $(Sc,Y)F_3$ exhibits a large pressure dependence of CTE.[38] Ferroelectric PT loses its NTE at the critical pressure of 0.9 GPa.[140] New compounds are expected to be explored with the property that NTE is little or weakly sensitive to pressure.

NTE has gained a good progress after two decades development. Many NTE materials have been discovered. However, there still remain challenges and questions for the applications of NTE materials. Some interesting phenomena have been found, but worth further studies in the following fields: multifunctionalization in NTE materials, NTE in semiconductors and Mott-insulators, new NTE alloys better than Invar alloys, multi-way to control thermal expansion of functional materials, particle size effect on thermal expansion and so on. There remains a big challenge for chemists to find a "perfect" NTE material which behaves the merits of isotropic NTE, controllable CTE, functionalizable, easy fabrication, low price and so on. The studies on NTE functional materials will definitely promote the progress of NTE materials development.

Acknowledgements

The authors acknowledge the financial support from the National Natural Science Foundation of China (Grant Nos. 21322102, 91422301, 21231001), program for Changjiang Scholars and Innovative Research Team in University (IRT1207), and the Fundamental Research Funds for the Central Universities, China (FRF-TP-14-012C1). The authors thank the contribution to the section of NTE in antiperovskite Mn_3AN from Dr. Ying Sun who works in Department of Physics, Beihang University, China.

Notes and references

[a] Department of Physical Chemistry, University of Science and Technology Beijing, Beijing 100083, China.
Email: xing@ustb.edu.cn

1 T. A. Mary, J. S. O. Evans, T. Vogt and A. W. Sleight, *Science*, 1996, **72**, 90.
2 J. S. O. Evans, *J. Chem. Soc*., *Dalton Trans*., 1999, 3317.
3 A. W. Sleight, *Inorg. Chem.*, 1998, **37**, 2854.
4 M. J. Dejneka, C. L. Chapman and S. T. Misture, *J. Am. Ceram. Soc.*, 2011, **94**, 2249.
5 W. Miller, C. W. Smith, D. S. Mackenziek and E. Evans, *J. Mater. Sci.*, 2009, **44**, 5441.
6 G. D. Barrera, J. A. O. Bruno, T. H. K. Barron and N. L. Allan, *J. Phys.: Condens. Matter*, 2005, **17**, 217.
7 K. Takenaka, *Sci. Technol. Adv. Mater*., 2012, **13**, 013001.
8 P. Mohn, *Nature*, 1999, **400**, 18.
9 A. Atkinson, S. Barnett, R. J. Gorte, J. T. S. Irvine, A. J. Mcevoy, M. Ogensen, S. C. Singhal and J. Vohs, *Nat. Mater.*, 2004, **3**, 17.
10 R. H. Baughman, A. A. Zakhidov and W. A. de Heer, *Science*, 2002, **297**, 787.
11 M. Munro, *J. Am. Ceram. Soc.*, 1997, **80**, 1919.
12 D. R. Hummer, P. J. Heaney and J. E. Post, *Powder Diffr.*, 2007, **22**, 352.
13 X. R. Xing, J. Chen, J. X. Deng and G.R. Liu, *J. Alloy.Compd.*, 2003, **360**, 286.
14 E. Gruneisen, *Handb. Phys.*, 1926, **10**, 1.
15 F. Sayetat, P. Fertey and M. Kessler, *J. Appl. Cryst.*, 1998, **31**, 121.
16 R. Roy, D. K. Agrawal and H. A. McKinstry, *Annu. Rev. Mater. Sci.*, 1989, **19**, 59.
17 H. Miyazak, I. Ushiroda, D. Itomura, T. Hirashita, N. Adachi and T. Ota. *Jpn. J. Appl. Phys.*, 2008, **47**, 7262.
18 J. S. O. Evans, T. A. Mary and A. W. Sleight, *J. Solid State Chem*., 1998, **137**, 148.
19 C. E. Guillaume, *CR. Acad. Sci.*, 1897, **125**, 235.
20 K. Scheel, *Verh. Deutsch. Phys. Ges.*, 1907, **9**, 3.
21 K. Scheel, *Verh. Deutsch. Phys. Ges.*, 1907, **9**, 719.
22 F. A. Hummel, *Foote Prints*, 1948, **20**, 3.
23 F. A. Hummel, *J. Am. Ceram. Soc.*, 1951, **34**, 235.
24 (a) M. Blackman, *Proc. Phys. Soc.*, 1957, **B70**, 827. (b) T. H. K. Barron, *Ann. Phys.* (New York), 1957, **1**, 77.
25 M. T. Dove, V. Heine and K. D. Hammonds, *Miner. Mag.*, 1995, **59**, 629.
26 J. Z. Tao and A.W. Sleight, *J. Solid State Chem.*, 2003, **173**, 442.
27 P. Lightfoot, D. A. Woodcock, M. J. Maple, L. A. Villaescusa and P. A. Wright, *J. Mater. Chem.*, 2001, **11**, 212.
28 S. Margadonna, K. Prassides and A. N. Fitch, *J. Am. Chem. Soc.*, 2004, **126**, 15390.
29 D. Dubbeldam, K. S. Walton, D. E. Ellis and R. Q. Snurr, *Angew. Chem. Int. Ed.*, 2007, **119**, 4580.
30 N. Lock, Y. Wu, M. Christensen, L. J. Cameron, V. K. Peterson, A. J. Bridgeman, C. J. Kepert and B. B. Iversen, *J. Phys. Chem. C,* 2010, **114**, 16181.
31 H. Zhou, R. Lin, C. He, Y. Zhang, N. Feng, Q. Wang, F. Deng, J. Zhang and X. Chen, *Nat. Commun.*, 2013, **4**, 2534.
32 S. E. Tallentire, F. Child, I. Fall, L. Vella-Zarb, I. R. Evans, M. G. Tucker, D. A. Keen, C. Wilson and J. S. O. Evans, *J. Am. Chem. Soc.*, 2013, **135**, 12849.
33 B. K. Greve, K. L. Martin, P. L. Lee, P. J. Chupas, K. W. Chapman and A. P. Wilkinson, *J. Am. Chem. Soc.*, 2010, **132**, 15496.
34 J. P. Attfield, *Nature*, 2011, **480**, 465.
35 C. R. Morelock, L. C. Gallington and A. P. Wilkinson, *J. Solid State Chem.*, 2015, **222**, 96.
36 C. R. Morelock, L. C. Gallington and A. P. Wilkinson, *Chem. Mater*., 2014, **26**, 1936.
37 (a) L. Hu, J. Chen, L. L. Fan, J. X. Deng, R. B. Yu and X. R. Xing, *J. Am. Ceram. Soc.*, 2014, **97**, 1009. (b) L. Hu, J. Chen, Z. Pan, J. X. Deng, R. B. Yu and X. R. Xing, *J. Am. Ceram. Soc.*, 2014, **97**, 1386.
38 C. R. Morelock, B. K. Greve, L. C. Gallington, K. W. Chapman and A. P. Wilkinson. *J. Appl. Phys.*, 2013, **114**, 213501.
39 L. Hu, J. Chen, L. L. Fan, Y. Ren, Y. C. Rong, Z. Pan, J. X. Deng, R. B. Yu and X. R. Xing, *J. Am. Chem. Soc.*, 2014, **136**, 13566.
40 K. Rottger, A. Endriss, J. Ihringer, S. Doyle and W. F. Kuhs, *Acta Crystallogr. B*, 1994, **50**, 644.

41 S. M. Bennington, J. C. Li, M. J. Harris and D. K. Rose, *Physica B*, 1999, **263**, 396.
42 (a) L. M. Sullivan and C. M. Lukehart, *Chem. Mater.*, 2005, **17**, 2136; (b) C. Lind, M. R. Coleman, L. C. Kozy, G. R. Sharma, *Phys. Status Solidi B*, 2011, **248**, 123.
43 (a) C. Verdon and D. C. Dunand, *Scr. Mater.*, 1997, **36**, 1075; (b) H. Holzer and D. C. Dunand, *J. Mater. Res.*, 1999, **14**, 780; (c) S. Yilmaz, *J. Phys. Condens. Matter*, 2002, **14**, 365.
44 (a) K. Kanamori, T. Kineri, R. Fukuda, T. Kawano and K. Nishio, *J. Mater. Sci.*, 2009, **44**, 855; (b) M. Kofteros, S. Rodriguez, V. Tandon and L. E. Murr, *Scr. Mater.*, 2001, **45**, 369; (c) X. Yang, X. Cheng, X. Yan, J. Yang, T. Fu and J. Qiu, *Compos. Sci. Technol.*, 2007, **67**, 1167; (d) X. Yang, J. Xu, H. Li, X. Cheng and X. Yan, *J. Am. Ceram. Soc.*, 2007, **90**, 1953; (e) L. Sun and P. Kwon, *J. Am. Ceram. Soc.*, 2010, **93**, 703.
45 K. Uchino, S. Nomura, L. E. Cross, R. E. Newnham and S. J. Jang, *J. Mater. Sci.*, 1981, **16,** 569.
46 J. H. Kim and A. Manthiram. *Chem. Mater.*, 2010, **22**, 822.
47 S. Zhang and F. Yu, *J. Am. Ceram. Soc.*, 2011, **94**, 3153.
48 R. C. Wetherhold and J. Z. Wang, *Compos. Sci. Technol.*, 1995, **53**, 1.
49 C. Hunter, *Solder. Surf. Mt. Tech.*, 2005, **19**, 16.
50 R. J. Zeches, M. D. Rossel, J. X. Zhang, A. J. Hatt, Q. He, C. H. Yang, A. Kumar, C. H. Wang, A. Melville, C. Adamo, G. Sheng, Y. H. Chu, J. F. Ihlefeld, R. Erni, C. Ederer, V. Gopalan, L. Q. Chen, D. G. Schlom, N. A. Spaldin, L. W. Martin and R. Ramesh, *Science*, 2009, **326**, 977.
51 A. V. Pogrebnyakov, J. M. Redwing, S. Raghavan, V. Vaithyanathan, D. G. Schlom, S. Y. Xu, Q. Li, D. A. Tenne, A. Soukiassian, X. X. Xi, M. D. Johannes, D. Kasinathan, W. E. Pickett, J. S. Wu and J. C. H. Spence, *Phys. Rev. Lett.*, 2004, **93**, 147006.
52 J. P. Locquet, J. Perret, J. Fompeyrine, E. Mächler, J. W. Seo and G. Van Tendeloo, *Nature*, 1998, **394**, 453.
53 J. H. Lee, L. Fang, E. Vlahos, X. Ke, Y. W. Jung, L. F. Kourkoutis, J. W. Kim, P. J. Ryan, T. Heeg, M. Roeckerath, V. Goian, M. Bernhagen, R. Uecker, P. C. Hammel, K. M. Rabe, S. Kamba, J. Schubert, J. W. Freeland, D. A. Muller, C. J. Fennie, P. Schiffer, V. Gopalan, E. Johnston-Halperin and D.G. Schlom, *Nature*, 2010, **466**, 954.
54 J. H. Haeni, P. Irvin, W. Chang, R. Uecker, P. Reiche, Y. L. Li, S. Choudhury, W. Tian, M. E. Hawley, B. Craigo, A. K. Tagantsev, X. Q. Pan, S. K. Streiffer, L. Q. Chen, S. W. Kirchoefer, J. Levy and D. G. Schlom, *Nature*, 2004, **430**, 758.
55 D. G. Schlom, L. Q. Chen, C. J. Fennie, V. Gopalan, D. A. Muller, X. Pan, R. Ramesh and R. Uecker, *MRS Bull.*, 2014, **39**, 118.
56 J. Wang, J. B. Neaton, H. Zheng, V. Nagarajan, S. B. Ogale, B. Liu, D. Viehland, V. Vaithyanathan, D. G. Schlom, U. V. Waghmare, N. A. Spaldin, K. M. Rabe, M. Wuttig and R. Ramesh, *Science*, 2003, **299**, 1719.
57 G. H. Haertling, *J. Am. Ceram. Soc.*, 1999, **82**, 797.
58 X. R. Xing, J. X. Deng, J. Chen and G. R. Liu, *Rare Metals*, 2003, **22**, 294.
59 J. Chen, X. R. Xing, R. B. Yu and G. R. Liu, *J. Am. Ceram. Soc.*, 2005, **88** 1356.
60 J. Chen, X. R. Xing, R. B. Yu, and G. R. Liu, *Appl. Phys. Lett.*, 2005, **87**, 231915.
61 X. R. Xing, J. X. Deng, Z. Q. Zhu and G. R. Liu. *J. Alloy. Compd.*, 2003, **353**, 1.
62 P. H. Hu, Z. M. Cao, J. Chen, J. X. Deng, C. Sun, R. B. Yu and X. R. Xing, *Mater. Lett.,* 2008, **62**, 4585.
63 J. Chen, X. R. Xing, J. X. Deng and G. R. Liu, *J. Alloy. Compd*., 2004, **372**, 259.
64 A. Chandra, D. Pandey, M. D. Mathews and A. K. Tyagi, *J. Mater. Res.*, 2005, **20**, 350.
65 C. Sun, Z. M. Cao, J. Chen, R. B. Yu, X. Y. Sun, P. H. Hu, G. R. Liu and X. R. Xing, *Phys. Stat. Sol.*, (b) 2008 **245**, 2520.
66 J. Chen, X. R. Xing, G. R. Liu, J. H. Li and Y. T. Liu, *Appl. Phys. Lett*., 2006, **89**, 101914.
67 J. Chen, L. L. Fan, Y. Ren, Z. Pan, J. X. Deng, R. B. Yu and X. R. Xing, *Phys. Rev. Lett.*, 2013, **110**, 115901.
68 P. H. Hu, J. Chen, C. Sun, J. X. Deng and X. R. Xing, *J. Am. Ceram. Soc.*, 2011, **94**, 3600.
69 J. Chen, X. R. Xing, C. Sun, P. H. Hu, R. B. Yu, X. W. Wang and L. H. Li, *J. Am. Chem. Soc.*, **2008**, 130, 1144.
70 P. H. Hu, J. Chen, J. X. Deng and X. R. Xing, *J. Am. Chem. Soc.*, **2010**, *132*, 1925.
71 P. H. Hu, J. Chen, X. Y. Sun, J. X. Deng, X. Chen, R. B. Yu, L. J. Qiao and X. R. Xing, *J. Mater. Chem.*, 2009, **19**, 1648.
72 P. H. Hu, H. J. Kang, J. Chen, J. X. Deng and X. R. Xing, *J. Mater. Chem.*, 2011, **21**, 16205.
73 J. Chen, F. F. Wang, Q. Huang, L. Hu, X. P Song, J. X. Deng, R. B. Yu and X. R. Xing, *Sci. Rep.*, 2013, **3**, 2458.
74 J. S. Forrester, E. H. Kisi, K. S. Knight and C. J. Howard, *J. Phys. Condens. Matter*, 2006, **18**, 233.
75 P. Bonneau, P. Garnier, G. Calvarin, E. Husson, J. R. Cacarri, A. W. Hewat and A. Morell, *J. Solid State Chem.*, 1991, **91**, 350.
76 Y. Jiang, R. Guo and A. S. Bhalla, *J. Appl. Phys.*, 1998, **84**, 5140.
77 N. Sidorov, V. Mitrofanov, V. Kuznetsov, A. Gutsol, V. Kalinnikov and S. Stefanovich, *Ferroelectrics*, 1993, **144**, 223.
78 S. B. Qadri, J. A. Bellotti, A. Garzarella and D. H. Wu, *Appl. Phys. Lett.*, 2005, **86**, 251914.
79 A. S. Bhalla, R. Guo, L. E. Cross, G. Burns, F. H. Dacol and R. R. Neurgaonkar, *Phys. Rev. B*, 1987, **36**, 2030.
80 K. Lin, H. Wu, F. Wang, Y. Rong, J. Chen, J. Deng, R. Yu, L. Fang, Q. Huang and X. R. Xing, *Dalton Trans.*, 2014, **43**, 7037.
81 I. M. Shmyt'ko, N. S. Afonikova and V. I. Torgashev, *Phys. Solid State,* 2002, **44**, 2309.
82 A. Say, O. Mys, A. Grabar, Y. Vysochanskii and R. Vlokh, *Phase Transit.*, 2009, **82**, 531.
83 G. Shirane and S. Hoshino, *J. Phys. Soc. Jpn.*, 1951, **6**, 265.
84 (a) J. Kobayashi, Y. Uesu and R. Ueda., *Phys. Rev.*, 1955, **99**, 1900; (b) A. M. Glazer and S. A. Mabud, *Acta Crystallorgr. B.*, 1979, **34**, 1065. (c) S. A. Mabud and A. M. Glazer, *J. Appl. Cryst.,* 1979, **12**, 49.
85 D. Taylor, *Br. Ceram. Trans. J.*, 1985, **84**, 181.
86 G. Shirane, K. Suzuki and A. Takeda, *J. Phys. Soc. Jpn.*, 1952, **7**, 12.

87 C. Bedoya, Ch. Muller, J. L. Baudour, F. Bouree, J. L. Soubeyroux and M. Roubin, *J. Phys. Condens. Matter*, 2001, **13**, 6453.
88 C. Muller, J. L. Baudour, C. Bedoy, F. Bouree, J. L. Soubeyroux and M. Roubin, *Acta Crystallogr. B*, 2000, **56**, 27.
89 V. V. S. S. Sunder and A. M. Umarji, *Mater. Res. Bull.*, 1995, **30**, 427.
90 L. E. Cross, S. J. Jang, R. E. Newnham, S. Nomura and K. Uchino, *Frrroekectrics*, 1980, **23**, 187.
91 S. N. Gvasaliya, B. Roessli, D. Sheptyakov, S. G. Lushnikov and T. A. Shaplygina, *Eur. Phys. J. B*, 2004, **40**, 235.
92 S. A. Ivanova, S. G. Erikssonb, R. Tellgrend and H. Rundlöf, *Mater. Res. Bull.*, 2004, **39**, 2317.
93 S. Bhattacharjee, K. Taji, C. Moriyoshi, Y. Kuroiwa and D. Pandey, *Phys. Rev. B*, 2011, **84**, 104116.
94 V. Kothai, A. Senyshyn and R. Ranjan, *J. Appl. Phys.,* 2013, **113**, 084102.
95 G. Shirane and A. Takeda, *J. Phys. Soc. Jpn.*, 1952, **7**, 1.
96 V. Mueller, L. Jäger, H. Beige, H. P. Abicht and T. Müller, *Solid State Commun.*, 2004, **129**, 757.
97 I. M. Shmyt'ko, N. S. Afonikova and V. I. Torgashev, *Phys. Solid State,* 2002, **44**, 2165.
98 Y. J. Feng, Z. Xu and X. Yao, *Chinese Sci. Bull.*, 2002, **47**, 575.
99 P. Yang, M. A. Rodriguez, G. R. Burns, M. E. Stavig and R. H. Moore, *J. Appl. Phys.*, 2004, **95**, 3632.
100 G. Rujijanagul and T. Bongkarn, *Phase Transit.*, 2007, **80**, 209.
101 B. Noheda, J. A. Gonzalo, J. D. Frutos, A. Gonzalez and C. Moure, *J. Mater. Sci. Lett.*, 1997, **16**, 101.
102 L. E. Cross, *Ferroelectrics*, 1987, **76**, 241.
103 T. Maiti, R. Guo and A. S. Bhalla, *J. Am. Ceram. Soc.*, 2008, **91**, 1769.
104 S. Wongsaenmai, R. Yimnirun, S. Ananta, R. Guo and A. S. Bhalla, *Mater. Lett.*, 2008, **62**, 352.
105 R. Wongmaneerung, R. Guo, A. Bhalla, R. Yimnirun and S. Ananta, *J. Alloy. Compd.*, 2008, **461**, 565.
106 V. V. Shvartsman and D. C. Lupascu, *J. Am. Ceram. Soc.*, 2012, **95**, 1.
107 M. Gorev, I. Flerov, V. Bondarev, P. Sciau and J. M. Savariault, *J. Phys.: Condens. Matter*, 2004, **16**, 7143.
108 L. Seveyrat, M. Lemercier, B. Guiffard, L. Lebrun and D. Guyomar, *Ceram. Int.*, 2009, **35**, 45.
109 G. Shirane, R, Pepinsy and B. C. Frazer, *Acta Cryst.*, 1956, **9**, 131.
110 R. E. Cohen, *Nature*, 1992, **358**, 136.
111 Y. Kuroiwa, S. Aoyagi, A. Sawada, J. Harada, E. Nishibori, M. Takata and M. Sakata, *Phys. Rev. Lett.*, 2001, **87**, 217601.
112 R. E. Eitel, C. A. Randall, T. R. Shrout, P. W. Rehrig, W. Hackenberger and S. E. Park, *Jpn. J. Appl. Phys.,* 2001, **40**, 5999.
113 V. S. S. Sai Sunder, A. Halliyal and A. M. Umarji, *J. Mater. Res.*, 1995, **10**, 1301.
114 R. Duan, R. F. Speyer, E. Alberta and T. R. Shrout, *J. Mater. Res.*, 2004, **19**, 2185.
115 M. R. Suchomel and P. K. Davies, *Appl. Phys. Lett.*, 2005, **86**, 262905.
116 D. M. Stein, M. R. Suchomel and P. K. Davies, *Appl. Phys. Lett.*, 2006, **89**, 132907.
117 J. Chen, X. L. Tan, W. Jo and J. Rödel, *J. Appl. Phys.*, 2009, **106**, 034109.
118 L. X. Zhang, J. Chen, H. Q. Zhao, L. L. Fan, Y. C. Rong, J. X. Deng, R. B. Yu and X. R. Xing. *Appl. Phys. Lett.*, 2013, **103**, 082902.
119 J. Chen, K. Nittala, J. L. Jones, P. H. Hu and X. R. Xing, *Appl. Phys. Lett*., 2010, **96**, 252908.
120 I. Grinberg and A. M. Rappe, *Phys. Rev. Lett.*, 2007, **98,** 037603.
121 I. Grinberga, M. R. Suchomel, P. K. Davies and A. M. Rappe , *J. Appl. Phys.*, 2005, **98**, 094111.
122 I. Grinberg, M. R. Suchomel, W. Dmowski, S. E. Mason, H. Wu, P. K. Davies and A. M. Rappe, *Phys. Rew. Lett.*, 2007, **98,** 107601.
123 T. T. Qi, I. Grinberg and A. M. Rappe，*Phys. Rew. B*, 2010, **82**, 134113.
124 I. Grinberg and A. M. Rappe. *Phase Transit.*, 2007, **80**, 351.
125 J. Chen, X. Y. Sun, J. X. Deng, Y. Zu, Y. T. Liu, J. H. Li and X. R. Xing, *J. Appl. Phys.*, **105**, 044105.
126 M. Yashima, K. Omoto, J. Chen, H. Kato and X. R. Xing. *Chem. Mater.*, 2011, **23**, 3135.
127 S. V. Halilov, M. Fornari and D. J. Singh, *Phys. Rev. B*, 2004, **69**, 174107.
128 J. Chen, P. H. Hu, X. Y. Sun and C. Sun, *Appl. Phys. Lett.*, 2007, **91**, 171907.
129 F. F. Wang, L. L. Fan, Y. Ren, J. Chen and X. R. Xing, *Appl. Phys. Lett.*, 2014, **104**, 252901.
130 A. A. Belik, M. Azuma, T. Saito, Y. Shimakawa and M. Takano, *Chem. Mater.,* 2005, **17***,* 269.
131 A. A. Belik, S. Iikubo, K. Kodama, N. Igawa, S. Shamoto, S. Niitaka, M.Azuma, Y. Shimakawa, M. Takano, F. Izumi and E. Takayama-Muromachi, *Chem. Mater.*, 2006**, 18***,* 798.
132 M. R. Suchomel, A. M. Fogg, M. Allix, H. Niu, J. B. Claridge and M. J. Rosseinsky, *Chem. Mater.*, 2006**, 18***,* 4987.
133 M. A. Khan, T. P. Comyn and A. J. Bell, *Appl. Phys. Lett.,* 2007, **91**, 032901.
134 L. X. Zhang, J. Chen, H. Q. Zhao, L. L. Fan, Y. C. Rong, J. X. Deng, R. B. Yu and X. R. Xing, *Dalton Trans.*, 2013, **42**, 585.
135 A. A. Belik, *J. Solid State Chem.*, 2012, **195**, 32.
136 S. C. Abrahams, S. K. Kurtz and P. B. Jamieson, *Phys. Rev*., 1968, **172**, 551.
137 N. Nakajima, Y. Yamamura and T. Tsujia, *Solid State Commun.*, 2003, **128**, 193.
138 T. Suzuki and A. Omote, *J. Am. Ceram. Soc.*, 2006, **89**, 691.
139 J. L. Zhu, H. W. Xu, J. Z. Zhang, C. Q. Jin, L. P. Wang and Y. S. Zhao, *J. Appl. Phys*., 2011, **110**, 084103.
140 J. L. Zhu, J. Z. Zhang, H. W. Xu, S. C. Vogel, C. Q. Jin, J. Frantti and Y. S. Zhao, *Sci. Rep*., 2014, **4**, 3700.
141 A. M. Glazer and S. A. Mabud, *Acta Crystallogr. B*, 1978, **34**, 1065.
142 J. Chen, K. Nittala, J. S. Forrester, J. L. Jones, J. X. Deng, R. B. Yu and X. R. Xing, *J. Am. Chem. Soc.*, 2011, **133**, 11114.
143 Y. He, *Thermochim. Acta*, 2004, **419**, 135.
144 S. C. Costa, P. S. Pizani, J. P. Rino and D. S. Borges, *J. Phys.: Condens. Matter*, 2005, **17**, 5771.
145 F. F. Wang, Y. Xie, J. Chen, H. G. Fu and X. R. Xing, *Appl. Phys. Lett.*, 2013, **103**, 221901.

146 L. Wang, P. F. Yuan, F. Wang, E. J. Liang, Q. Sun, Z. X. Guo and Y. Jia, *Mater. Res. Bull.*, 2014, **49**, 509.
147 H. Fang, Y. Wang, S. Shang and Z.-K. Liu, *Phys. Rev. B*, 2015, **91**, 024104.
148 F. F. Wang, Y. Xie, J. Chen, H. G. Fu and X. R. Xing, *Phys. Chem. Chem. Phys.*, 2014, **16**, 5237.
149 R. J. Weiss, *Proc. Phys. Soc.*, 1963, 82281.
150 A. Fujita, K. Fukamichi, J. T. Wang and Y. Kawazoe, *Phys, Rev. B*, 2003, **68**, 104431.
151 Y. Takahashi and H. Nakano, *J. Phys.: Condens. Matter,* 2006, **18**, 521.
152 (a) R. Minakata, M. Shiga and Y. Nakamura, *J. Phys. Soc. Jpn*, 1976, **41**, 1435; (b) H. Nakamura, H. Wada, K. Yoshimura, M. Shiga, Y. Nakamura, J. Sakurai and Y. Komura, *J. Phys. F: Met. Phys.*, 1988, **18**, 981.
153 Y. M. Hao, X. M. Zhang, B. W. Wang, Y. Z. Yuang and F. Wang, *J. Appl. Phys.*, 2010, **108**, 023915.
154 P. Álvarez-Alonso, P. Gorria, J. A. Blanco, J. Sánchez-Marcos, G. J. Cuello, I. Puente-Orench, J. A. Rodríguez-Velamazán, G. Garbarino, I. de Pedro, J. R. Fernández and J. L. Sánchez Llamazares, *Phys. Rev. B*, 2012, **86**, 184411.
155 D. Givord and R. Lemaire, *IEEE T. Magn.*, 1974, **10**, 109.
156 A. V. Andreev, F. R. de Boer, T. H. Jacobs and K. H. J. Buschow, *Physica B*, 1991, **175**, 361.
157 R. J. Huang, Y. Liu, W. Fan, J. Tan, F. Xiao, L. Qian and L. Li, *J. Am. Chem. Soc.*, 2013, **135**, 11469.
158 C. Fukarnichi, T. H. Chiang, E. Matsubara and Y. Waseda, *Sci. Rep. RITU*, 1995, **A41**, 9.
159 K. H. J. Buschow and R. Grössinger, *J. Less-Common Met.*, 1987, **135**, 39.
160 N. Yang, K. W. Dennis, R. W. McCallum, M. J. Kramer, Y. Zhang and P. L. Lee, *J. Magn. Magn. Mater.*, 2005, **295**, 65.
161 T. Kiyama, K. Yoshimura, K. Kosuge Y. Ikeda and Y. Bando. *Phys. Rev. B*, 1996, **54**, 756.
162 T. Taniguchi, S. Mizusaki, N. Okada, Y. Nagata, K. Mori, T. Wuernisha, T. Kamiyama, N. Hiraoka, M. Itou, Y. Sakurai, T. C. Ozawa, Y. Noro and H. Samata, *Phys. Rev. B*, 2007, **75**, 024414.
163 S. Khmelevskyi, I. Turek and P. Mohn, *Phys, Rev. Lett.*, 2003, **91**, 037201.
164 E. F. Wassermann, *Warrtsndale, PA: The Minerals, Metals and Materials Society*, 1997, 6374.
165 E. F. Wasserman, *Ferromagnetic Materials*, ed. K. H. J. Buschow and E. P. Wohlfartht, Elsevier Science Publishers B.V. 1990, vol. 5, ch. 3, pp. 238-322.
166 P. A. Algarabel and M. R. Ibarra, *J. Magn. Magn. Mater.*, 1992, **110**, 323.
167 Y. Hao, F. Liang, X. Zhang, F. Wang and Y. Wu, *J. Rare Earth.*, 2011, **29**, 772.
168 Y. M. Hao, M. Tan, W. Wang and F. Wang, *Chinese. Phys. B*, 2010, **19**, 067502.
169 M. Shiga and Y. Nakamura, *J. Phys. Soc. Jpn.*, 1979, **47**, 1446.
170 H. Wada and M. Shii, *J. Magn. Magn. Mater.*, 1992, **104**, 1925.
171 J. Rohrkamp, O. Heyer, T. Fickenscher, R. Pöttgen, S. Jodlauk, H. Hartmann, T. Lorenz and J. A. Mydosh, *J. Phys.: Condens. Matter*, 2007, **19**, 486204.
172 K. Takenaka and H. Takagi, *Appl. Phys. Lett.*, 2005, **87**, 261902.
173 K. Takenaka, K. Asano, M. Misawa and H. Takagi, *Appl. Phys Lett.*, 2008, **92**, 011927.
174 Y. Sun, C. Wang, Y. C. Wen, L. H. Chu, H. Pan, M. Nie and M. B. Tang, *J. Am. Ceram. Soc.*, 2010, **93**, 2178.
175 R. J. Huang, L. F. Li, F. S Cai, X. D Xu and L.H Qian, *Appl. Phys. Lett.*, 2008, **93**, 081902.
176 T. Hamada and K. Takenaka, *J. Appl. Phys.*, 2011, **109**, 07E309.
177 K. Takenaka and H. Takagi, *Appl. Phys. Lett.*, 2009, **94**, 131904.
178 C. Wang, L. H. Chu, Q. R. Yao, Y. Sun, M. M. Wu, L. Ding, J. Yan, Y. Y. Na, W. H. Tang, G. N. Li, Q. Huang and J. W. Lynn, *Phys. Rev. B,* 2012, **85**, 220103.
179 X. Y. Song, Z. H. Sun, Q. Huang, M. Rettenmayr, X. M. Liu, M. Seyring, G. N. Li, G. H. Rao and F. X. Yin, *Adv. Mater.*, 2011, **23**, 4690.
180 S. P. Singh, D. Pandey, S. Yoon, S. Baik and N. Shin, *Appl. Phys. Lett.*, 2007, **90**, 242915.
181 R. V. Demin, L. I. Korolevaa, R. V. Privezentsev and N. A. Kozlovskaya, *Phys. Lett. A*, 2004, **325**, 426.
182 J. L. Garcia-Mufioz, M. Suaaidi and C. Ritter, *Physica B*, 1997, **234**, 854.
183 H. Zhang, R. Flacau, J. L. Sun, G. B. Li, F. H. Liao and J. H. Lin, *Inorg. Chem.*, 2014, **53**, 4535.
184 R. Saha, A. Shireen, A. K. Bera, S. N. Shirodka, Y. Sundarayya, N. Kalarikkal, S. M. Yusuf, U. V. Waghmare, A. Sundaresan and C. N. R. Rao, *J. Solid State Chem.*, 2011, **184**, 494.
185 O. Volkova, Y. Arango, N. Tristan, V. Kataev, E. Gudilin, D. Meier, T. Lorenz, B. Büchner and A. Vasil'ev, *JETP Lett.*, 2005, **82**, 444.
186 X. G. Zheng, H. Kubozono, H. Yamada, K. Kato, Y. Ishiwata and C. N. Xu, *Nat. Nanotechnol.*, 2008, **3**, 724.
187 S. Kitani, M. Tachibana, N. Taira and H. Kawaji, *Phys. Rev. B*, 2013, **87**, 064402.
188 J. Hemberger, H. A. Krug von Nidda, V. Tsurkan and A. Loidl, *Phys. Rev. Lett.*, 2007, **98**, 147203.
189 V. Tsurkan, D. Ehlers, V. Felea, H. A. Krug von Nidda and A. Loidl, *Phys. Rev. B*, 2013, **88**, 144417.
190 B. A. Hunter, B. J. Kennedy and T. Vogt, *Phys. Rev. B*, 2004, **69**, 020410.
191 W. H. Li, S. Y. Wu, C. C. Yang, S. K. Lai, K. C. Lee, H. L. Huang and H. D. Yang, *Phys. Rev. Lett.*, 2002, **89**, 135504.
192 R. J. Weiss, *Proc. Phys. Soc. London*, 1963, **82**, 281.
193 M. Schilfgaarde, I. A. Abrikosov and B. Johansson, *Nature*, 1999, **400**, 46.
194 E. F. Wassermann, *J. Magn. Magn. Mater.*, 1991, **100**, 346.
195 M. Shiga, *Curr. Opin. Solid St. M.*, 1996, **1**, 340.
196 A. G. Kuchin, I. V. Medvedeva, V. S. Gaviko, V. A. Kazantsev, *J. Alloy. Compd.*, 1999, **289**, 18.
197 P. Álvare, P. Gorria, J. S. Marcos, I. P. Orench, J. A. R. Velamazán, G. Cuello, J. L. S. Llamazares and J. A. Blanco, *J. Phys.: Conf. Ser.,* 2011, **325**, 012011.

198 X. Ze, Y. Ishikawa, S. Ishio and M. Takahashi, *J. Phys. F*, 1985, **15**, 1787.
199 A. Fujita, T. Suzuki, N. Kataoka and K. Fukamiihi, *Phys. Rev. B*, 1994, **50**, 6199.
200 K. Fukamiii and H. Saito, *Phys Status Solidi A-Appl. Res.*, 1972, **10**, 129.
201 H. Masumoto, M. Kikuchi and T. Nakayarna, *Meter. Trans. JIM*, 1963, **24**, 42.
202 Y. Nakamura, *J. Magn. Magn. Mater.*, 1983, **31**, 829.
203 A. V. Andreev and A. Lindbaum, *J. Alloy. Compd.*, 2000, **297**, 43.
204 P. Gorria, P. Álvarez-Alonso, J. Sánchez-Marcosb, J. L. Sánchez Llamazaresa, M. J. Pérezav and J. A. Blancoa, *Acta Mater.*, 2009, **57**, 1724.
205 N. Yang, K. W. Dennis, R. W. McCallum, M. J. Kramer, Y. Zhang and P. L. Lee, *J. Magn. Magn. Mater.*, 2007, **311**, 630.
206 D. Sanavi Khoshnoud, N. Tajabor and F. Pourarian, *J. Alloy. Compd.*, 2012, **537**, 106.
207 Y. M. Hao, L. An, J. Guo and K. Lu, *J. Chinese Ceram. Soc.*, 2009, **37**, 715.
208 Y. M. Hao, Y. Zhou and M. Zhao, *J. Appl. Phys.*, 2005, **97**, 116102.
209 J. L. Wang, S. J. Campbell, O. Tegus, C. Marquina and M. R. Ibarra, *Phys. Rev. B*, 2007, **75**, 174423.
210 Y. M. Hao, Y. Zhou and M. Zhao, *Adv. Eng. Mater.*, 2005, **7**, 517.
211 L. Jia, J. R. Sun, H. W. Zhang, F. X. Hu, C. Dong and B. G. Shen, *J. Phys.: Condens. Matter*, 2006, **18**, 9999.
212 Z. Gu and W. Y. Ching, *Phys. Rev. B*, 1987, **36**, 8530.
213 I. S. Dubenko, S. A. Granovskiy, E. Gratz, R. Z. Levitin, A. Lindbaum and A. S. Markosyan, *J. Magn. Magn. Mater.*, 1996, **157**, 629.
214 A. de Visser, K. Bakker and J. Pierre, *Physica B*, 1993, **186**, 577.
215 F. G. Aliev, R. Villar, S. Vieira, M. A. Lopez de la Torre, R. V. Scolozdra and M. B. Maple, *Phys. Rev. B*, 1993, **47**, 769.
216 G. K. White, *J. Phys.: Condens. Matter*, 1989, **1**, 6987.
217 G. W. Wiener and J. A. Berger, *Trans. AIME.* 1955, **203**, 360.
218 P. Tong, B. S. Wang and Y. P. Sun, *Chinese Phys. B,* 2013, **22**, 067501.
219 Y. Sun, C. Wang, Y. C. Wen, K. G. Zhu and J. T. Zhao, *Appl. Phys. Lett.*, 2007, **91**, 231913.
220 K. Takenaka, M. Ichigo, T. Hamada, A. Ozawa, T. Shibayama, T. Inagaki and K. Asano, *Sci. Technol. Adv. Mater.*, 2014, **15**, 015009.
221 W. S. Kim, E. O. Chi, J. C. Kim, N. H. Hur, K. W. Lee and Y. N. Choi, *Phys. Rev. B*, 2003, **68**, 172402.
222 Y. Sun, C. Wang, Y. C. Wen, L. H. Chu, M. Nie and F. S. Liu, *J. Am. Ceram. Soc.*, 2010, **93**, 650.
223 S. Iikubo, K. Kodama, K. Takenaka, H. Takagi, and S. Shamoto, *Phys. Rev. B*, 2008, **77**, 020409.
224 S. Iikubo, K. Kodama, K. Takenaka, H. Takagi, M. Takigawa and S. Shamoto, *Phys. Rev. Lett.*, 2008, **101**, 205901.
225 P. Tong, D. Louca, G. King, A. Llobet, J. C. Lin and Y. P. Sun, *Appl. Phys. Lett.*, 2013, **102**, 041908.
226 J. Matsuno, K. Takenaka, H. Takagi, D. Matsumura, Y. Nishihata and J. Mizuki, *Appl. Phys. Lett.*, 2009, **94**, 181904.
227 J. P. Jardin and J. Labbe, *J. Solid State Chem.*, 1983, **46**, 275.
228 K. Kodama, S. Iikubo, K. Takenaka, M. Takigawa, H. Takagi, and S. Shamoto, *Phys. Rev. B*, 2010, **81**, 224419.
229 Q. Huang, A. Santoro, J. W. Lynn, R. W. Erwin, J. A. Borchers, J. L. Peng and R. L. Greene, *Phys. Rev. B*, 1997, **55**, 14987.
230 T. Chatterji, F. Fauth, B. Ouladdiaf, P. Mandal and B. Ghosh, *Phys. Rev. B*, 2003, **68**, 052406.
231 T. Chatterji, D. Riley, F. Fauth, P. Mandal and B. Ghosh, *Phys. Rev. B*, 2006, **73**, 094444.
232 T. Chatterjia, B. Ouladdiafa, P. Mandalc and B. Ghosh, *Solid State Commun.*, 2004, **131**, 75.
233 B. Dabrowski, M. Avdeev, O. Chmaissem, S. Kolesnik, P. W. Klamut, M. Maxwell and J. D. Jorgensen, *Phys. Rev. B*, 2005, **71**, 104411.
234 G. L. Harding, P. C. Lanchester and R. Street, *J. Phys. C: Solid State Phys.*, 1971, **4**, 2923.
235 C. R. Kmety, J. L. Manson, Q. Huang, J. W. Lynn, R. W. Erwin, J. S. Miller and A. J. Epstein, *Phys. Rev. B*, 1999, **60**, 60.
236 X. L. Chen, Z. R. Yang, W. Tong, Z. H. Huang, L. Zhang, S. L. Zhang, W. H. Song, L. Pi, Y. P. Sun, M. L. Tian and Y. H. Zhang, *J. Appl. Phys.*, 2014, **115**, 083916.
237 F. Yokaichiya, A. Krimmel, V. Tsurkan, I. Margiolaki, P. Thompson, H. N. Bordallo, A. Buchsteiner, N. Stüßer, D. N. Argyriou and A. Loidl, *Phys. Rev. B*, 2009, **79**, 064423.
238 M. Tachibana, N. Taira, H. Kawaji, *Solid State Commun.*, 2011, **151**, 1776.
239 J. Hemberger, P. Lunkenheimer, R. Fichtl, H. A. Krug von Nidda, V. Tsurkan and A. Loidl, *Nature*, 2005, **434**, 364.
240 A. L. Goodwin, *Nat. Nanotechnol*. 2008, **3**, 711.
241 K. V. Zakharchenko, M. I. Katsnelson and A. Fasolino, *Phys. Rev. Lett.*, 2009, **102**, 046808.
242 C. Y. Li, C. M. Wu, S. K. Karna, C. W. Wang, D. Hsu, C. J. Wang and W. H. Li, *Phys. Rev. B*, 2011, **83**, 174446.
243 P. Badrinarayanan, Md. I. Ahmad, M. Akinc and M. R. Kessler, *Mater. Chem. Phys.,* 2011, **131**, 12.
244 L. Li, Y. Zhang, Y. W. Yang, X. H. Huang, G. H. Li and L. D. Zhang, *Appl. Phys. Lett.,* 2005, **87**, 031912.
245 Y. Yamamoto, T. Miura, M. Suzuki, N. Kawamura, H. Miyagawa, T. Nakamura, K. Kobayashi, T. Teranishi and H. Hori, *Phys. Rev. Lett.*, 2006, **93**, 139902.
246 J. D. Bucci, B. K. Robertson and W. J. James, *J. Appl. Cryst.*, 1972, **5**, 187.
247 C. H. Xu, C. Z. Wang, C. T. Chan and K. M. Ho, *Phys. Rev. B*, 1991, **43**, 5024.
248 M. Leszczynski, V. B. Pluzhnikov, A. Czopnik, J. Bak-Misiuk, T. Slupinski, *J. Appl. Phys.*,1997, **82**, 4678.
249 T. F. Qi, O. B. Korneta, S. Parkin, L. E. De Long, P. Schlottmann and G. Cao, *Phys. Rev. Lett.*, 2010, **105**, 177203.
250 T. F. Qi, O. B. Korneta, S. Parkin, J. Hu and G. Cao, *Phys. Rev. B*, 2012, **85**, 165143.
251 Y. W. Long, N. Hayashi, T. Saito, M. Azuma, S. Muranaka and Y. Shimakawa, *Nature*, 2009, **458**, 60.
252 M. Azuma, W. Chen, H. Seki, M. Czapski, S. Olga, K. Oka, M. Mizumaki, T. Watanuki, N. Ishimatsu, N. Kawamura, S. Ishiwata, M.

G. Tucker, Y. Shimakawa and J. P. Attfield. *Nat. Commun.*, 2011, **2**, 347.

253 N. V. Anshukova, B. M. Bulychev, A. I. Golovashkin, L. I. Ivanova, I. B. Krynetskii, A. A. Minakov and A. P. Rusakov, *J. Exp. Theor. Phys.*, 2003, **97**, 70.

254 J. J. Neumeier, T. Tomita, M. Debessai, J. S. Schilling, P. W. Barnes, D. G. Hinks and J. D. Jorgensen, *Phys. Rev. B*, 2005, **72**, 220505.

255 S. L. Bud'fko, N. Ni, S. Nandi, G. M. Schmiedeshoff and P. C. Canfield, *Phys. Rev. B*, 2009, **79**, 054525.

256 T. Klimczuk, H. C. Walker, R. Springell, A. B. Shick, A. H. Hill, P. Gaczyński, K. Gofryk, S. A. J. Kimber, C. Ritter, E. Colineau, J. C. Griveau, D. Bouëxière, R. Eloirdi, R. J. Cava and R. Caciuffo, *Phys. Rev. B*, 2012, **85**, 174506.

257 S. A. J. Kimber, D. N. Argyriou, F. Yokaichiya, K. Habicht, S. Gerischer, T. Hansen, T. Chatterji, R. Klingeler, C. Hess, G. Behr, A. Kondrat and B. Büchner, *Phys. Rev. B*, 2008, **78**, 140503.

258 A. Rebello, J. J. Neumeier, Z. Gao, Y. Qi and Y. Ma, *Phys. Rev. B*, 2012, **86**, 104303.

259 A. Pandey, D. G. Quirinale, W. Jayasekara, A. Sapkota, M. G. Kim, R. S. Dhaka, Y. Lee, T. W. Heitmann, P. W. Stephens, V. Ogloblichev, A. Kreyssig, R. J. McQueeney, A. I. Goldman, A. Kaminski, B. N. Harmon, Y. Furukawa and D. C. Johnston, *Phys. Rev. B*, 2013, **88**, 014526.

260 Z. J. Yang, M. Yewondwossen, D. W. Lawther, S. P. Ritcey, D. J. W. Geldart and R. A. Dunlap, *J. Supercond.*, 1995, **8**, 233.

261 S. V. Pryanichnikov, S. G. Titova, G. A. Kalyuzhnaya, Yu. I. Gorina and P. A. Slepukhin, *J. Exp. Theor. Phys.*, 2008, **107**, 69.

262 J. D. Jorgensen, D. G. Hinks, P. G. Radaelli, W. I. F. David and R. M. Ibberson, *arXiv:cond-mat/0205486*, 2002.

263 P. A. Alekseev, J. M. Mignot, E. V. Nefeodova, K. S. Nemkovski, V. N. Lazukov, N. N. Tiden, A. P. Menushenkov, R. V. Chernikov, K. V. Klementiev, A. Ochiai, A. V. Golubkov, R. I. Bewley, A. V. Rybina and I. P. Sadikov, *Phys. Rev. B,* 2006, **74**, 035114.

264 J. Arvanitidis, K. Papagelis, S. Margadonna, K. Prassides and A. N. Fitch, *Nature*, 2003, **425**, 599.

265 S. Margadonna, K. Prassides, M. Chondroudi, J. R. Salvadorc and M. G. Kanatzidis, *Chem. Commun.*, 2005, 5754.

266 W. Miiller, M. Avdeev, Q. Zhou, B. J. Kennedy, N. Sharma, R. Kutteh, G. J. Kearley, S. Schmid,K. S. Knight, P. E. R. Blanchard and C. D. Ling, *J. Am. Chem. Soc.*, 2012, **134**, 3265.

267 W. C. M. Mattens, H. Holscher, G. J. M. Tuin, A. C. Molenan and F. R. de Boerthermal, *J. Magn. Magn. Mater.*, 1980, **15**, 982.

268 B. Kindler, D. Finsterbusch, R. Graf, F. Ritter, W. Assmus and B. Luthi, *Phys. Rev. B*, 1994, **50**, 704.

269 R. Schefzyk, F. Steglich, T. Penney and F. Holtzberg, *J. Magn. Magn. Mater.*, 1986, **54**, 341.

270 A. Jayaraman, E. Bucher, P. D. Dernier and L. D. Longinotti, *Phys. Rev. Lett.*, 1973, **31**, 700.

271 I. Yamada, K. Shiro, H. Etani, S. Marukawa, N. Hayashi, M. Mizumaki, Y. Kusano, S. Ueda, H. Abe and T. Irifune, *Inorg. Chem.*, 2014, **53**, 10563.

272 I. Yamada, K. Tsuchida, K. Ohgushi, N. Hayashi, J. Kim, N. Tsuji, R. Takahashi, M. Matsushita, N. Nishiyama, T. Inoue, T. Irifune, K. Kato, M. Takata and M. Takano, *Angew. Chem. Int. Ed.*, 2011, **50**, 6579.

273 Y. Long, T. Saito, T. Tohyama, K. Oka, M. Azuma and Y. Shimakawa, *Inorg. Chem.*, 2009, **48**, 8489.

274 I. Yamada, H. Etani, K. Tsuchida, S. Marukawa, N. Hayashi, T. Kawakami, M. Mizumaki, K. Ohgushi, Y. Kusano, J. Kim, N. Tsuji, R. Takahashi, N. Nishiyama, T. Inoue, T. Irifune and M. Takano, *Inorg. Chem.*, 2013, **52**, 13751.

275 H. Etani, I. Yamada, K. Ohgushi, N. Hayashi, Y. Kusano, M. Mizumaki, J. Kim, N. Tsuji, R. Takahashi, N. Nishiyama, T. Inoue, T. Irifune and M. Takano, *J. Am. Chem. Soc.*, 2013, **135**, 6100.

276 K. Oka, M. Mizumaki, C. Sakaguchi, A. Sinclair, C. Ritter, P. Attfield and M. Azuma, *Phys. Rev. B*, 2013, **88**, 014112.

277 S. Ishiwata, M. Azuma, M. Hanawa, Y. Moritomo, Y. Ohishi, K. Kato, M. Takata, E. Nishibori, M. Sakata, I. Terasaki and M. Takano, *Phys. Rev. B*, 2005, **72**, 045104.

278 K. Oka, K. Nabetani, C. Sakaguchi, H. Seki, M. Czapski, Y. Shimakawa and M. Azuma, *Appl. Phys. Lett.*, 2013, **103**, 061909.

279 S. Margadonna, J. Arvanitidis, K. Papagelis and K. Prassides, *Chem. Mater.*, 2005, **17***,* 4474.

280 Y. Yamanari, Y. Suzuki, K. Imai, E. Shikoh, A. Fujiwara, N. Kawasaki, N. Ikeda, Y. Kubozono and T. Kambe, *Phys. Rev. B*, 2011, **83**, 245103.

281 J. R. Salvador, F. Guo, T. Hogan and M. G. Kanatzidis, *Nature*, 2003, **425**, 702.

282 S. Margadonna, K. Prassides, A. N. Fitch, J. R. Salvador and M. G. Kanatzidis, *J. Am. Chem. Soc.*, 2004, **126**, 4498.

283 S. Bobev, D. J. Williams, J. D. Thompson and J. L. Sarrao, *Solid State Commun.*, 2004, **131**, 431.

284 Y. Janssen, S. Chang, B. K. Cho, A. Llobet, K. W. Dennis, R. W. McCallum, R. J. McQueeney and P. C. Canfield, *J. Alloy. Compd.*, 2005, **389**, 10.

285 F. R. Drymiotis, Y. Lee, G. Lawes, J. C. Lashley, T. Kimura, S. M. Shapiro, A. Migliori, V. Correa and R. A. Fisher, *Phys. Rev. B*, 2005, **71**, 174304.

286 C. H. Booth, A. D. Christianson, J. M. Lawrence, L. D. Pham, J. C. Lashley and F. R. Drymiotis, *Phys. Rev. B*, 2007, **75**, 012301.

287 B. P. Doyle, E. Carleschi, E. Magnano, M. Malvestuto, A. A. Dee, A. S. Wills, Y. Janssen and P. C. Canfield, *Phys. Rev. B*, 2007, **75**, 235109.

288 G. K. White, *Cryogenics*, 1962, **2**, 292.

289 H. Fujishita, Y. Hayashi, M. Saito, H. Unno, H. Kaneko, H. Okamoto, M. Ohashi, Y. Kobayashi and M. Sato, *Eur. Phys. J. B*, 2012, **85**, 52.

290 M. S. da Luz, J. J. Neumeier, R. K. Bollinger, A. S. Sefat, M. A. McGuire, R. Jin, B. C. Sales and D. Mandrus, *Phys. Rev. B*, 2009, **79**, 214505.

291 H. Fujishita, S. Murakami, N. Nakamura, Y. Kanou and H. Okamoto, *Solid State Commun.*, 2008, **145**, 246.

292 S. L. Bud'ko, N. Ni and P. C. Canfield, *Philos. Mag.*, 2010, **90**, 1219.

293 H. Fujishita, T. Yamada, S. Nakada, H. Okamoto, S. Shitara, M. Kato and Y. Koike, *Solid State Commun*., 2010, **150**, 711.

294 M. A. Simpson and T. F. Smith, *J. Low Temp. Phys.*, 1978, **32**, 57.

295 N. Oeschler, P. Gegenwart, F. Weickert, I. Zerec, P. Thalmeierand, F. Steglich, E. D. Bauer, N. A. Frederick and M. B. Maple, *Phys. Rev. B*, 2004, **69**, 235108.
296 A. Gasparini, Y. K. Huang, J. Hartbaum, H. Löhneysen and A. de Visser, *Phys. Rev. B*, 2010, **82**, 052502.
297 F. Hardy, P. Adelmann, T. Wolf, H. Löhneysen and C. Meingast, *Phys. Rev. Lett.*, 2009, **102**, 187004.
298 F. Gugenberger, C. Meingast, G. Roth, K. Grube, V. Breit, T. Weber, H. Wühl, S. Uchida and Y. Nakamura, *Phys. Rev. B*, 1994, **49**, 13137.
299 A. C. Bailey and B. Yates, *J. Appl. Phys.*, 1970, **41**, 5088.
300 K. V. Zakharchenko, J. H. Los, M. I. Katsnelson and A. Fasolino, *Phys. Rev. B*, 2010, **81**, 235439.
301 H. You, U. Welp and Y. Fang, *Phys. Rev. B*, 1991, **43**, 3660.
302 C. A. M. dos Santos, J. J. Neumeier, Y. K. Yu, R. K. Bollinger, R. Jin, D. Mandrus and B. C. Sales, *Phys. Rev. B*, 2006, **74**, 132402.
303 Y. Yiu, V. O. Garlea, M. A. McGuire, A. Huq, D. Mandrus and S. E. Nagler, *Phys. Rev. B*, 2012, **86**, 054111.
304 A. E. Böhmer, P. Burger, F. Hardy, T. Wolf, P. Schweiss, R. Fromknecht, H. v. Löhneysen, C. Meingast, H. K. Mak, R. Lortz, S. Kasahara, T. Terashima, T. Shibauchi and Y. Matsuda, *Phys. Rev. B*, 2012, **86**, 094521.
305 S. Nandi, M. G. Kim, A. Kreyssig, R. M. Fernandes, D. K. Pratt, A. Thaler, N. Ni, S. L. Bud'ko, P. C. Canfield, J. Schmalian, R. J. McQueeney and A. I. Goldman, *Phys. Rev. Lett.*, 2010, **104**, 057006.
306 Q. Huang, Y. Qiu, W. Bao, M. A. Green, J. W. Lynn, Y. C. Gasparovic, T. Wu, G. Wu and X. H. Chen, *Phys. Rev. Lett.*, 2008, **101**, 257003.
307 Y. Su, P. Link, A. Schneidewind, Th. Wolf, P. Adelmann, Y. Xiao, M. Meven, R. Mittal, M. Rotter, D. Johrendt, Th. Brueckel and M. Loewenhaupt, arXiv:0807.1743, 2008.
308 P. C. Canfield, S. L. Bud'ko, N. Ni, A. Kreyssig, A. I. Goldman, R. J. McQueeney, M. S. Torikachvili, D. N. Argyriou, G. Luke and W. Yu, *Physica C*, 2009, **469**, 404.
309 J. Zhao, Q. Huang, C. de la Cruz, J. W. Lynn, M. D. Lumsden, Z. A. Ren, J. Yang, X. Shen, X. Dong, Z. Zhao and P. Dai, *Phys. Rev. B*, 2008, **78**, 132504.
310 R. Mittal, L. Pintschovius, D. Lamago, R. Heid, K. P. Bohnen, D. Reznik, S. L. Chaplot, Y. Su, N. Kumar, S. K. Dhar, A. Thamizhavel, Th. Brueckel, *Phys. Rev. Lett.*, 2009, **102**, 217001.
311 R. Hoffmann and C. Zheng, *J. Phys. Chem*., 1985, **89**, 4175.
312 V. K. Anand, D. G. Quirinale, Y. Lee, B. N. Harmon, Y. Furukawa, V. V. Ogloblichev, A. Huq, D. L. Abernathy, P. W. Stephens, R. J. McQueeney, A. Kreyssig, A. I. Goldman and D. C. Johnston, *arXiv:1406.7249*, 2014.
313 D. G. Quirinale, V. K. Anand, M. G. Kim, A. Pandey, A. Huq, P. W. Stephens, T. W. Heitmann, A. Kreyssig, R. J. McQueeney, D. C. Johnston and A. I. Goldman, *Phys. Rev. B*, 2013, **88**, 174420.
314 V. Pasler, P. Schweiss, C. Meingast, B. Obst, H. Wühl, A. I. Rykov and S. Tajima, *Phys. Rev. Lett.*, 1998, **81**, 1094.
315 T. Asahi, H. Suzuki, M. Nakamura, H. Takano and J. Kobayashi, *Phys. Rev. B*, 1997, **55**, 9125.
316 C. Meingast, O. Kraut, T. Wolf, H. Wühl, A. Erb and G. Müller-Vogt, *Phys. Rev. Lett.*,1991, **67**, 1634.
317 V. Srikanth, E. C. Subbarao, D. K. Agrawal, C. Y. Huang, R. Roy and G. V. Rao, *J. Am. Ceram. Soc.*, 1991, **74**, 365.
318 J. Tao and A. Sleight, *J. Solid State Chem.*, 2003, **173**, 45.
319 S. C. Peter, M. Chondroudi, C. D. Malliakas, M. Balasubramanian and M. G. Kanatzidis, *J. Am. Chem. Soc.*, 2011, **133**, 13840.
320 P. J. Chupas, S. Chaudhuri, J. C. Hanson, X. Qiu, P. L. Lee, S. D. Shastri, S. J. Billinge, C. P. Grey, *J. Am. Chem. Soc.*, 2004, **126**, 4756.
321 B. J. Kennedy and T. Vogt, *Mater. Res. Bull.*, 2002, **37**, 77.
322 L. Han, Y. Wang, L. Guo, L. Zhao and Y. Tao, *Nanoscale*, 2014, **6**, 5907.
323 Z. Hu, J. D. Jorgensen, S. Teslic, S. Short, D. N. Argyriou, J. S. O. Evans and A. W. Sleight, *Physica B*, 1997, **241**, 370.
324 J. D. Jorgensen, Z. Hu, S. Short, A. W. Sleight and J. S. O. Evans, *J. Appl. Phys.*, 2001, **89**, 3184.
325 M. Cetinko, A. P. Wilkinson and C. Lind, *Phys. Rev. B*, 2009, **79**, 224118.

